INFORMATION TO USERS

This manuscript has been reproduced from the microfilm master. UMI films the text directly from the original or copy submitted. Thus, some thesis and dissertation copies are in typewriter face, while others may be from any type of computer printer.

The quality of this reproduction is dependent upon the quality of the copy submitted. Broken or indistinct print, colored or poor quality illustrations and photographs, print bleedthrough, substandard margins, and improper alignment can adversely affect reproduction.

In the unlikely event that the author did not send UMI a complete manuscript and there are missing pages, these will be noted. Also, if unauthorized copyright material had to be removed, a note will indicate the deletion.

Oversize materials (e.g., maps, drawings, charts) are reproduced by sectioning the original, beginning at the upper left-hand corner and continuing from left to right in equal sections with small overlaps.

Photographs included in the original manuscript have been reproduced xerographically in this copy. Higher quality 6" x 9" black and white photographic prints are available for any photographs or illustrations appearing in this copy for an additional charge. Contact UMI directly to order.

Bell & Howell Information and Learning
300 North Zeeb Road, Ann Arbor, MI 48106-1346 USA
800-521-0600

Université d'Ottawa · University of Ottawa

Cation distribution in the europium iron garnet series $Eu_3Fe_{5-x}Al_xO_{12}$

by
Mingyu Li

The thesis submitted to
the school of Graduate Studies and Research in
partial fulfillment of the requirements for
the degree of M.Sc. in physics

Department of Physics
University of Ottawa
Ottawa, Ontario
Canada

May 2000

Abstract

The cation distributions in europium iron garnet $Eu_3Fe_{5-x}Al_xO_{12}$ series have not been determined yet since they were synthesized and studied by Yamaguchi and Sakuraba twenty years ago. In this thesis, the Fe-Al distributions over the octahedral (*a*) and tetrahedral (*d*) sites in the europium iron garnet $Eu_3Fe_{5-x}Al_xO_{12}$ series have been determined by powder X-ray diffraction (XRD) and ^{57}Fe Mössbauer spectroscopy (^{57}Fe MS). The ^{57}Fe MS spectra are collected at temperatures above the Néel temperatures of the studied samples and the cation distributions are derived from both the raw and thickness-corrected MS spectra. It is found that Al atoms occupy both the *a* and *d* sites. Higher Al concentration in the *d* sites is interpreted as the evidence that Al atoms enter preferentially the *d* sites due to the smaller size of Al ions compared with Fe ions. MS gives more reliable results of the Fe-Al distributions than XRD, which could be ascribed to the sensitivity of MS to the local environment around the iron nucleus at the specific site.

ACKNOWLEDGMENTS

I am indebted to my supervisor, Professor Z. M. Stadnik, for his constant and timely support.

I wish to acknowledge the financial support of the University of Ottawa in the form of the tuition fee wavers.

I am thankful to Dr. C. Benson and the technicians for their assistance with the first-year labs. Thanks are extended to all in the Department of Physics for their help on countless occasions.

I would like to thank all my family members for their endless support, patience and encouragement.

Contents

Chapter 1

Introduction

1.1 Garnet structure

The determination of a garnet structure was first made on natural minerals nearly eighty years ago[1]. The garnet structure has been widely studied in the last fifty years[2]. Structural refinements were first carried out on synthetic yttrium iron garnet (YIG) crystals[3–5]. It was established that garnets are cubic compounds that belong to the space group $Ia3d$ (O_h^{10}) containing 8 formulas with 160 atoms per unit cell[6].

The general chemical formula of a garnet is $\{X_3\}[Y_2](Z_3)O_{12}$, where { }, [ ] and ( ) represent eightfold dodecahedral (*c* sites), sixfold octahedral (*a* sites) and fourfold tetrahedral (*d* sites) coordination, and X, Y and Z denote the cations in each particular site, respectively[7]. The arrangement of cations in the garnet structure is shown in **Fig. 1.1**[8] and the co-ordination about one oxygen ion is shown in **Fig. 1.2**[9]. Oxygen atoms are situated in a general position with variable coordinates (*h* sites). Each *h* site is at the corner of four polyhedra sites (one *d* site, one *a* site and two *c* sites), as shown in **Fig. 1.2.** Each *c* site is surrounded by four *c* sites, four *a* sites and six *d* sites. Each *a* site is surrounded by eight *a* sites at the corners of a body-centered cube, six *d* sites and six *c* sites. Each *d* sites is surrounded by four *d* sites, four *a* sites and six *c* sites[10]. The *a* and *d* sites share corners to form a cubic framework structure. The X cations occupy *c* sites in the channels within this framework. The special *c*, *a* and *d* sites have no degrees of

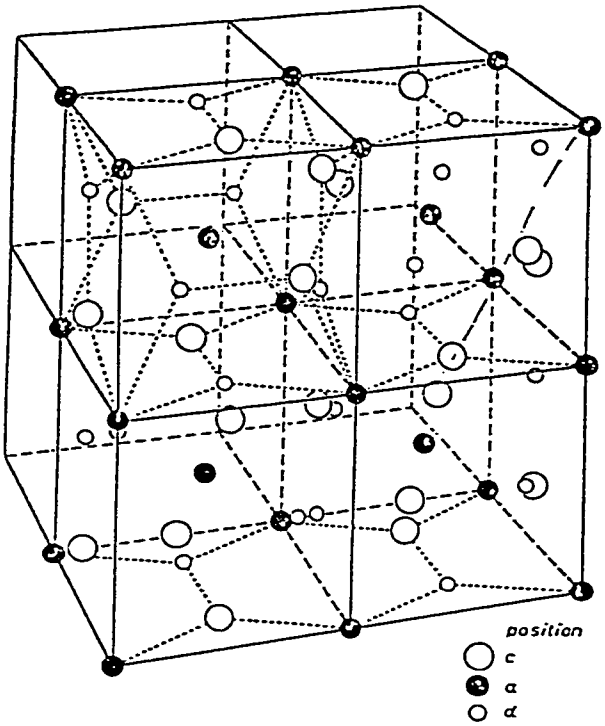

Fig. 1.1. Arrangement of cations in the garnet structure[8].

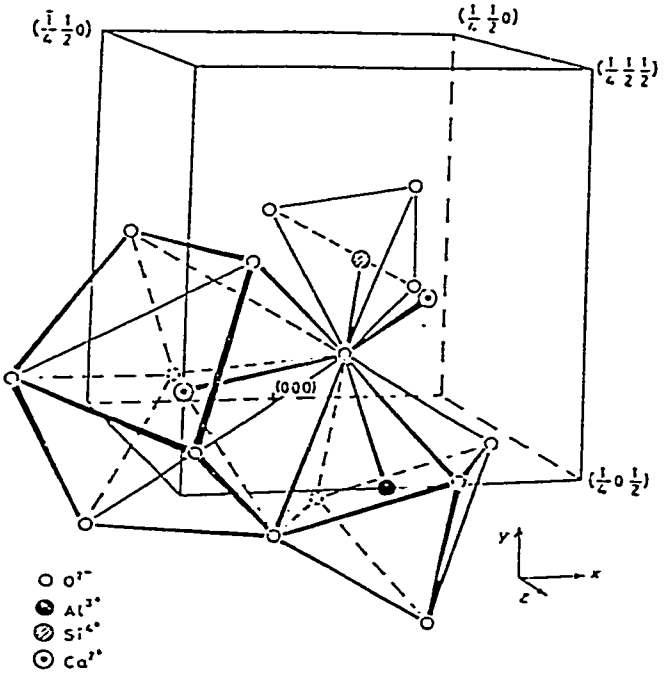

Fig. 1.2. Co-ordination about an oxygen ion in a garnet[9].

freedom; the *h* sites are general and therefore have three degrees of freedom. A description of the sites occupied by the different ions is shown in **Table 1.1.**

It should be pointed out that the structure is amenable to substitution at the *c*, *a* and *d* sites and a large variety of cations can be allowed in these positions. The primary consideration of the site occupancy by cations is the ionic size. The ionic radius increases with the coordination number. The large X cations include Eu^{3+}, Ca^{3+}, Mn^{3+}, Fe^{3+}, Mg^{3+}. The intermediate-sized Y cations include Fe^{3+}, Cr^{3+}, Al^{3+}, Ti^{3+}. The smaller Z cations are Fe^{3+}, Si^{3+}, Al^{3+}, Ti^{3+}[11, 12]. This list is not exhaustive and many other cations may enter the structure[13].

Table 1.1. Description of the garnet structure.

Point symmetry	222	$\bar{3}$	$\bar{4}$	$\bar{1}$
Space group position	24c	16a	24d	96h
Typical ideal formula	$\{X_3\}$	$[Y_2]$	(Z_3)	O_{12}
Coordination to oxygen	8	6	4	
Type of polyhedron	dodecahedron	octahedron	tetrahedron	

1.2 Properties of garnets

Generally, all physical phenomena characteristic of solids are in some way related to their crystal structures. Here, the crystal structure does not only mean the symmetry of the crystals, but also means the types of atoms and their specific arrangement in the crystals. A lot of research has been done in the case of garnets. There is no doubt that any special properties of garnets must be a direct consequence of the structure and the particular ions in the crystals.

• Magnetic properties

There are three major types of magnetic ordering that are relevant to garnets. They are ferromagnetic, antiferromagnetic and ferrimagnetic. The most important garnets in industry applications are those that are ferrimagnetic, such as yttrium, rare earth and the substituted garnets. The study of those garnets continues due to their wide range of technological applications. For instance, single crystals of yttrium iron garnet have been known to be applicable in the microwave-device field[14,15]; ion-implanted garnet films with large magneto-optical effects can be developed into high-density memory devices because of their large Faraday rotation and good corrosion resistance[16–18]. Since the discovery of the magnetic garnets in 1958, they have turned out to be the most promising materials for magnetic devices, such as printers, memory devices and many others[19,20].

• Optical properties

Aluminum garnets have good optical properties. It is well known that yttrium aluminum garnet (YAG) is the most important solid-state laser host material. The Nd:YAG laser has been widely used in commercial, medical, military and industrial applications since its discovery in 1964[21]. Iron garnets are transparent within the infrared region[22]. The magnetic optical effects in iron garnets make them suitable for displays[23], printers[24], bubble applications[25], gyrolasers[26] or optical-communication[27]. Finally, silicon-doped iron garnets

have photoinduced effects which increase the potentiality of these materials in solid-state devices[28].

The thermal and elastic properties of garnets have also been studied[29,30], which led to other industrial applications. For instance, the thermal properties of garnets are very useful in the process of garnet growth[31].

1.3 Purpose of this thesis

The europium iron garnets ($Eu_3Fe_{5-x}Al_xO_{12}$) were synthesized by Yamaguchi and Sakuraba[32]. The lattice constants of these garnets were evaluated from X-ray diffraction measurements, but their structure has not been determined[32]. The magnetization measurements have been made on the single crystals of this series[32], but the assignment of Al^{+3} to the *a* and/or *d* sites has not been determined yet. The cation distribution is important for the preparation of magnetic materials with controlled properties. For example, it is known that the substitution of nonmagnetic ions for iron changes the magnetic moment by altering the difference in the number of magnetic ions in the *a* and *d* sites in the yttrium iron garnet (YIG)[33-35]. The neighboring cations of the central iron ions have a substantial effect on the electric field gradient (EFG) at the Fe nucleus[36]. Therefore, one must know the cation distribution in a chemical formula for a calculation of the EFG. The knowledge of the cation distribution also helps to understand the growth of single crystals because the chemical composition can be related to the temperature and pressure of the formation[37].

The determination of the cation distribution in the $Eu_3Fe_{5-x}Al_xO_{12}$ series is the main purpose of this study. The second goal of this study is to carry out the refinement of the crystal structure of this series.

1.4 Scope of the thesis

The thesis contains the research results from both powder X-ray diffraction (XRD) at room temperature and Mössbauer spectroscopy (MS) methods in the temperature range 298–1023 K. The XRD patterns were indexed and crystal structure refinements were carried out on the basis of the *Ia3d* space group. The MS data analysis and some relevant methodological aspects are also discussed. The derived iron distribution from the two methods have then been compared.

Chapter 2

Methodology

Many experiments show that no single technique is able to give the complete cation distribution in the garnets and it is necessary to combine different techniques[38]. In this thesis, two techniques are applied to the studied samples which are XRD and ^{57}Fe MS.

2.1 X-ray diffraction

2.1.1 Review of crystal diffraction

The extension of Fourier analysis to the periodic electron density function n(**r**) leads to[39]

$$n(\mathbf{r}) = \sum_{G} n_G \exp(i\mathbf{G}\cdot\mathbf{r}), \tag{2.1}$$

where **G** is the vector of a reciprocal lattice, **r** is the position of a lattice point and n_G can be derived from **Eq. 2.1**[39]

$$n_G = \frac{1}{V_C}\int_{cell} dV n(\mathbf{r})\exp(-i\mathbf{G}\cdot\mathbf{r}). \tag{2.2}$$

The diffraction condition for a crystal is derived from the above definitions. The incident radiation has a wave vector **k**. The scattered ray has a wave vector **k′** and $\Delta\mathbf{k} = \mathbf{k}'-\mathbf{k}$. Considering two volume elements **r** apart in a crystal, the difference of the phase factor is exp[-i$\Delta\mathbf{k}\cdot\mathbf{r}$]. The scattering amplitude is defined as[39]

$$F = \int dVn(\mathbf{r}) \exp(-i\Delta\mathbf{k}\cdot\mathbf{r}) \tag{2.3}$$

$$= \sum_G \int dVn_G \exp[i(\mathbf{G} - \Delta\mathbf{k}\cdot\mathbf{r}]. \tag{2.4}$$

When the scattering vector is equal to the reciprocal lattice vector $\Delta\mathbf{k} = \mathbf{G}$, **Eq. 2.4** yields $F = Vn_G$. If $n_G \neq 0$, a constructive interference peak will show up at **G**. So, $\Delta\mathbf{k} = \mathbf{G}$ is the diffraction condition, which means that the set of reciprocal lattice vectors **G** determines all possible diffraction peaks. If 2θ is the angle separating incident and diffracted beams, the diffraction condition leads to the following expression (*Bragg's Law*)

$$2d_{hkl} \sin\theta = n\lambda, \tag{2.5}$$

where n is the order of diffraction. The condition for Bragg reflection is shown in **Fig.2.1**[40].

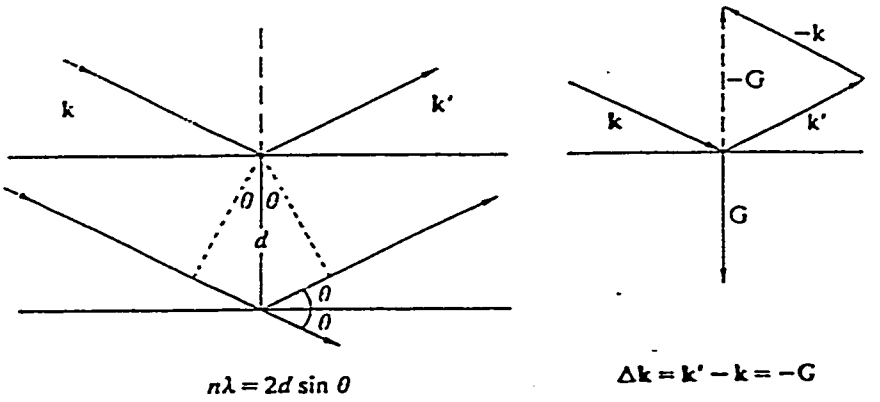

Fig. 2.1. Diffraction by an array of point scatters may be considered as Bragg reflection from planar arrays[40].

When the lattice cell is conventional instead of primitive, some values of n_G in **Eq. 2.4** may be equal to zero. The peaks corresponding to zero-amplitude **G**'s would not appear in the diffraction spectra. The set of conditions that determine the allowed and forbidden Miller indices (*hkl*) are called the extinction rules for the crystals. Different *Bravais* lattices have different extinction rules. For example, the sum of Miller indices *h*, *k* and *l* in a body-centered cubic lattice must be an even integer[40]. There are three types of *Bravais* lattices in a cubic system. They are simple cubic [**P**(a)], face-centered cubic [**F**(a)] and body-centered cubic [**I**(a)]. The lattice constant (the side length of the conventional cubic cell) is *a*.

The extinction rules of cubic structures[40]

Simple cubic	all *h*, *k*, *l* allowed	first reflection (100)
Body-centered cubic	only *h*+*k*+*l* even allowed	first reflection (110)
Face-centered cubic	*h*, *k*, *l* all odd or all even allowed	first reflection (111)

Crystal structures can be determined by diffraction of X-ray, neutron or electron beams. The intensity distribution of the diffraction pattern is related to the Fourier transform of the crystal structure[41]. The garnet structure belongs to the body-centered cubic system.

2.1.2 Background and definitions in the Rietveld analysis

The Rietveld method was first reported at the Seventh Congress of the International Union of Crystallography (IUCr) in Moscow in 1966[42]. It has become generally accepted for X-ray as well as neutron powder diffraction since 1977[43-45].

A crystal structure refinement is a fitting process to obtain the best fit between the entire observed XRD pattern and the entire calculated pattern for the crystal structures, diffraction optical effects, instrumental factors and other specimen characteristics[46]. In the Rietveld method, the fitting is done by using a least-squares method. Crystal parameters[46] and profile values[47] are optimized until the best agreement is obtained between the observed and calculated intensities.

The basic idea about a least-squares analysis is to minimize the difference between the calculated and observed values until the smallest residual S_y is obtained[46]. In the XRD pattern analysis, S_y is defined as

$$S_y = \sum_i w_i \left(y_{io} - y_{ic}\right)^2, \tag{2.6}$$

where w_i is equal to $1/y_{io}$, y_{io} is the total observed intensity at the ith step, and y_{ic} is the calculated intensity at the ith step.

An expression which describes the powder XRD pattern as a function of parameters contributing to the intensities can be written as[48]

$$I(k) = S \cdot P \cdot C, \tag{2.7}$$

where $I(k)$ is the integrated intensity of the kth reflection, S represents all structure-independent values, including the unit cell volume and 2θ-independent values, P represents the product of all structure-independent but diffraction-angle-dependent

parameters and C represents the contribution from the crystal structure and sample characteristics.

S can be defined as

$$S = I_0 \cdot \left(\frac{A\lambda^3}{32\pi r}\right) \cdot \left[\left(\frac{\mu_0}{4\pi}\right)^2 \frac{e^4}{m^2}\right] \cdot \left(\frac{1}{2\mu}\right) \cdot \left(\frac{1}{V^2}\right), \tag{2.8}$$

with intensity I_0 [$Jsec^{-1}m^{-2}$] of incident beam, cross sectional area A [m^2] of incident beam, wavelength λ [μ], goniometer radius r [m], which is described in Chapter 3, $\mu_0 = 4\pi\times10^{-7}m\cdot kg\cdot C^{-2}$, charge of the electron e [C], mass of the electron m [kg], volume of a unit cell V [m^3], linear absorption coefficient μ [m^{-1}]. The value of S is usually incorporated into the scale factor, being refined in the least-squares procedure.

P can be expressed as

$$P = L \cdot p \cdot D, \tag{2.9}$$

where L represents the Lorentz factor

$$L = \frac{1}{2\sin^2\theta \cdot \cos\theta} = \frac{1}{\sin 2\theta \cdot \sin\theta} = \csc 2\theta \cdot \csc\theta \ , \tag{2.10}$$

p represents the polarization factor

$$p = \frac{1+\cos^2 2\theta_m \cdot \cos^2 2\theta}{1+\cos^2 2\theta_m} \ , \tag{2.11}$$

where θ_m is a monochromator correction term for diffraction angle θ. D is a correction term for various divergence slit configurations.

The structure and sample-dependent expression C can be written as

$$C = PO_k \cdot M_k \cdot \left|F_k\right|^2 \ , \tag{2.12}$$

where PO_k is the simple preferred orientation correction in which the March algorithm[49] is applied, M_k is the multiplicity of the kth reflection and F_k is the structure factor

expression with an anisotropic displacement factor matrix. Because the preferred orientation produces systematic distortions of the reflection intensities, the intensity of a *k*th reflection is corrected by the preferred orientation function[50]

$$PO_k = \left(r^2 \cdot \cos^2 \alpha + \frac{\sin^2 \alpha}{r} \right)^{-\frac{3}{2}}, \tag{2.13}$$

where r is an adjustable parameter since r only can be determined from the fit of the intensities and α is the angle between the crystal plane *(hkl)* and the *PO* vector. The structure factor is defined as[46]

$$F_k = \sum_{j=1}^{n} f_j \cdot O_j \cdot e^{\left[2\pi i \left(h_k^i r_j - h_j^i B_j h_k\right)\right]}, \tag{2.14}$$

where f_j is the scattering factor or scattering length of atom j, and h_k, r_j and B_j are matrices representing the Miller indices, atomic coordinates and anisotropic displacement factors, respectively.

A powder diffraction pattern of a crystal is a collection of individual reflection profiles. Each profile has a peak height, a peak position, a breath, tails and an integrated area. $I(k)$ is proportional to the integrated area. Many Bragg reflections contribute to the intensity y_i observed at any arbitrarily chosen point i in the pattern. The basic philosophy of a crystal structure refinement is to fit these parameters to give the best match with the observed intensities. However, the fitted profiles from the least-squares process are still not good enough compared with the real diffraction profiles. This is because the least-square process does not consider the shape of a peak. In order to have a more reliable fitting result, an error function G is applied to the calculated integrated intensities (e.g. Gauss function) giving a distribution of intensities around the peak position[46]. Thus, a

real reflection can be simulated. Because the G can be applied to each step intensity, the least- squares parameters can be fitted based on step intensities and not only on integrated intensities. This concept can be expressed as[51]

$$y_{ic} = y_{ib} + \sum_{p=p_1}^{p_2} \sum_{k=k_1}^{k_2} G_{ipk} \cdot I_{pk} \ , \tag{2.15}$$

where y_{ic} is the net intensity calculated at point i in the pattern, y_{ib} is the background intensity, G_{ik} is a normalized peak profile function, I_{pk} is the intensity of the kth Bragg reflection of phase p and k_1 ....k_2 are the reflections contributing to the intensity at point i.

The following are some symmetric analytical profile functions that have been used[52]:

a) Gauss $$G_{ik} = \frac{\sqrt{C_1}}{H_k \sqrt{\pi}} \cdot e^{-C_1 X_{ik}^2} \ , \tag{2.16}$$

b) Lorentz $$G_{ik} = \frac{\sqrt{C_0}}{H_k \pi \cdot \left(1 + C_0 X_{ik}^2\right)}, \tag{2.17}$$

c) Pseudo Voigt $$G_{ik} = \gamma \cdot \frac{\sqrt{C_0}}{H_k \pi \cdot \left(1 + C_0 X_{ik}^2\right)} + \left(1 - \gamma\right) \cdot \frac{\sqrt{C_1}}{H_k \sqrt{\pi}} \cdot e^{-C_1 X_{ik}^2} \ , \tag{2.18}$$

d) Pearson VII $$G_{ik} = \frac{\Gamma(\gamma)}{\Gamma\left(\gamma - \frac{1}{2}\right)} \cdot \frac{2\sqrt{C_2}}{H_k \sqrt{\pi}} \cdot \left(1 + 4C_2 X_{ik}^2\right)^{-\gamma} \ , \tag{2.19}$$

e) Voigt $$G_{ik} = \frac{\sqrt{C_1}}{H_{Gk} \sqrt{\pi}} \cdot \mathrm{Re}\left[w\left(\sqrt{C_1} X_{ik} + i C_3 H_{Lk}\right)\right]. \tag{2.20}$$

Here $C_0 = 4$, $C_1 = 4\ln 2$, $C_2 = 2^{1/\gamma}-1$, $C_3 = 2^{-3/2}$, H_k is the full width at half maximum (FWHM) of the kth Bragg reflection, $X_{ik} = 2\theta_i - 2\theta_k$, γ is a refinable mixing parameter, Γ denotes the gamma function and w is the complex error function.

The dependence of the breadth H of the reflection profiles measured as FWHM has typically been modeled as[53]

$$H^2 = U\tan^2\theta + V\tan\theta + W, \tag{2.21}$$

where U, V and W are the refinable parameters.

The mixing parameter γ is defined as

$$\gamma = \gamma_1 + \gamma_2 \cdot 2\theta + \gamma_3 \cdot (2\theta)^2, \tag{2.22}$$

where γ_1, γ_2 and γ_3 are refinable parameters.

The background y_{ib} may be obtained by linear interpolation between reference points or by refinement of the parameters in a function[54]

$$y_{ib} = \sum_{m=-1}^{4} B_m (2\theta_i)^m . \tag{2.23}$$

In order to make sure that the best fit of the entire calculated pattern to the entire observed pattern has been obtained, one needs various criteria to make the judgment[54]. Some often-used criteria are given as

R-pattern
$$R_p = \frac{\sum |y_{io} - y_{ic}|}{\sum y_{io}}, \tag{2.24}$$

R-weighted pattern
$$R_{wp} = \sqrt{\frac{\sum w_i (y_{io} - y_{ic})^2}{\sum w_i y_{io}^2}}, \tag{2.25}$$

R-Bragg factor
$$R_B = \frac{\sum |I_{ko} - I_{kc}|}{\sum I_{ko}}, \tag{2.26}$$

R-structure factor
$$R_F = \frac{\sum |(I_{ko}^{1/2} - I_{kc}^{1/2})|}{\sum I_{ko}^{1/2}}. \tag{2.27}$$

Here I_{ko} and I_{kc} are the observed and calculated intensities assigned to the kth Bragg reflection at the end of the refinement cycles , respectively.

The so-called goodness of fit indicator, S, is defined as

$$S = \sqrt{\frac{S_y}{N-P+C}} = \frac{R_{wp}}{R_{exp}}, \tag{2.28}$$

where

$$R_{exp} = \sqrt{\frac{N-P+C}{\sum w_i y_{io}}} . \tag{2.29}$$

Here N is the number of steps, P is the parameter varied in the calculated model and C is the applied constraints.

Among these R's, R_{wp} is the most meaningful criterion from the mathematical point of view because it represents the residual being minimized. It is also the best one that reflects the progress of the refinement[55].

2.2 Theory of Mössbauer spectroscopy

The Mössbauer effect (ME) is alternatively known as a recoil-free nuclear resonance emission and absorption. The phenomenon was discovered in 1958 by the German physicist R. L. Mössbauer, who was awarded the Nobel Prize for this work in 1960[56].

In a typical Mössbauer experiment, a γ–ray source is set into slow oscillatory motion relative to a sample under study. The sample can only absorb those γ rays that are appropriate to a transition between the nuclear energy levels in the sample material. As the half-width of the γ–ray line is fairly small (e.g., 4.9×10^{-9} eV for ^{57}Fe), the probability of the ME is very sensitive to even quite small energy changes. Such small changes occur in the energy state of the nucleus as a result of interaction of the nuclear charge and

moments with the external environment (hyperfine interaction), such as the electron shell and the other atoms of the crystal. For this reason, the source and absorber must have identical atoms. If the source is moved at various velocities, the resonance can be created with the aid of the Doppler effect[57]. In general, a Mössbauer spectrum reflects the nature and the strength of the hyperfine interactions. Most valuable chemical and physical information can be extracted from the hyperfine interactions. The parameters that provide such information are the isomer shift, the electric quadrupole splitting and the magnetic hyperfine splitting.

2.2.1 Isomer shift

The nucleus is not a point charge; it has a finite radius and, in most cases, the excited and ground states have different radii. Because of the Coulomb interaction of the nuclear charge and the electron charge, the nuclear energy levels are slightly different in atoms of different compounds.

The atomic nucleus can be considered to be spherical with a radius R. The electron charge Ze is distributed homogeneously within it. At a distance r from the center of the atomic nucleus, the electrostatic potential is given by

$$V = \frac{Ze}{r}, \qquad \text{for r>R,} \tag{2.30}$$

and by

$$V' = \frac{Ze}{R}\left(\frac{3}{2} - \frac{r^2}{2R^2}\right), \qquad \text{for r≤R.} \tag{2.31}$$

As the s electrons with orbital quantum number l=0 also have a finite density within the atomic nucleus, the energy state of the nucleus is affected by the charge originating from the electrons in the sphere of radius R. On this basis, the energy shift of energy states can be given as[58]

$$\delta E = \int_0^{\infty} \rho(V' - V) 4\pi r^2 dr = \frac{4\pi\rho Ze}{R} \int_0^R \left(\frac{3}{2} - \frac{r^2}{2R^2} - \frac{R}{r} \right) r^2 dr . \qquad (2.32)$$

Therefore,

$$\delta E = -\frac{2\pi}{5} Ze\rho R^2 = \frac{2\pi}{5} Ze^2 |\psi(0)|^2 R^2 , \qquad (2.33)$$

where $\rho = -e|\psi(0)|^2$ is the charge density originating from the s electrons in the atomic nucleus.

The atomic nuclei have different radii in the excited and ground states ($R_g \neq R_e$), and therefore δE will also have different values in these states. The difference between the two δE's can be written as

$$\delta E_e - \delta E_g = \frac{2\pi}{5} Ze^2 |\psi(0)|^2 (R_e^2 - R_g^2) . \qquad (2.34)$$

Mössbauer atoms in the radiation source and in the absorber may have different chemical environments (types of chemical bonds, oxidation state, etc.), from which it follows that $|\psi_a(0)|^2 \neq |\psi_s(0)|^2$. Hence, the energy between the excited state and the ground state, E_0, is different for the MS atoms in the source and the absorber, respectively. The difference, ΔE_0, is the isomer shift, denoted by δ

$$\delta = E_0^a - E_0^s = \frac{2\pi}{5} Ze^2 \left(R_e^2 - R_g^2 \right) \left(|\psi_a(0)|^2 - |\psi_s(0)|^2 \right) . \qquad (2.35)$$

The origin of the isomer shift is shown in **Fig. 2.2**[59]. The isomer shift is generally given in units of velocity (mm/s or cm/s).

The value of $|\psi(0)|^2$ is determined by the degree of occupation of the *s* orbitals, and also by the degree of occupation of the orbitals with the orbital quantum number $l > 0$, because of the shielding effect on the *s* electrons. The density of the *s* electrons at the position of the nucleus can be estimated from the Fermi-Serge equation

$$|\psi_{n,s}(0)|^2 = \frac{ZZ_{eff}^2}{\pi a_0^3 n_{eff}^3}\left(1-\frac{d\sigma}{dn}\right), \tag{2.36}$$

where Z is the nuclear charge, Z_{eff} is the effective nuclear charge taking into account the shielding effect of the electrons, a_0 is the Bohr radius of the ground-state atom, $\sigma = n-n_{eff}$ is the quantum deficiency and n, n_{eff} are the principal quantum number and the effective principal quantum number, respectively[58].

2.2.2 Quadrupole splitting

If the nucleus has spin $I > 1$, it will possess a quadrupole moment (eQ) arising from the non-uniform distribution of charge. The asymmetrical charge distribution also gives rise to an electric field gradient (EFG) that differs from zero on the site of the atom nucleus. The interaction of the nuclear electric quadrupole moment and the electric field gradient at the site of the atom nucleus can be expressed by the Hamilton operator[60]

$$\mathbf{H} = \frac{e^2qQ}{4I(2I-1)}\left[3\mathbf{I}_z^2 - \mathbf{I}(\mathbf{I}+1)+\eta\left(\mathbf{I}_x^2-\mathbf{I}_y^2\right)\right], \tag{2.37}$$

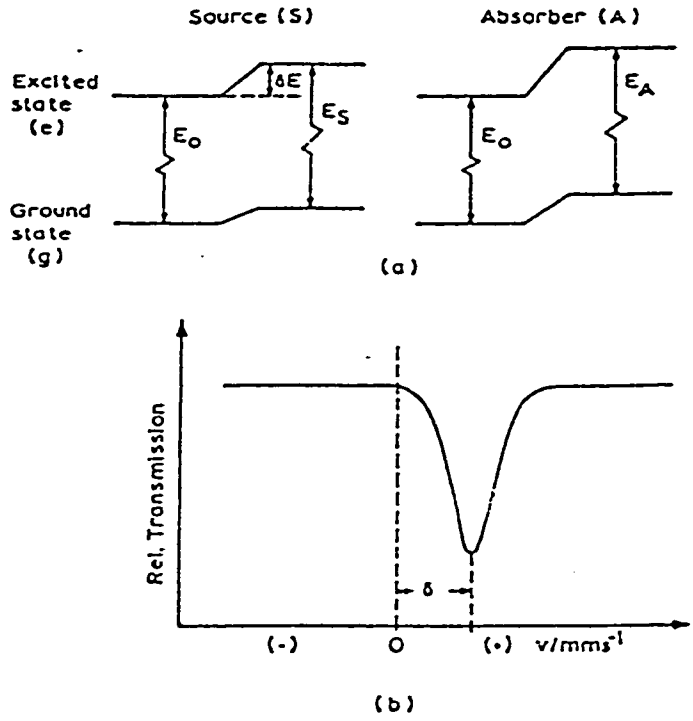

Fig. 2.2. Origin of the isomer shift. (a) Electric monopole interaction between the nuclear charge and electrons at the nucleus shifts nuclear energy levels without changing the degeneracy; (b) Resultant Mössbauer spectrum (schematic)[59].

where eq is the absolute value of the EFG in the z direction ($eq = |V_{zz}| = \left|\frac{\partial^2 V}{\partial Z^2}\right|$) at the site of the atomic nucleus, I is the spin quantum number, $\mathbf{I}$ is the spin operator and $\mathbf{I}_x$, $\mathbf{I}_y$, $\mathbf{I}_z$ are the conventional spin operators. η is defined as

$$\eta = \frac{V_{xx} - V_{yy}}{V_{zz}} \quad , \tag{2.38}$$

where the indices are chosen so that

$$|V_{zz}| \geq |V_{xx}| \geq |V_{yy}| \quad . \tag{2.39}$$

For $I \leq 3/2$, the eigenvalues of the above Hamilton operator are described by the equation

$$E_Q = \frac{e^2 qQ}{4I(2I-1)}\left[3m_I^2 - I(I+1)\right]\left(1+\frac{\eta^2}{3}\right)^{1/2}, \qquad (2.40)$$

where m_I is the magnetic quantum number, with values of I, $I-1$,...., $-I$.

The magnetic quantum numbers determine the number of energy levels. Therefore, they determine the number of Mössbauer lines. As an example, the effect of electric quadrupole interaction in ^{57}Fe with $I = 3/2$ in the excited energy state (14.4keV) and $I = 1/2$ in the ground state is shown in **Fig. 2.3** [59]. The ground state ($I = 1/2$) is not split because there is not a spectroscopic quadrupole moment in nuclei with $I = 0, 1/2$. The excited state ($I = 3/2$) splits into two degenerate substates $|3/2, \pm 3/2\rangle$ and $|3/2, \pm 1/2\rangle$. Therefore, only two γ-ray transitions are allowed and a doublet would be seen in the spectrum.

2.2.3 Magnetic hyperfine interaction

The interaction between the magnetic dipole moment of the nucleus (μ) and the magnetic field (H) at the nucleus is called the magnetic dipole interaction or the nuclear Zeeman effect. The Hamilton operator of this interaction is given by

$$\mathbf{H}_m = -\boldsymbol{\mu}\mathbf{H} = -g\mu_m \mathbf{I}\mathbf{H}, \qquad (2.41)$$

where g is the nuclear Landè factor and μ_m is the nuclear magneton ($\mu_m = e\hbar / 2Mc$, M– mass of the nucleus). Accordingly, the individual energy levels are

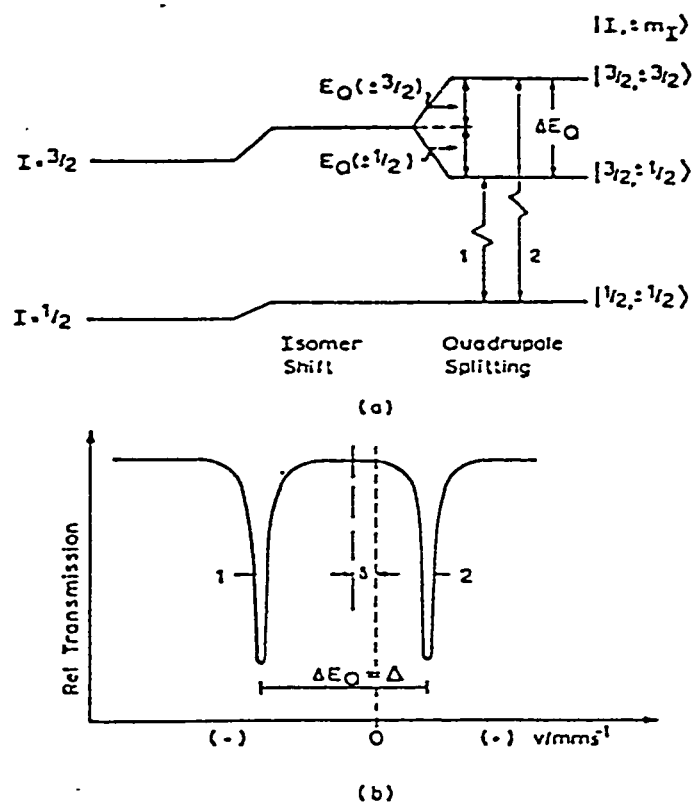

Fig. 2.3. Quadrupole splitting in ^{57}Fe with I = 3/2 in the excited state and I = 1/2 in the ground state. (a) The I = 3/2 level is split into two sublevels $|I,\pm m_I\rangle$ by the electric quadrupole interaction. The ground state level with I = 1/2 is not split because there is no spectroscopic quadrupole moment in a nucleus with I = 1/2. The levels with I = 3/2 and I = 1/2 are shifted by the electric monopole interaction (giving rise to the isomer shift). (b) Resultant Mössbauer spectrum (schematic)[59].

$$E_m = -\mu H m_I \frac{1}{I} = -g\mu_m H m_I \,. \tag{2.42}$$

The nuclear Zeeman effect splits the nuclear state with spin quantum number I into $2I$+1 equally spaced and non-degenerate substates $|I, m_I\rangle$. The only transitions possible between the energy levels of the ground and excited states are those for which $\Delta m_I = 0,\pm 1$. For the effect of magnetic dipole interaction in ^{57}Fe, the I = 3/2 level is split

into four substates and the ground state with $I = 1/2$ into two substates. Therefore, six transitions are allowed in total, as shown in **Fig. 2.4**[59].

In a Mössbauer experiment with a single-line source and a magnetically ordered substance as an absorber, a resonance sextet is usually observed and the centroid is shifted from zero velocity by the isomer shift. There are various sources contributing to the effective magnetic field. The following are the most important sources[59]:

- The Fermi contact field H_c, which not only originates from the direct interaction of the unpaired *s* electrons and the atomic nucleus, but also results from the polarization of the paired *s* electrons;
- The contribution H_L from the orbital motion of valence electrons with the total orbital momentum quantum number L;
- The contribution H_D arising from the electron spin of the atom under consideration.

The magnetic and quadrupole hyperfine interactions may occur simultaneously and are superimposed on one another. **Fig. 2.4** illustrates such a situation[59].

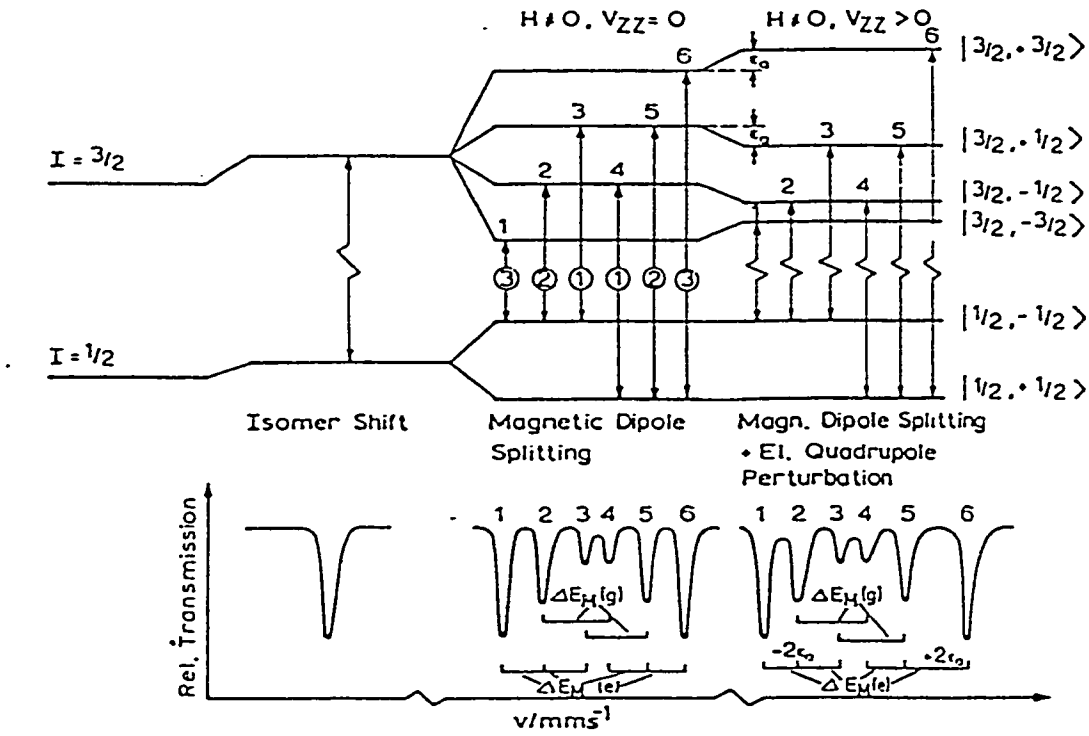

Fig. 2.4. Magnetic dipole splitting (nuclear Zeeman effect) in ^{57}Fe without ($H \neq 0$, $V_{ZZ} = 0$) and with electric quadrupole perturbation ($H \neq 0$, $V_{zz} > 0$) and resultant Mössbauer spectra (schematic)[61]. The centers of gravity of the nuclear levels are shifted by electric monopole interaction, which is always present[59].

2.2.4 Determination of cation distribution by MS

The application of MS in quantitative analysis is based on the fact that, for a very thin sample[61], the area of the MS lines is proportional to the number of MS atoms in the sample. The relationship between the area A of the lines and the number n of the MS atoms can be written as[58]

$$A = k \cdot f \cdot n, \tag{2.43}$$

where f is the recoil-free fraction of the γ radiation (the Debye-Waller factor) and k is a constant including several parameters, such as the cross-section of resonance absorption, the intensity of radiation and the measurement time.

In almost all cases, k and f are not the same for those MS atoms in different environments. Thus, in order to get the ratio of the concentrations of the MS atoms in different sites, k and f must be determined exactly. In practice, empirically determined k and f values are very often used. With the aid of these factors, the line areas can be used to determine the concentrations of the MS atoms in different states.

If the Debye model[62,63] gives a satisfactory description of the lattice vibrations, then

$$f(T) = \exp\left[\frac{-3E_r^2}{Mc^2 k\theta_D}\left(\frac{1}{4}+\frac{T^2}{\theta_D^2}\int_0^{\theta_D/T}\frac{xdx}{e^x-1}\right)\right], \tag{2.44}$$

where E_γ is the γ-ray energy, θ_D is the Debye temperature, k is the Boltzmann constant, c is the velocity of light and M is the mass of the Mössbauer nucleus.

If $T \ll \theta_D$, **Eq.2.51** may be approximated by

$$f(T) = \exp\left[\frac{-E_r^2}{2Mc^2k\theta_D}\left(\frac{3}{2}+\frac{\pi^2T^2}{\theta_D^2}\right)\right], \tag{2.45}$$

and in the high-temperature region, $T > \theta_D/2$,

$$f(T) = \exp\left[\frac{-3E_r^2T}{Mc^2k\theta_D^2}\right]. \tag{2.46}$$

θ_D can be obtained from the temperature dependence $\delta(T)$ of the center shift of the MS spectra. $\delta(T)$ in the Debye approximation can be written as[64]

$$\delta(T) = \delta_0 - \frac{9}{2}\frac{kT}{Mc}\left(\frac{T}{\theta_D}\right)^3\int_0^{\theta_D/T}\frac{x^3dx}{e^x-1}. \tag{2.47}$$

where δ_0 is the intrinsic isomer shift.

In order to determine f in the Debye model or to find the ratio of the MS atoms in different sites, θ_D should be determined. Based on **Eq. 2.47**, θ_D can be calculated by fitting the curve $\delta(T)$. Then, the fraction f at any temperature can be evaluated from **Eq. 2.44**. Therefore, the ratio of the MS atoms in different sites can be derived. The determination of θ_D for the a and d sites in garnet structure will be further discussed in Chapter 4.

Chapter 3

Experimental

The europium iron garnet series $Eu_3Fe_{5-x}Al_xO_{12}$ was measured by both XRD and MS. This chapter gives a brief introduction to the two experimental techniques and the procedure for the data collection in each technique. The raw data correction, corrected data fitting and the relevant computer programs are also described.

3.1 Powder X-ray diffraction

3.1.1 Sample preparation

The europium iron garnet samples were the same as those studied by Y. Yamaguchi and T. Sakuraba[65]. The single crystal samples were grown from a Pb-PbF_2 flux, cut parallel to (110), polished and annealed at 1250 °C for 24 hours in air. The sample forms and the corresponding Néel temperatures are shown in **Table 3.1**.

Table 3.1. The sample forms and Néel temperatures, T_c, of the $Eu_3Fe_{5-x}Al_xO_{12}$ series. *P* refers to a polycrystalline sample and *S* means a single crystal. T_c was measured by a Faraday balance in a magnetic field of 500 Oe[65].

x	0	0.1	0.15	0.2	0.3	0.5	0.6	0.8	1.0	1.5
Form	*P*	*P*	*S*	*P*	*P*	*P*	*P*	*P*	*P*	*S*
T_c (K)	-	558	-	548	536	511	498	474	448	-

The Rietveld refinement of a crystal structure of the europium iron garnet series needs XRD patterns of very good quality[66]. The Rietveld refinement is much more successful if accurate and precise data are collected. Therefore, the sample preparation is

of critical importance in the XRD measurement. In order to have the collection of accurate and precise data in the XRD experiment, careful attention is required to the method of the sample preparation. The samples must be sufficiently ground and correctly mounted in an appropriate sample holder with a suitable thickness and area.

- Grinding problems

  Using powder that is too coarse can give rise to inaccurate and imprecise intensities. Unusually intense and sharp reflections are often obtained from material that is poorly ground. On the other hand, overgrinding materials can broaden some or all reflections (anisotropic grinding effects) and produce small amount of amorphous surface layers[67].

- Sample holder and sample area

  XRD method requires mounting of the sample in an appropriate holder in order to avoid a rise in systematic errors which can affect both reflection positions and intensities[68]. Sufficient sample area is also important because the X-ray beam must be fully within the sample.

- Sample thickness

  The thickness of a powder sample must be appropriate so that essentially all of the incident X-ray beam interacts with the sample and does not pass through it[68].

The studied samples were first ground in a silica mortar. Then the fine powder was mixed with methanol and allowed to dry on a low-background sample holder in order to form a thin flat sample. The diameter of the sample on the holder was around 1.5 cm. The holder is made from a piece of a single crystal of Si which gives a small contribution to the background of the XRD spectrum.

3.1.2 X'Pert scanning diffractometer

X'Pert is a multi-purpose system designed to provide analyses for a number of individual and combined applications. It can contain two vertical goniometers, each equipped for particular applications. The X'Pert system uses a PW3710 diffractomer control unit to control either one or two goniometers depending on the application requirements. The outlook of the X'Pert system is shown in **Fig. 3.1**[69].

XRD measurements of powder samples were performed using the Philips X'Pert scanning diffractometer equipped with a PW3020 vertical goniometer. This goniometer has a 173 mm radius and uses DC-motors instead of conventional stepper motors. θ and 2θ angles are monitored via two optically encoded disks mounted directly on the drive shaft. This allows a minimum 2θ angle increment of 0.0001° to be achieved. The PW3020 vertical goniometer is shown is **Fig. 3.2**[69].

The diffractometer is also equipped with a PW1386/55 automatic divergent slit. This variable divergent slit is mechanically coupled to the θ-axis in order to keep the illuminated sample area at a constant length of 12.5 mm. By using the variable slit, the high-angle intensity loss can be avoided and it allows the diffractometer to work at very low angles without having to put up with high background. The variable divergence slit is a pair of molybdenum rods which are mounted on a drum driven by the θ-axis of the goniometer. As the diffraction angle changes, the angle of view is adjusted. This gives a constant specimen irradiation length. A 0.1 mm receiving slit was used in the XRD measurements in order to have the optimum intensity and resolution[68]. The PW1386/55 automatic divergent slit is shown in **Fig. 3.3**[69]. The geometric arrangement of the powder diffractometer is shown in **Fig. 3.4**[68].

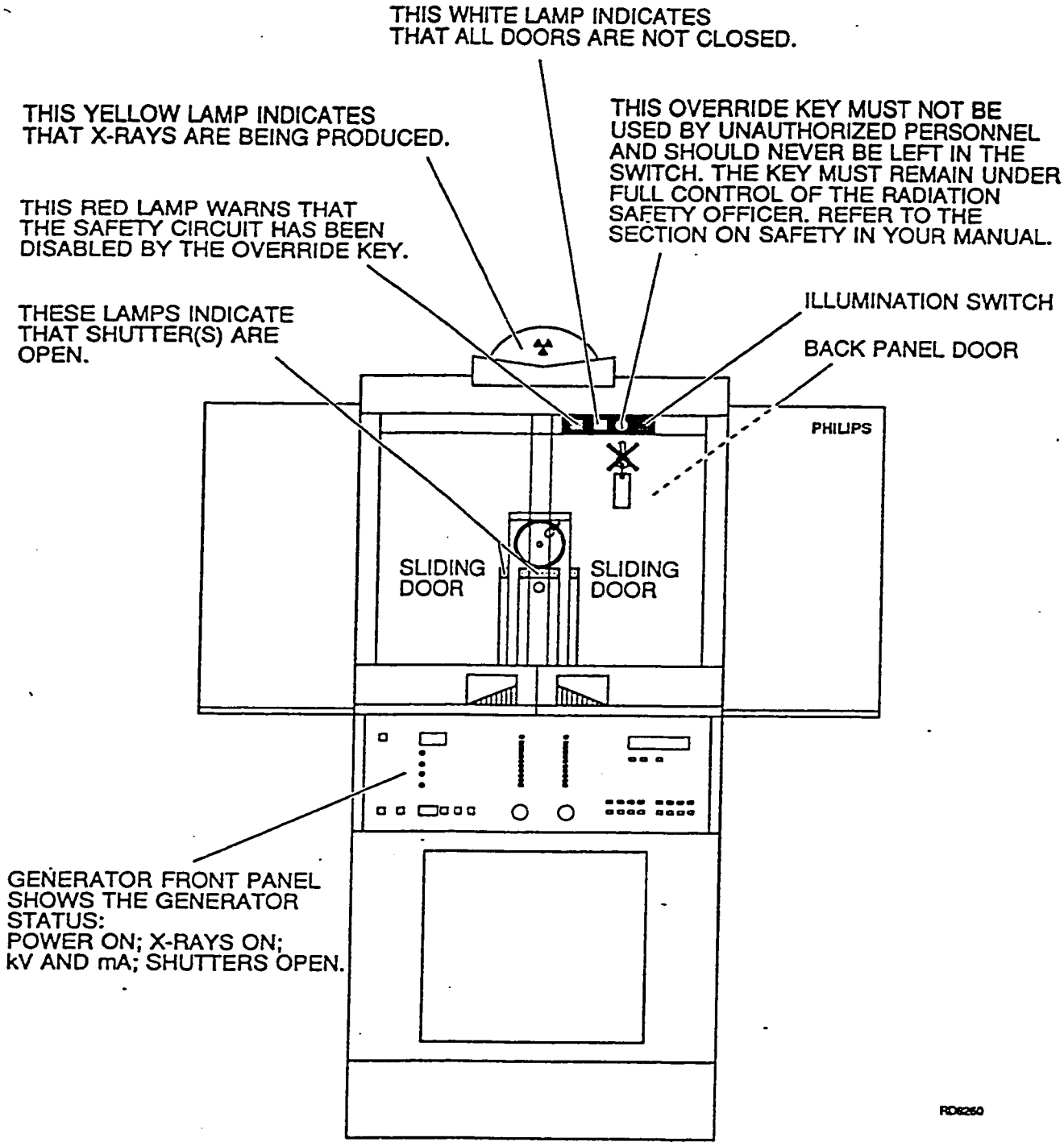

Fig. 3.1. Front view of the X'Pert system[69].

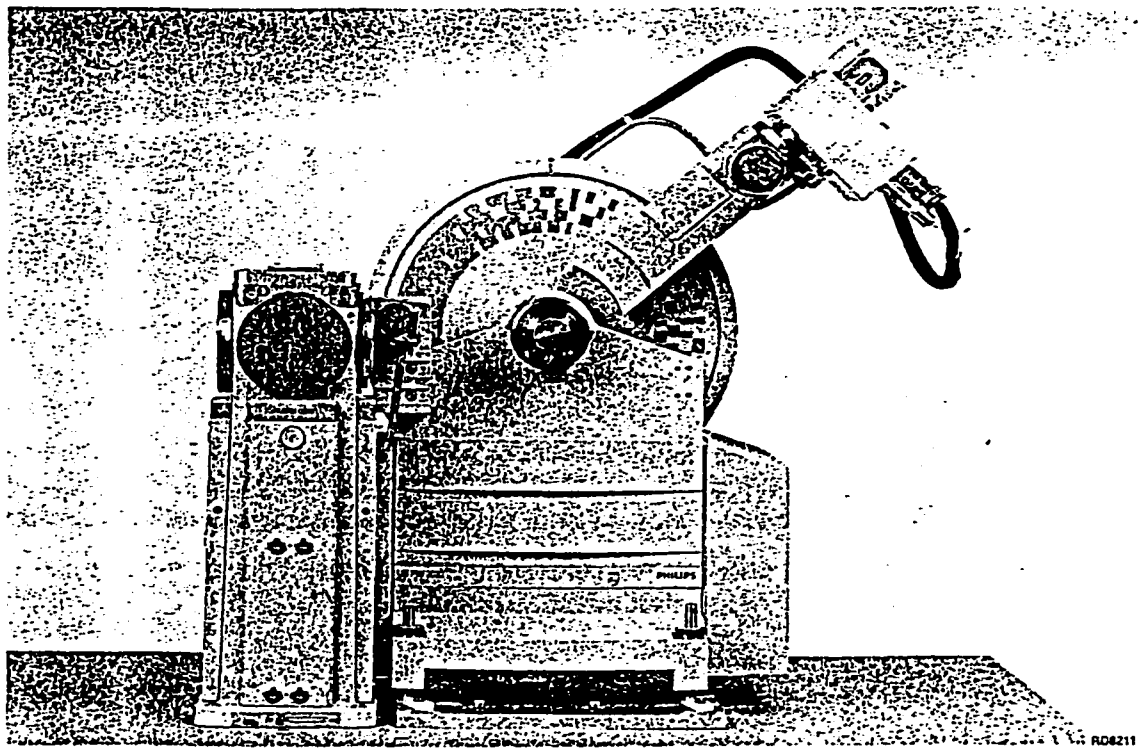

Fig. 3.2. PW3020 vertical goniometer[69].

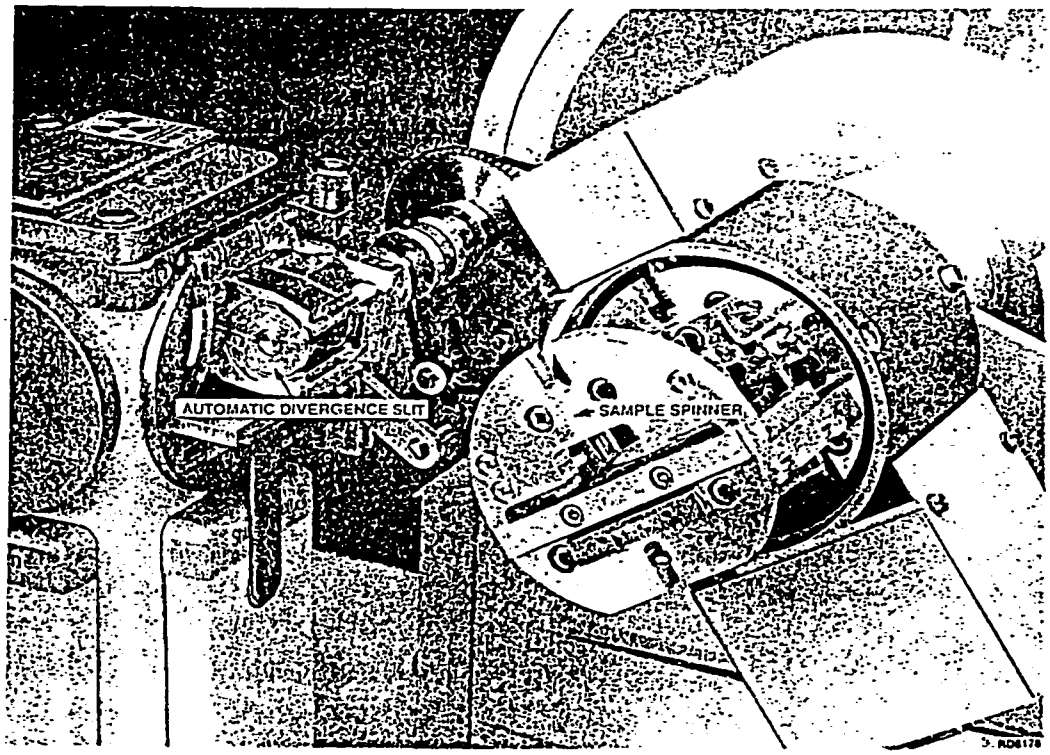

Fig. 3.3. PW1386/55 automatic divergent slit[69].

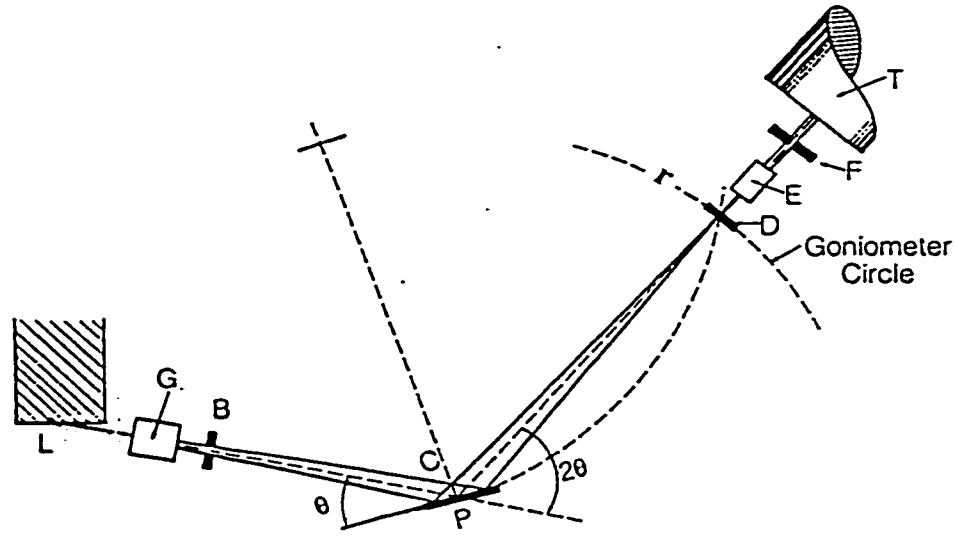

Fig 3.4. Geometric arrangement of the powder diffractometer. **G, E**–parallel plate collimator; **B**–divergence slit; **C**–flat surface of a specimen; **D**–receiving slit; **F**–scatter slit; **T**–radiation detector; **P**–the axis of the specimen; **r**–the radius of the goniometer circle[68].

With these settings, the instrumental resolution was 0.007 $Å^{-1}$. This resolution was determined from the FWHM of the (111) peak of a Si standard. Cu$K\alpha$ radiation was employed and the $K\beta$ line was eliminated by using a Kevex PSi2 Peltier cooled Si detector. A value of 1.5405981 Å was taken for the Cu$K\alpha_1$ wavelength throughout all the calculations[70]. The XRD spectra of garnet samples are shown in **Figs. 3.5** and **3.6**.

3.1.2 2θ correction and data fitting

Two spectra were measured for each sample. The first spectrum was obtained by using a pure sample. The second one was measured for a mixture of the garnet sample and a 10% by weight Si standard reference material 640b[71]. Diffraction peaks of the latter were fitted to a set of Lorentzians[72]. A parabolic background was assumed for each fitted 2θ segment. The results of the fits are given in terms of peak positions, widths, heights and integrated areas.

The 2θ angles were corrected for the possible instrumental aberration and specimen displacement[73]. First, the difference of the peak positions of the Si standard and that of the Si standard mixed with a specimen was calculated, $\Delta(2\theta)_{Si-fit} = 2\theta_{Si-expt} - 2\theta_{Si-std}$. Next, this difference was fitted to a spline function of $2\theta_{expt}$, which is referred to as $\Delta(2\theta)_{Si-fit}$[73]. An example of a spline fit for the sample $Eu_3Fe_{4.5}Al_{0.5}O_{12}$ is shown in **Fig. 3.7**. Compared with the forth-order polynominal fit, the spline fit is more reliable since the fitting curve goes through all the data points. Then, all the peak positions were corrected according to the equation $2\theta_{corr} = 2\theta_{expt} - \Delta(2\theta)_{Si-fit}$.

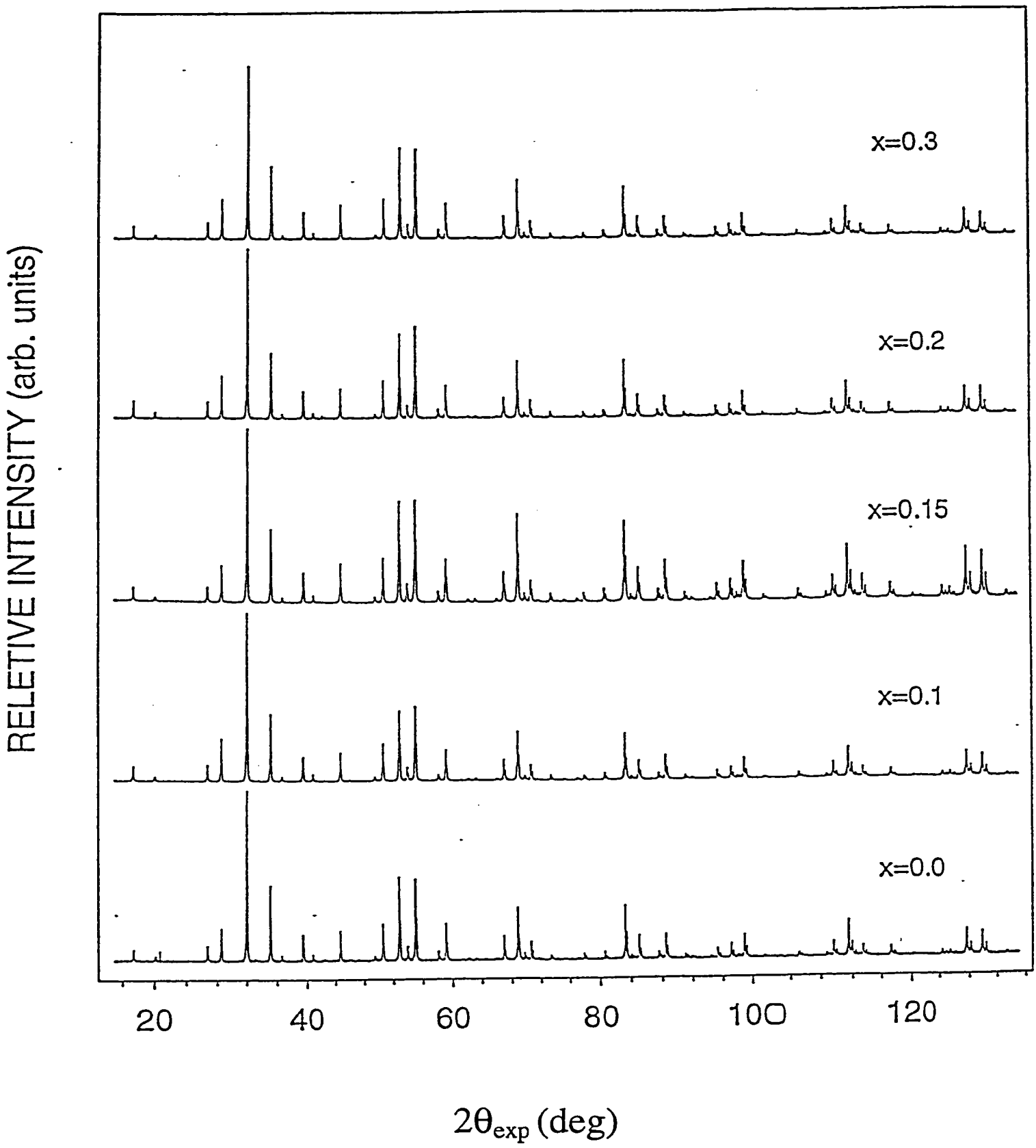

Fig. 3.5. The XRD spectra of $Eu_3Fe_{5-x}Al_xO_{12}$ series with x from 0.0 to 0.3.

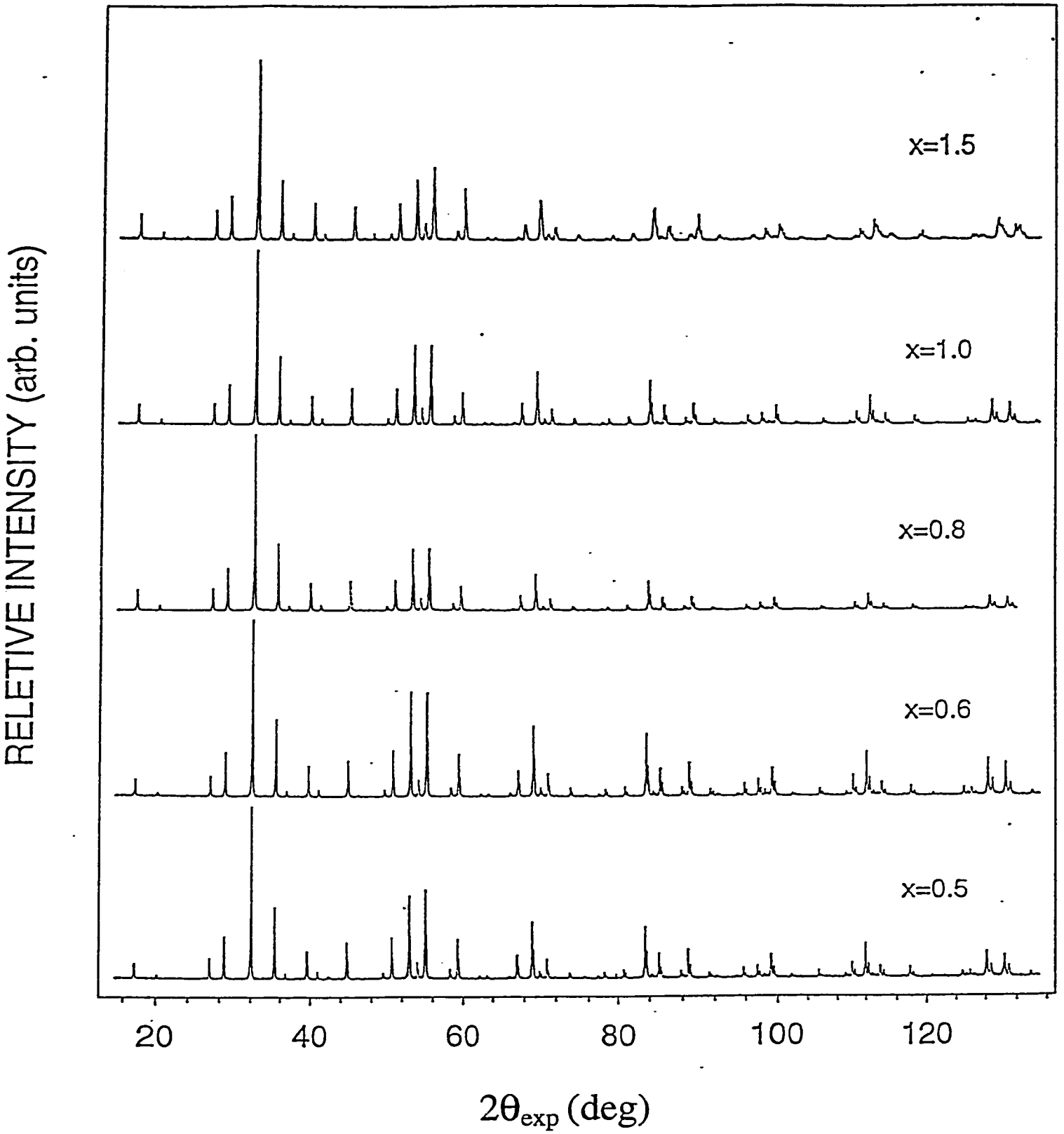

Fig. 3.6. The XRD spectra of $Eu_3Fe_{5-x}Al_xO_{12}$ series with x from 0.5 to 1.5.

Three Fortran programs were used for indexing the XRD spectra: Dicvol 91[74], Lsucri[75] and Treor 90[76]. The extinction rules and the type of the *Bravis* lattice for the $Eu_3Fe_{5-x}Al_xO_{12}$ series, which were described in Chapter 2, were chosen for these programs as the prerequisites. The corrected positions of 30 peaks with the highest intensity were entered into these programs. The results from the Dicvol 91 program were used; the other two programs gave the same results. The output of these indexing programs gives the calculated peak positions, Miller indices and the crystal lattice constant *a*.

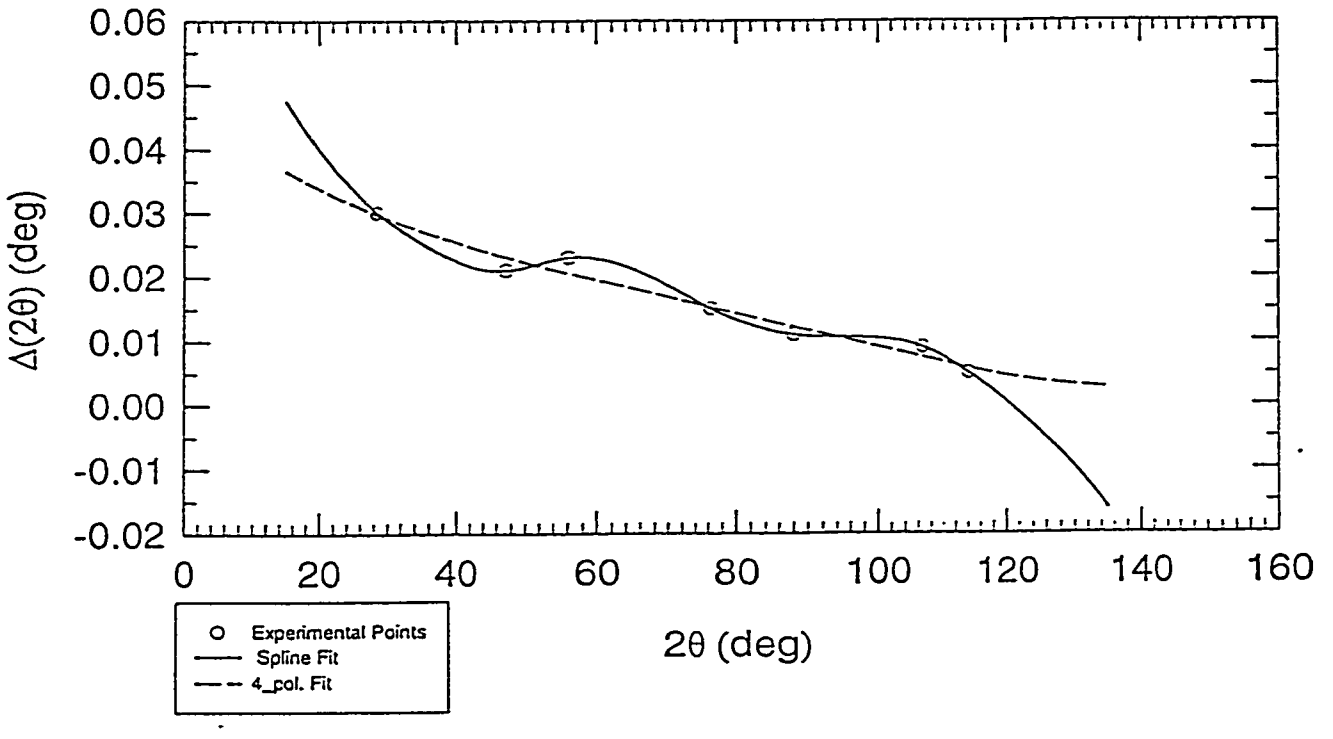

Fig. 3.7. The $\Delta(2\theta)_{Si\text{-}fit}$ calculated from the XRD spectrum of the sample $Eu_3Fe_{4.5}Al_{0.5}O_{12}$ fitted to the forth-order polynomial and the spline functions.

3.1.4 The Rietveld analysis

The Rietveld analysis was applied to the corrected spectra. The diffraction profiles were modeled by using a pseudo-Voigt function. The crystal lattice constant, the space group *Ia3d* and the corresponding site occupancies for each site were entered into the program first. The total site occupancies for the *c*, *a*, *d* and *h* sites are 1/4, 1/6, 1/4 and 1, respectively, and are fixed in the fitting process. They are defined as the ratios of the total coordinates for each particular site and the total coordinates for the free oxygen atom. For the $Eu_3Fe_{5-x}Al_xO_{12}$ series, both Fe^{3+} and Al^{3+} ions occupy the *a* and *d* sites. Therefore, the respective site occupancies of Fe and Al atoms in the *a* or *d* sites were varied. The parameters U, V, W and K were varied[77]. In addition to these non-structural parameters, the positional parameters of oxygen, *x*, *y* and *z*, and isotropic thermal parameters were also varied[78]. The 2θ angle range from 30° to 80° was chosen for the first-step fitting because of the broadened Bragg lines in the high-angle region and less accurate line positions in the low-angle region. Then, the fitting was extended to the full angle range from 15° to 135°. The fitting results gave the refined lattice constants, the site occupancies of the two types of atoms in the *a* and *d* sites, the overall thermal factors, the isotropic thermal factors, the positional parameters of oxgen and U, V, W, K values[78]. Since the total site occupancies and the number of atoms in each site are constant in a garnet chemical formula, the cation distribution in a particular site was derived from the ratios of the site occupancies of each type of atoms and the total site occupancy for this site. For example, the number of iron ions in the *a* site is $n_{Fe} = 2\frac{m_{Fe}}{(1/6)}$, where m_{Fe} is the fitted

Fe^{3+} site occupancy at the *a* site, 2 is the total number of ions at the *a* site for one garnet chemical formula and 1/6 is the total site occupancy of the *a* site.

3.2 Mössbauer spectroscopy

3.2.1 Sample preparation

The thickness of the MS absorber is important due to the following two reasons. First, the measured linewidth will increase as the absorber thickness increases. This will decrease the resolution of a multiple-line spectrum or the precision with which a single line will be located. An increase in absorber thickness also diminishes the transmission of resonant radiation as a result of non-resonant scattering[79]. Second, the absorber must have a finite thickness in order to have the resonance to be observed at all and to collect a spectrum in a reasonable time. For these two reasons, there must be an optimum absorber thickness for transmission geometry.

The optimum absorber thickness was investigated by Long *et al.* based on an evaluation of the electronic and the recoilless nuclear absorption of γ rays[80]. The evaluation leads to the conclusion that the ideal absorber thickness is between $1/\mu_e$ and $2/\mu_e$, where μ_e is the electronic mass absorption coefficient for the Mössbauer γ rays[80].

The absorber thickness was from 15 mg/cm^2 to 30 mg/cm^2 which was calculated based on the optimal thickness evaluation by Long *et al.*[80]. The sample holder was made of pure boron nitride. The absorber holder has the same diameter of 1.2 cm.

3.2.2 MS spectrometer

The MS spectra of the $Eu_3Fe_{5-x}Al_xO_{12}$ series were recorded with a 1024 multichannel analyser using a constant-acceleration electromechanical drive system. The Doppler motion is provided by the electromechanical drive system which is controlled by a servo-amplifier. The amplifier is fed with a reference voltage wave form which repeats itself exactly with a frequency of between about 5 and 40 Hz. The actual drive or transducer embodies two coils, one of which produces a voltage proportional to the actual velocity of the shaft (pick-up coil), and the other one controls the velocity of the shaft (drive coil). The servo-amplifier compares this signal to the reference wave form and applies corrections to the drive coil to minimize any differences. In this way, the center shaft, which is rigidly connected to the MS source, executes an accurate periodic motion. A schematic arrangement for the spectrometer is shown as **Fig. 3.8**[81]. The spectra were obtained between 298 K and 1028 K with the 14.4 keV γ rays from the $^{57}Co(Rh)$ source. The velocity scale was calibrated at room temperature by measuring the spectra of 6.35-μm Fe foil. The accumulated counts per channel were typically about a few millions. For high temperature measurements, the MS spectra were made by using an oven for which the temperature could be monitored and adjusted. The temperature control was achieved to within ±1 K. The oven was connected to a diffusion pump which produced a vacuum in the oven of about 10^{-5} Torr. The oven was water cooled.

Three samples with x = 0.0, 1.0 and 1.5 were measured continually in the temperature range 298–1023 K .

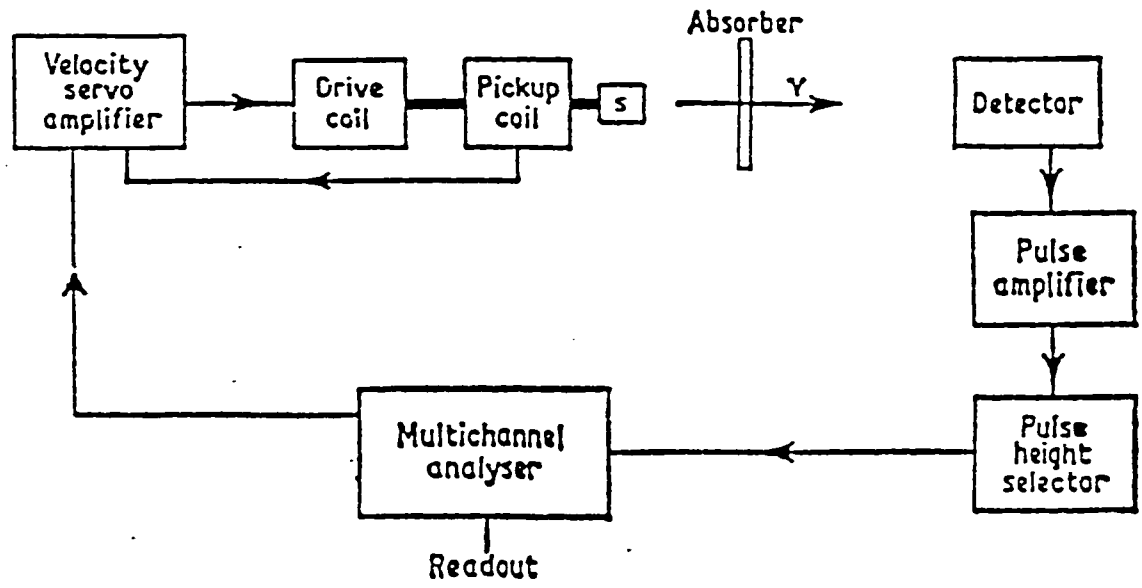

Fig. 3.8. Schematic arrangement for a constant acceleration spectrometer[81].

3.2.3 Fitting program

The MS spectra of the studied samples were fitted by using the computer program Normos 90[82]. The spectra were obtained at temperatures above T_c. Therefore, only the quadrupole splitting doublets from the iron atoms in the *a* and *d* sites were observed. All the spectra were fitted to Lorenzian lines using the usual constraints of equal area and width for the two lines of each doublet. The fitting results gave the background of the spectrum, widths and areas of the fitted doublets, isomer shifts and quadrupole splittings.

Chapter 4

Results and discussion

In the first section of this chapter, the results of the $Eu_3Fe_{5-x}Al_xO_{12}$ series from the XRD pattern indexing and Rietveld analysis are presented and discussed. In the second section, the MS spectra of the studied samples with x = 0.0, 1.0 and 1.5 measured in the high-temperature region are described, the relevant fitted parameters are given and the method of determining the Debye temperature θ_D is discussed.

4.1 Powder X-ray diffraction

4.1.1 XRD spectra

The XRD spectra of the studied samples measured in the 2θ range 15°–135° (**Figs. 3.5** and **3.6**) show the presence of many Bragg lines. The weaker lines are usually not observed in the spectra measured with a scintillation detector. This increased sensitivity for the weak lines is due to the solid-state detector which has a higher counting efficiency (due to the elimination of a monochromator in the diffracted beam) and a lower background counting rate as compared to a conventional scintillation detector.

It should be noticed that the splitting of diffraction peaks for large 2θ values is due to $K\alpha_2$ radiation. The positions of all the detected Bragg lines corresponding to $K\alpha_1$ in terms of the angle 2θ, the lattice constant a and the spacing d, as well as the Miller indices for all observed peaks and their relative intensities (normalized to a maximum of

100.0), were determined from the Fortran programs Ito, Treor 90 and Dicvol 91, as described in Chapter 3. Based on the fitting results, $\Delta(2\theta)$ and $\Delta(d)$ were calculated; $\Delta(2\theta)$ and $\Delta(d)$ are the differences between the observed and calculated values for 2θ and d, respectively. All these parameters for the studied samples are presented in **Tables. 4.1–4.10**.

Every single observed Bragg line can be indexed to the **I**(a) structure. It is noticeable that even the peaks with an intensity as small as 0.4% of the maximum intensity, as shown in **Table 4.8**, could be detected and indexed to the **I**(a) structure. There is an excellent agreement between $2\theta_{obs}$ and $2\theta_{cal}$, as well as between d_{obs} and d_{cal}, as shown in **Tables 4.1–4.10**.

The a values for the 10 studied samples are also in a good agreement with the values reported by Yamaguchi and Sakuraba[65]. The a values are given in **Table 4.11** and **Fig. 4.1**. It can be seen (**Fig. 4.1**) that the a value decreases with the increasing of nominal composition x. This is due to the fact that the larger-size Fe ions were substituted by the smaller-size Al ions in the crystal structure. The size of the a site is not the same as that of the d site. The Al atoms enter the a and d sites randomly. Therefore, the a values do not change linearly with x, as shown in **Fig. 4.1**.

These results lead to the conclusion that the structure of the $Eu_3Fe_{5-x}Al_xO_{12}$ series belongs to the body-centered cubic *Bravis* lattice. The cubic lattice constant a for each sample was used in the Rietveld refinement process as an input parameter.

Table 4.1. The observed and calculated structure parameters for the europium iron garnet $Eu_3Fe_5O_{12}$. $2\theta_{obs}$–position of the observed Bragg lines in degrees, $2\theta_{cal}$–position of the calculated Bragg lines in degrees, $\Delta(2\theta)$–the difference between $2\theta_{obs}$ and $2\theta_{cal}$ in degrees, d_{obs}–the observed spacing distance in Å, d_{cal}–the calculated spacing distance in Å, $\Delta(d)$ –the difference between d_{obs} and d_{cal} in Å, Int–the relative intensity.

h	k	l	$2\theta_{obs}$	$2\theta_{cal}$	$\Delta(2\theta)$	d_{obs}	d_{cal}	Δd	Int
2	1	1	17.404	17.362	0.0418	5.0914	5.1035	-0.0122	5.3
2	2	0	20.134	20.074	0.0599	4.4068	4.4198	-0.0130	2.7
3	2	1	26.682	26.660	0.0223	3.3383	3.3410	-0.0027	7.4
4	0	0	28.557	28.538	0.0189	3.1232	3.1253	-0.0020	20.0
4	2	0	32.007	31.992	0.0152	2.7940	2.7953	-0.0013	100.0
4	2	2	35.153	35.140	0.0131	2.5508	2.5518	-0.0009	41.1
4	3	1	36.633	36.625	0.0084	2.4511	2.4516	-0.0005	3.3
5	2	1	39.459	39.449	0.0096	2.2818	2.2824	-0.0005	14.9
4	4	0	40.809	40.800	0.0093	2.2094	2.2099	-0.0005	3.4
6	1	1	44.653	44.648	0.0048	2.0277	2.0279	-0.0002	18.8
6	3	1	49.412	49.407	0.0053	1.8430	1.8432	-0.0002	2.5
4	4	4	50.536	50.543	-0.0071	1.8046	1.8044	0.0002	24.4
6	4	0	52.753	52.762	-0.0093	1.7339	1.7336	0.0003	53.1
7	2	1	53.842	53.848	-0.0056	1.7013	1.7012	0.0002	9.2
6	4	2	54.908	54.918	-0.0101	1.6708	1.6705	0.0003	54.8
6	5	1	58.041	58.050	-0.0086	1.5878	1.5876	0.0002	4.6
8	0	0	59.058	59.070	-0.0116	1.5629	1.5626	0.0003	23.3
6	5	3	62.052	62.067	-0.0153	1.4945	1.4942	0.0003	1.0
6	6	0	63.039	63.048	-0.0088	1.4734	1.4733	0.0002	1.5
7	5	2	65.936	65.941	-0.0046	1.4155	1.4155	0.0001	1.0
8	4	0	66.880	66.890	-0.0101	1.3978	1.3977	0.0002	14.9
8	4	2	68.762	68.770	-0.0075	1.3641	1.3640	0.0001	35.0
9	2	1	69.682	69.700	-0.0181	1.3483	1.3480	0.0003	3.4
6	6	4	70.616	70.625	-0.0092	1.3328	1.3326	0.0002	12.7
8	5	1	71.540	71.545	-0.0051	1.3178	1.3177	0.0001	1.1
9	3	2	73.372	73.370	0.0016	1.2894	1.2894	0.0000	2.9
8	4	4	74.270	74.277	-0.0065	1.2760	1.2759	0.0001	0.8
9	4	1	75.173	75.179	-0.0055	1.2629	1.2628	0.0001	0.9
10	1	1	76.966	76.972	-0.0057	1.2379	1.2378	0.0001	1.4
10	2	0	77.856	77.863	-0.0073	1.2259	1.2258	0.0001	3.9
10	3	1	80.515	80.521	-0.0062	1.1920	1.1919	0.0001	4.8
10	4	0	83.155	83.159	-0.0037	1.1607	1.1607	0.0000	35.2
9	6	1	84.019	84.034	-0.0154	1.1510	1.1508	0.0002	2.8
10	4	2	84.912	84.909	0.0034	1.1411	1.1412	0.0000	15.6
11	2	1	87.530	87.525	0.0049	1.1136	1.1137	0.0000	3.7
8	8	0	88.393	88.396	-0.0028	1.1050	1.1049	0.0000	15.7
11	3	2	91.006	91.007	-0.0007	1.0799	1.0799	0.0000	2.6
10	6	0	91.880	91.877	0.0029	1.0719	1.0720	0.0000	2.1
9	6	5	94.470	94.492	-0.0220	1.0492	1.0491	0.0002	1.3
12	0	0	95.360	95.365	-0.0054	1.0418	1.0417	0.0000	6.1
12	2	0	97.116	97.116	-0.0002	1.0276	1.0276	0.0000	8.8
10	7	1	98.008	97.994	0.0140	1.0206	1.0207	-0.0001	2.2
12	2	2	98.872	98.874	-0.0017	1.0140	1.0140	0.0000	15.5
11	6	1	101.548	101.526	0.0216	0.9944	0.9945	-0.0002	1.2
9	9	2	105.104	105.104	0.0001	0.9703	0.9703	0.0000	2.8
13	2	1	108.745	108.743	0.0022	0.9477	0.9477	0.0000	1.6

Table 4.1. (*continued*)

h	k	l	$2\theta_{obs}$	$2\theta_{cal}$	$\Delta(2\theta)$	d_{obs}	d_{cal}	Δd	Int
12	4	4	109.668	109.664	0.0037	0.9423	0.9423	0.0000	9.2
12	6	0	111.527	111.524	0.0035	0.9318	0.9318	0.0000	20.8
13	3	2	112.457	112.462	-0.0050	0.9267	0.9266	0.0000	2.2
12	6	2	113.408	113.407	0.0011	0.9216	0.9216	0.0000	7.0
8	8	8	117.266	117.259	0.0073	0.9021	0.9022	0.0000	5.8
14	1	1	120.259	120.237	0.0224	0.8883	0.8884	-0.0001	1.0
14	3	1	124.363	124.355	0.0077	0.8710	0.8710	0.0000	2.5
12	8	0	125.431	125.416	0.0149	0.8667	0.8668	-0.0001	2.4
14	4	0	127.593	127.581	0.0118	0.8585	0.8586	0.0000	14.5
14	4	2	129.825	129.811	0.0138	0.8505	0.8506	0.0000	13.1
14	5	1	133.307	133.300	0.0067	0.8390	0.8390	0.0000	1.4

Table 4.2. The observed and calculated structure parameters for the europium iron garnet $Eu_3Fe_{4.9}Al_{0.1}O_{12}$. $2\theta_{obs}$–position of the observed Bragg lines in degrees. $2\theta_{cal}$–position of the calculated Bragg lines in degrees, $\Delta(2\theta)$–the difference between $2\theta_{obs}$ and $2\theta_{cal}$ in degrees, d_{obs}–the observed spacing distance in Å, d_{cal}–the calculated spacing distance in Å, $\Delta(d)$ –the difference between d_{obs} and d_{cal} in Å, Int–the relative intensity.

h	k	l	$2\theta_{obs}$	$2\theta_{cal}$	$\Delta(2\theta)$	d_{obs}	d_{cal}	Δd	Int
2	1	1	17.345	17.371	-0.0261	5.1085	5.1009	-0.0076	7.2
2	2	0	20.071	20.084	-0.0133	4.4204	4.4175	-0.0029	2.1
3	2	1	26.680	26.674	0.0065	3.3385	3.3393	0.0008	8.9
4	0	0	28.560	28.553	0.0071	3.1229	3.1237	0.0008	22.3
4	2	0	32.021	32.008	0.0126	2.7928	2.7939	0.0011	100.0
4	2	2	35.175	35.158	0.0167	2.5493	2.5505	0.0012	38.5
4	3	1	36.669	36.644	0.0252	2.4488	2.4504	0.0016	2.1
5	2	1	39.492	39.470	0.0218	2.2800	2.2812	0.0012	14.5
4	4	0	40.849	40.821	0.0277	2.2073	2.2088	0.0014	3.8
6	1	1	44.692	44.672	0.0200	2.0260	2.0269	0.0009	17.8
6	2	0	45.902	45.898	0.0042	1.9754	1.9756	0.0002	0.6
6	3	1	49.444	49.433	0.0106	1.8419	1.8422	0.0004	2.5
4	4	4	50.578	50.570	0.0075	1.8032	1.8035	0.0003	23.4
6	4	0	52.793	52.791	0.0019	1.7326	1.7327	0.0001	47.0
7	2	1	53.879	53.877	0.0019	1.7003	1.7003	0.0001	8.3
6	4	2	54.946	54.948	-0.0022	1.6697	1.6697	-0.0001	48.0
6	5	1	58.081	58.082	-0.0008	1.5868	1.5868	0.0000	3.8
8	0	0	59.095	59.102	-0.0074	1.5620	1.5618	-0.0002	19.9
8	1	1	60.135	60.112	0.0227	1.5375	1.5380	0.0005	0.2
8	2	0	61.086	61.112	-0.0260	1.5158	1.5152	-0.0006	0.2
6	5	3	62.090	62.102	-0.0122	1.4937	1.4934	-0.0003	1.2
6	6	0	63.065	63.083	-0.0184	1.4729	1.4725	-0.0004	1.4
8	3	1	64.047	64.056	-0.0092	1.4527	1.4525	-0.0002	0.3
7	5	2	65.962	65.978	-0.0162	1.4151	1.4147	-0.0003	1.3
8	4	0	66.918	66.928	-0.0104	1.3971	1.3969	-0.0002	13.4
8	4	2	68.799	68.809	-0.0102	1.3635	1.3633	-0.0002	32.9
9	2	1	69.728	69.741	-0.0126	1.3475	1.3473	-0.0002	3.0
6	6	4	70.656	70.666	-0.0103	1.3321	1.3319	-0.0002	10.2
8	5	1	71.570	71.587	-0.0169	1.3173	1.3171	-0.0003	0.4
9	3	2	73.408	73.414	-0.0057	1.2888	1.2887	-0.0001	3.1
9	4	1	75.202	75.223	-0.0212	1.2625	1.2622	-0.0003	0.8
10	2	0	77.915	77.910	0.0048	1.2251	1.2252	0.0001	3.4
10	3	1	80.573	80.570	0.0026	1.1913	1.1913	0.0000	4.4
10	4	0	83.215	83.210	0.0048	1.1600	1.1601	0.0001	29.9
9	6	1	84.084	84.087	-0.0027	1.1503	1.1502	0.0000	2.1
10	4	2	84.966	84.962	0.0043	1.1406	1.1406	0.0000	12.8
11	2	1	87.590	87.581	0.0093	1.1130	1.1131	0.0001	4.0
8	8	0	88.459	88.452	0.0067	1.1043	1.1044	0.0001	15.7
11	3	2	91.078	91.066	0.0122	1.0793	1.0794	0.0001	2.3
10	6	0	91.941	91.937	0.0039	1.0714	1.0714	0.0000	1.2
9	6	5	94.568	94.555	0.0132	1.0484	1.0485	0.0001	0.8
12	0	0	95.435	95.429	0.0058	1.0412	1.0412	0.0000	5.3
12	1	1	96.323	96.305	0.0182	1.0339	1.0341	0.0001	0.7
12	2	0	97.194	97.182	0.0120	1.0270	1.0271	0.0001	7.3
10	7	1	98.080	98.061	0.0192	1.0200	1.0202	0.0001	2.1
12	2	2	98.952	98.942	0.0104	1.0134	1.0135	0.0001	12.7

Table 4.2. (*continued*)

h	k	l	$2\theta_{obs}$	$2\theta_{cal}$	$\Delta(2\theta)$	d_{obs}	d_{cal}	Δd	Int
11	6	1	101.609	101.598	0.0115	0.9939	0.9940	0.0001	1.0
12	4	0	102.510	102.488	0.0218	0.9876	0.9878	0.0002	0.2
9	9	2	105.191	105.180	0.0113	0.9697	0.9698	0.0001	3.0
10	8	2	106.084	106.084	-0.0003	0.9640	0.9640	0.0000	0.5
13	2	1	108.832	108.824	0.0082	0.9472	0.9472	0.0000	1.7
12	4	4	109.749	109.747	0.0023	0.9418	0.9418	0.0000	8.5
12	6	0	111.611	111.609	0.0021	0.9313	0.9313	0.0000	18.2
13	3	2	112.552	112.549	0.0031	0.9262	0.9262	0.0000	2.0
12	6	2	113.497	113.495	0.0017	0.9211	0.9211	0.0000	6.2
10	9	3	116.396	116.378	0.0185	0.9064	0.9065	0.0001	0.5
8	8	8	117.345	117.354	-0.0090	0.9018	0.9017	0.0000	5.0
14	1	1	120.340	120.338	0.0023	0.8879	0.8880	0.0000	1.0
14	2	0	121.355	121.352	0.0027	0.8835	0.8835	0.0000	0.7
14	3	1	124.450	124.465	-0.0153	0.8706	0.8705	-0.0001	2.5
12	8	0	125.503	125.529	-0.0257	0.8664	0.8663	-0.0001	3.0
14	4	0	127.674	127.699	-0.0252	0.8582	0.8581	-0.0001	14.4
14	3	3	128.787	128.808	-0.0215	0.8542	0.8541	-0.0001	0.7
14	4	2	129.904	129.935	-0.0313	0.8503	0.8502	-0.0001	13.3
14	5	1	133.417	133.435	-0.0180	0.8386	0.8386	-0.0001	1.3
12	8	4	134.631	134.647	-0.0158	0.8349	0.8348	0.0000	1.0

Table 4.3. The observed and calculated structure parameters for the europium iron garnet $Eu_3Fe_{4.85}Al_{0.15}O_{12}$. $2\theta_{obs}$–position of the observed Bragg lines in degrees, $2\theta_{cal}$–position of the calculated Bragg lines in degrees, $\Delta(2\theta)$–the difference between $2\theta_{obs}$ and $2\theta_{cal}$ in degrees, d_{obs}–the observed spacing distance in Å, d_{cal}–the calculated spacing distance in Å, $\Delta(d)$ –the difference between d_{obs} and d_{cal} in Å, Int–the relative intensity.

h	k	l	$2\theta_{obs}$	$2\theta_{cal}$	$\Delta(2\theta)$	d_{obs}	d_{cal}	Δd	Int
2	1	1	17.360	17.377	-0.0167	5.1042	5.0993	0.0049	6.8
2	2	0	20.084	20.091	-0.0068	4.4176	4.4161	0.0015	2.1
3	2	1	26.666	26.682	-0.0162	3.3403	3.3383	0.0020	8.6
4	0	0	28.545	28.562	-0.0172	3.1245	3.1227	0.0018	20.4
4	2	0	32.005	32.019	-0.0138	2.7942	2.7930	0.0012	100
4	2	2	35.153	35.170	-0.0168	2.5508	2.5497	0.0012	41.9
4	3	1	36.645	36.657	-0.0115	2.4503	2.4496	0.0007	3.0
5	2	1	39.470	39.483	-0.0133	2.2812	2.2805	0.0007	18.4
4	4	0	44.675	44.687	-0.0120	2.0268	2.0263	0.0005	22.1
6	2	0	45.893	45.913	-0.0203	1.9758	1.9750	0.0008	0.6
6	3	1	49.444	49.450	-0.0062	1.8419	1.8417	0.0002	3.3
4	4	4	50.576	50.588	-0.0118	1.8033	1.8029	0.0004	26.4
6	4	0	52.801	52.809	-0.0083	1.7324	1.7321	0.0003	61.7
7	2	1	53.884	53.896	-0.0117	1.7001	1.6998	0.0003	11.2
6	4	2	54.960	54.967	-0.0072	1.6693	1.6691	0.0002	62.3
6	5	1	58.092	58.102	-0.0101	1.5866	1.5863	0.0003	6.9
8	0	0	59.123	59.123	-0.0002	1.5613	1.5613	0.0000	27.1
6	5	3	62.111	62.124	-0.0132	1.4932	1.4929	0.0003	2.0
6	6	0	63.098	63.106	-0.0079	1.4722	1.4720	0.0002	2.0
7	5	2	65.999	66.002	-0.0030	1.4143	1.4143	0.0001	1.6
8	4	0	66.945	66.953	-0.0076	1.3966	1.3965	0.0001	19.8
8	4	2	68.826	68.834	-0.0082	1.3630	1.3628	0.0001	54.0
9	2	1	69.753	69.766	-0.0130	1.3471	1.3469	0.0002	5.4
6	6	4	70.686	70.692	-0.0062	1.3316	1.3315	0.0001	13.1
8	5	1	71.609	71.613	-0.0043	1.3167	1.3166	0.0001	1.1
9	3	2	73.433	73.441	-0.0079	1.2884	1.2883	0.0001	5.3
9	4	1	75.244	75.251	-0.0074	1.2619	1.2618	0.0001	1.6
10	1	1	77.042	77.047	-0.0049	1.2368	1.2368	0.0001	2.2
10	2	0	77.940	77.940	0.0003	1.2248	1.2248	0.0000	5.6
10	3	1	80.611	80.601	0.0096	1.1908	1.1909	-0.0001	8.2
10	4	0	83.255	83.243	0.0123	1.1596	1.1597	-0.0001	52.7
9	6	1	84.128	84.120	0.0084	1.1498	1.1499	-0.0001	3.6
10	4	2	85.004	84.995	0.0088	1.1401	1.1402	-0.0001	21.1
11	2	1	87.633	87.616	0.0173	1.1126	1.1128	-0.0002	8.1
8	8	0	88.507	88.488	0.0191	1.1038	1.1040	-0.0002	26.4
11	3	2	91.114	91.103	0.0110	1.0789	1.0790	-0.0001	5.4
10	6	0	91.981	91.975	0.0061	1.0710	1.0711	-0.0001	2.5
9	6	5	94.597	94.594	0.0027	1.0482	1.0482	-0.0000	1.7
12	0	0	95.478	95.469	0.0087	1.0408	1.0409	-0.0001	11.0
12	2	0	97.230	97.223	0.0066	1.0267	1.0267	-0.0001	13.4
10	7	1	98.107	98.103	0.0041	1.0198	1.0199	0.0000	4.8
12	2	2	98.987	98.984	0.0027	1.0131	1.0131	0.0000	25.4
11	6	1	101.646	101.642	0.0037	9.9368	9.9371	0.0000	2.9
9	9	2	105.233	105.228	0.0055	9.6943	9.6947	0.0000	6.1
10	8	2	106.137	106.133	0.0042	9.6365	9.6368	0.0000	1.1

Table 4.3. (*continued*)

h	k	l	$2\theta_{obs}$	$2\theta_{cal}$	$\Delta(2\theta)$	d_{obs}	d_{cal}	Δd	Int
13	2	1	108.892	108.875	0.0171	9.4682	9.4692	-0.0001	3.7
12	4	4	109.812	109.799	0.0134	9.4144	9.4152	-0.0001	14.5
12	6	0	111.668	111.663	0.0052	9.3097	9.3100	0.0000	31.8
13	3	2	112.607	112.604	0.0038	9.2585	9.2587	0.0000	4.3
12	6	2	113.559	113.551	0.0077	9.2079	9.2083	0.0000	14.6
10	9	3	116.481	116.436	0.0448	9.0595	9.0617	-0.0002	0.8
8	8	8	117.412	117.414	-0.0023	9.0145	9.0144	0.0000	8.8
14	1	1	120.394	120.401	-0.0074	8.8771	8.8767	0.0000	1.9
14	2	0	121.409	121.417	-0.0079	8.8326	8.8323	0.0000	1.5
14	3	1	124.535	124.535	-0.0000	8.7027	8.7027	0.0000	6.2
12	8	0	125.601	125.596	0.0054	8.6607	8.6609	0.0000	5.6
14	4	0	127.771	127.774	-0.0028	8.5787	8.5786	0.0000	28.9
14	3	3	128.913	128.885	0.0284	8.5374	8.5385	-0.0001	1.7
14	4	2	133.510	133.520	-0.0104	8.3835	8.3832	0.0000	3.0

Table 4.4. The observed and calculated structure parameters for the europium iron garnet $Eu_3Fe_{4.8}Al_{0.2}O_{12}$. $2\theta_{obs}$–position of the observed Bragg lines in degrees, $2\theta_{cal}$–position of the calculated Bragg lines in degrees, $\Delta(2\theta)$–the difference between $2\theta_{obs}$ and $2\theta_{cal}$ in degrees, d_{obs}–the observed spacing distance in Å, d_{cal}–the calculated spacing distance in Å, $\Delta(d)$ –the difference between d_{obs} and d_{cal} in Å. Int–the relative intensity.

h	k	l	$2\theta_{obs}$	$2\theta_{cal}$	$\Delta(2\theta)$	d_{obs}	d_{cal}	Δd	Int
2	1	1	17.377	17.378	-0.0012	5.0992	5.0989	0.0003	8.5
2	2	0	20.098	20.093	0.0054	4.4146	4.4157	-0.0012	2.5
3	2	1	26.683	26.685	-0.0016	3.3382	3.3380	0.0002	9.0
4	0	0	28.559	28.565	-0.0058	3.1230	3.1224	0.0006	22.2
4	2	0	32.018	32.022	-0.0038	2.7931	2.7928	0.0003	100.0
4	2	2	35.169	35.173	-0.0041	2.5497	2.5494	0.0003	40.7
4	3	1	36.659	36.659	-0.0003	2.4494	2.4494	0.0000	2.7
5	2	1	39.485	39.487	-0.0019	2.2804	2.2803	0.0001	15.7
4	4	0	40.830	40.839	-0.0086	2.2083	2.2079	0.0004	3.1
6	1	1	44.686	44.691	-0.0051	2.0263	2.0261	0.0002	19.4
6	3	1	49.449	49.455	-0.0059	1.8417	1.8415	0.0002	2.6
4	4	4	50.589	50.593	-0.0035	1.8028	1.8027	0.0001	23.5
6	4	0	52.813	52.814	-0.0013	1.7320	1.7320	0.0000	55.2
7	2	1	53.899	53.901	-0.0018	1.6997	1.6996	0.0001	8.0
6	4	2	54.973	54.973	0.0005	1.6690	1.6690	0.0000	56.8
6	5	1	58.112	58.108	0.0043	1.5861	1.5862	-0.0001	5.1
8	0	0	59.129	59.129	0.0001	1.5612	1.5612	0.0000	21.3
6	5	3	62.128	62.130	-0.0023	1.4928	1.4928	0.0000	1.2
6	6	0	63.107	63.112	-0.0050	1.4720	1.4719	0.0001	1.6
7	5	2	66.003	66.009	-0.0055	1.4143	1.4142	0.0001	1.3
8	4	0	66.956	66.959	-0.0032	1.3964	1.3964	0.0001	13.2
8	4	2	68.837	68.841	-0.0041	1.3628	1.3627	0.0001	36.1
9	2	1	69.774	69.773	0.0010	1.3468	1.3468	0.0000	3.2
6	6	4	70.695	70.699	-0.0044	1.3315	1.3314	0.0001	11.5
9	3	2	73.441	73.448	-0.0074	1.2883	1.2882	0.0001	3.4
9	4	1	75.249	75.259	-0.0101	1.2618	1.2616	0.0001	0.6
10	1	1	77.054	77.055	-0.0009	1.2367	1.2367	0.0000	1.4
10	2	0	77.940	77.948	-0.0079	1.2248	1.2247	0.0001	3.2
10	3	1	80.606	80.610	-0.0039	1.1909	1.1908	0.0000	5.1
10	4	0	83.248	83.252	-0.0036	1.1597	1.1596	0.0000	34.8
9	6	1	84.109	84.129	-0.0197	1.1500	1.1498	0.0002	1.9
10	4	2	85.003	85.004	-0.0014	1.1402	1.1401	0.0000	13.8
11	2	1	87.626	87.625	0.0006	1.1127	1.1127	0.0000	4.0
8	8	0	88.498	88.498	0.0003	1.1039	1.1039	0.0000	13.0
11	3	2	91.109	91.113	-0.0043	1.0790	1.0789	0.0000	2.8
10	6	0	91.977	91.985	-0.0084	1.0710	1.0710	0.0001	1.6
9	6	5	94.595	94.605	-0.0103	1.0482	1.0481	0.0001	0.9
12	0	0	95.482	95.480	0.0016	1.0408	1.0408	0.0000	6.1
12	2	0	97.235	97.235	0.0002	1.0266	1.0266	0.0000	7.5
10	7	1	98.120	98.115	0.0055	1.0197	1.0198	0.0000	2.6
12	2	2	98.996	98.996	-0.0001	1.0130	1.0130	0.0000	14.8
11	6	1	101.658	101.655	0.0033	0.9936	0.9936	0.0000	1.6
9	9	2	105.241	105.241	0.0003	0.9694	0.9694	0.0000	3.2
13	2	1	108.881	108.889	-0.0080	0.9469	0.9468	0.0000	1.5
12	4	4	109.814	109.813	0.0010	0.9414	0.9414	0.0000	8.8
12	6	0	111.677	111.678	-0.0005	0.9309	0.9309	0.0000	19.4

Table 4.4. (*continued*)

h	k	l	$2\theta_{obs}$	$2\theta_{cal}$	$\Delta(2\theta)$	d_{obs}	d_{cal}	Δd	Int
13	3	2	112.609	112.619	-0.0097	0.9258	0.9258	0.0001	2.1
12	6	2	113.568	113.567	0.0015	0.9207	0.9207	0.0000	7.0
8	8	8	117.429	117.431	-0.0016	0.9014	0.9014	0.0000	6.2
14	1	1	120.410	120.419	-0.0090	0.8876	0.8876	0.0000	1.1
14	2	0	121.434	121.435	-0.0013	0.8832	0.8831	0.0000	0.7
14	3	1	124.566	124.554	0.0121	0.8701	0.8702	0.0000	3.2
12	8	0	125.640	125.619	0.0207	0.8659	0.8660	-0.0001	2.7
14	4	0	127.813	127.794	0.0188	0.8577	0.8578	-0.0001	16.2
14	4	2	130.057	130.035	0.0218	0.8497	0.8498	-0.0001	14.8
14	5	1	133.581	133.543	0.0376	0.8381	0.8382	-0.0001	1.5

Table 4.5. The observed and calculated structure parameters for the europium iron garnet $Eu_3Fe_{4.7}Al_{0.3}O_{12}$. $2\theta_{obs}$–position of the observed Bragg lines in degrees, $2\theta_{cal}$–position of the calculated Bragg lines in degrees, $\Delta(2\theta)$–the difference between $2\theta_{obs}$ and $2\theta_{cal}$ in degrees, d_{obs}–the observed spacing distance in Å, d_{cal}–the calculated spacing distance in Å, $\Delta(d)$ –the difference between d_{obs} and d_{cal} in Å, Int–the relative intensity.

h	k	l	$2\theta_{obs}$	$2\theta_{cal}$	$\Delta(2\theta)$	d_{obs}	d_{cal}	Δd	Int
2	1	1	17.430	17.388	0.0420	5.0838	5.0960	-0.0122	7.0
2	2	0	20.145	20.104	0.0411	4.4044	4.4133	-0.0089	2.4
3	2	1	26.716	26.700	0.0163	3.3341	3.3361	-0.0020	10.0
4	0	0	28.596	28.581	0.0150	3.1191	3.1207	-0.0016	25.7
4	2	0	32.050	32.040	0.0099	2.7904	2.7912	-0.0008	100.0
4	2	2	35.201	35.193	0.0077	2.5475	2.5480	-0.0005	46.1
4	3	1	36.686	36.680	0.0056	2.4477	2.4480	-0.0004	2.5
5	2	1	39.514	39.510	0.0042	2.2788	2.2790	-0.0002	19.2
4	4	0	40.871	40.862	0.0086	2.2062	2.2066	-0.0004	4.3
6	1	1	44.719	44.717	0.0016	2.0249	2.0250	-0.0001	20.5
6	2	0	45.966	45.945	0.0214	1.9728	1.9737	-0.0009	0.7
6	3	1	49.485	49.484	0.0008	1.8404	1.8405	-0.0000	2.9
4	4	4	50.626	50.623	0.0033	1.8016	1.8017	-0.0001	28.1
6	4	0	52.849	52.846	0.0031	1.7309	1.7310	-0.0001	61.1
7	2	1	53.938	53.933	0.0048	1.6985	1.6987	-0.0001	10.2
6	4	2	55.009	55.006	0.0034	1.6680	1.6681	-0.0001	62.7
6	5	1	58.152	58.143	0.0089	1.5851	1.5853	-0.0002	5.8
8	0	0	59.171	59.165	0.0059	1.5602	1.5603	-0.0001	25.3
6	5	3	62.175	62.169	0.0063	1.4918	1.4920	-0.0001	1.5
6	6	0	63.151	63.151	-0.0002	1.4711	1.4711	0.0000	1.4
7	5	2	66.050	66.050	0.0001	1.4134	1.4134	0.0000	1.1
8	4	0	67.004	67.001	0.0026	1.3956	1.3956	0.0000	16.4
8	4	2	68.887	68.885	0.0022	1.3619	1.3620	0.0000	40.5
9	2	1	69.819	69.818	0.0015	1.3460	1.3460	0.0000	4.2
6	6	4	70.747	70.745	0.0024	1.3306	1.3307	0.0000	13.0
8	5	1	71.680	71.667	0.0135	1.3156	1.3158	-0.0002	0.8
9	3	2	73.498	73.496	0.0020	1.2875	1.2875	0.0000	3.6
9	4	1	75.309	75.308	0.0007	1.2609	1.2609	0.0000	1.2
10	1	1	77.098	77.106	-0.0077	1.2361	1.2360	0.0001	1.3
10	2	0	77.994	78.000	-0.0055	1.2241	1.2240	0.0001	3.7
10	3	1	80.667	80.664	0.0030	1.1901	1.1902	0.0000	5.2
10	4	0	83.311	83.308	0.0027	1.1590	1.1590	0.0000	35.6
9	6	1	84.187	84.186	0.0007	1.1491	1.1491	0.0000	2.5
10	4	2	85.065	85.063	0.0021	1.1395	1.1395	0.0000	16.0
11	2	1	87.691	87.687	0.0044	1.1120	1.1120	0.0000	4.8
8	8	0	88.561	88.560	0.0012	1.1033	1.1033	0.0000	15.2
11	3	2	91.185	91.178	0.0067	1.0783	1.0783	0.0001	2.8
10	6	0	92.052	92.051	0.0006	1.0704	1.0704	0.0000	1.8
9	6	5	94.675	94.674	0.0006	1.0475	1.0475	0.0000	1.1
12	0	0	95.553	95.551	0.0024	1.0402	1.0402	0.0000	6.5
12	2	0	97.306	97.307	-0.0012	1.0261	1.0261	0.0000	8.8
10	7	1	98.191	98.188	0.0030	1.0192	1.0192	0.0000	2.9
12	2	2	99.071	99.071	0.0002	1.0125	1.0125	0.0000	16.0
11	6	1	101.728	101.733	-0.0050	0.9931	0.9931	0.0000	1.7
9	9	2	105.321	105.324	-0.0032	0.9689	0.9688	0.0000	3.7
10	8	2	106.223	106.231	-0.0081	0.9631	0.9631	0.0001	1.0

Table 4.5. (*continued*)

h	k	l	$2\theta_{obs}$	$2\theta_{cal}$	$\Delta(2\theta)$	d_{obs}	d_{cal}	Δd	Int
13	2	1	108.983	108.978	0.0047	0.9463	0.9463	0.0000	2.0
12	4	4	109.902	109.904	-0.0018	0.9409	0.9409	0.0000	9.5
12	6	0	111.766	111.772	-0.0055	0.9304	0.9304	0.0000	19.7
13	3	2	112.710	112.714	-0.0044	0.9253	0.9253	0.0000	2.3
12	6	2	113.655	113.664	-0.0089	0.9203	0.9202	0.0000	6.8
8	8	8	117.531	117.536	-0.0046	0.9009	0.9009	0.0000	5.9
14	1	1	120.511	120.531	-0.0195	0.8872	0.8871	0.0001	1.0
14	2	0	121.541	121.549	-0.0081	0.8827	0.8827	0.0000	0.8
14	3	1	124.663	124.675	-0.0124	0.8698	0.8697	0.0000	3.3
12	8	0	125.725	125.744	-0.0186	0.8656	0.8655	0.0001	2.8
14	4	0	127.909	127.925	-0.0155	0.8574	0.8573	0.0001	16.2
14	3	3	129.083	129.039	0.0436	0.8531	0.8533	-0.0002	0.8
14	4	2	130.159	130.172	-0.0132	0.8494	0.8493	0.0000	13.8
14	5	1	133.662	133.692	-0.0302	0.8379	0.8378	0.0001	1.9

Table 4.6. The observed and calculated structure parameters for the europium iron garnet $Eu_3Fe_{4.5}Al_{0.5}O_{12}$. $2\theta_{obs}$–position of the observed Bragg lines in degrees, $2\theta_{cal}$–position of the calculated Bragg lines in degrees, $\Delta(2\theta)$–the difference between $2\theta_{obs}$ and $2\theta_{cal}$ in degrees, d_{obs}–the observed spacing distance in Å, d_{cal}–the calculated spacing distance in Å, $\Delta(d)$ –the difference between d_{obs} and d_{cal} in Å, Int–the relative intensity.

h	k	l	$2\theta_{obs}$	$2\theta_{cal}$	$\Delta(2\theta)$	d_{obs}	d_{cal}	Δd	Int
2	1	1	17.376	17.402	-0.0263	5.0995	5.0919	0.0076	8.1
2	2	0	20.104	20.121	-0.0165	4.4133	4.4097	0.0036	2.1
3	2	1	26.702	26.722	-0.0199	3.3358	3.3334	0.0024	10.5
4	0	0	28.591	28.605	-0.0138	3.1196	3.1181	0.0015	23.5
4	2	0	32.057	32.067	-0.0100	2.7898	2.7889	0.0008	100.0
3	3	2	33.669	33.678	-0.0086	2.6598	2.6591	0.0007	0.9
4	2	2	35.215	35.223	-0.0080	2.5465	2.5459	0.0006	41.6
4	3	1	36.698	36.711	-0.0134	2.4469	2.4461	0.0009	3.8
5	2	1	39.534	39.543	-0.0094	2.2777	2.2772	0.0005	16.7
4	4	0	40.899	40.897	0.0018	2.2047	2.2048	-0.0001	3.7
6	1	1	44.755	44.756	-0.0009	2.0233	2.0233	0.0000	22.3
6	2	0	45.987	45.984	0.0028	1.9720	1.9721	-0.0001	0.2
6	3	1	49.529	49.527	0.0016	1.8389	1.8390	-0.0001	2.7
4	4	4	50.659	50.667	-0.0079	1.8005	1.8002	0.0003	24.2
6	4	0	52.886	52.893	-0.0065	1.7298	1.7296	0.0002	52.3
7	2	1	53.978	53.981	-0.0028	1.6974	1.6973	0.0001	8.7
6	4	2	55.049	55.054	-0.0054	1.6669	1.6667	0.0002	53.3
6	5	1	58.191	58.195	-0.0042	1.5841	1.5840	0.0001	5.0
8	0	0	59.215	59.218	-0.0032	1.5591	1.5591	0.0001	22.4
6	5	3	62.215	62.225	-0.0101	1.4910	1.4907	0.0002	1.2
6	6	0	63.216	63.209	0.0072	1.4697	1.4698	-0.0002	1.7
7	5	2	66.105	66.111	-0.0058	1.4123	1.4122	0.0001	1.4
8	4	0	67.056	67.063	-0.0074	1.3946	1.3945	0.0001	14.4
8	4	2	68.944	68.949	-0.0050	1.3609	1.3609	0.0001	34.9
9	2	1	69.879	69.883	-0.0038	1.3450	1.3449	0.0001	4.1
6	6	4	70.809	70.811	-0.0021	1.3296	1.3296	0.0000	10.2
9	3	2	73.573	73.566	0.0071	1.2863	1.2864	-0.0001	3.3
9	4	1	75.381	75.381	0.0004	1.2599	1.2599	0.0000	1.0
10	1	1	77.186	77.180	0.0057	1.2349	1.2350	-0.0001	1.6
10	2	0	78.074	78.075	-0.0013	1.2230	1.2230	0.0000	3.4
10	3	1	80.749	80.744	0.0055	1.1891	1.1892	-0.0001	5.5
10	4	0	83.395	83.392	0.0034	1.1580	1.1580	0.0000	30.5
9	6	1	84.265	84.271	-0.0059	1.1482	1.1482	0.0001	2.0
10	4	2	85.149	85.149	0.0002	1.1386	1.1386	0.0000	13.3
11	2	1	87.782	87.777	0.0055	1.1111	1.1111	-0.0001	3.9
8	8	0	88.653	88.651	0.0019	1.1024	1.1024	0.0000	14.9
11	3	2	91.280	91.274	0.0061	1.0774	1.0775	-0.0001	2.9
10	6	0	92.150	92.149	0.0015	1.0695	1.0695	0.0000	1.4
9	6	5	94.767	94.776	-0.0090	1.0467	1.0467	0.0001	1.0
12	0	0	95.652	95.654	-0.0018	1.0394	1.0394	0.0000	5.3
12	2	0	97.417	97.414	0.0033	1.0252	1.0252	0.0000	7.6
10	7	1	98.296	98.296	-0.0001	1.0184	1.0184	0.0000	2.4
12	2	2	99.185	99.181	0.0044	1.0116	1.0116	0.0000	13.4
11	6	1	101.861	101.848	0.0129	0.9922	0.9923	-0.0001	1.5
9	9	2	105.445	105.447	-0.0020	0.9681	0.9681	0.0000	3.0
13	2	1	109.120	109.110	0.0105	0.9455	0.9455	-0.0001	2.2

Table 4.6. (*continued*)

h	k	l	$2\theta_{obs}$	$2\theta_{cal}$	$\Delta(2\theta)$	d_{obs}	d_{cal}	Δd	Int
12	4	4	110.036	110.037	-0.0013	0.9402	0.9401	0.0000	8.7
12	6	0	111.915	111.910	0.0052	0.9296	0.9296	0.0000	18.8
13	3	2	112.863	112.855	0.0078	0.9245	0.9245	0.0000	2.1
12	6	2	113.808	113.807	0.0007	0.9195	0.9195	0.0000	6.4
10	9	3	116.721	116.707	0.0137	0.9048	0.9048	-0.0001	0.6
8	8	8	117.691	117.690	0.0008	0.9001	0.9001	0.0000	6.3
14	1	1	120.708	120.695	0.0134	0.8863	0.8864	-0.0001	0.9
14	2	0	121.714	121.717	-0.0026	0.8819	0.8819	0.0000	0.8
14	3	1	124.851	124.854	-0.0032	0.8690	0.8690	0.0000	3.0
12	8	0	125.933	125.927	0.0065	0.8648	0.8648	0.0000	2.8
14	4	0	128.128	128.117	0.0115	0.8566	0.8566	0.0000	13.8
14	4	2	130.384	130.374	0.0099	0.8486	0.8486	0.0000	12.5

Table 4.7. The observed and calculated structure parameters for the europium iron garnet $Eu_3Fe_{4.4}Al_{0.6}O_{12}$. $2\theta_{obs}$–position of the observed Bragg lines in degrees, $2\theta_{cal}$–position of the calculated Bragg lines in degrees, $\Delta(2\theta)$–the difference between $2\theta_{obs}$ and $2\theta_{cal}$ in degrees, d_{obs}–the observed spacing distance in Å, d_{cal}–the calculated spacing distance in Å, $\Delta(d)$ –the difference between d_{obs} and d_{cal} in Å, Int–the relative intensity.

h	k	l	$2\theta_{obs}$	$2\theta_{cal}$	$\Delta(2\theta)$	d_{obs}	d_{cal}	Δd	Int
2	1	1	17.402	17.412	-0.0097	5.0919	5.0891	0.0028	6.2
2	2	0	20.114	20.131	-0.0174	4.4111	4.4073	0.0038	1.6
3	2	1	26.734	26.737	-0.0025	3.3319	3.3316	0.0003	9.8
4	0	0	28.622	28.621	0.0015	3.1163	3.1164	-0.0002	23.6
4	2	0	32.085	32.085	0.0003	2.7874	2.7874	0.0000	100.0
4	2	2	35.244	35.243	0.0015	2.5445	2.5446	-0.0001	45.0
4	3	1	36.745	36.732	0.0132	2.4439	2.4447	-0.0008	3.5
5	2	1	39.568	39.566	0.0024	2.2758	2.2759	-0.0001	18.5
4	4	0	40.923	40.920	0.0028	2.2035	2.2037	-0.0001	3.9
6	1	1	44.781	44.781	-0.0002	2.0222	2.0222	0.0000	20.6
6	2	0	46.015	46.010	0.0046	1.9708	1.9710	-0.0002	1.1
6	3	1	49.550	49.556	-0.0058	1.8382	1.8380	0.0002	2.8
4	4	4	50.695	50.696	-0.0011	1.7993	1.7993	0.0000	28.6
6	4	0	52.925	52.923	0.0019	1.7286	1.7287	-0.0001	66.2
7	2	1	54.011	54.012	-0.0012	1.6964	1.6964	0.0000	10.8
6	4	2	55.086	55.087	-0.0005	1.6658	1.6658	0.0000	67.8
6	5	1	58.229	58.229	-0.0004	1.5832	1.5832	0.0000	6.2
8	0	0	59.251	59.253	-0.0022	1.5583	1.5582	0.0001	26.8
6	5	3	62.276	62.262	0.0137	1.4896	1.4899	-0.0003	1.7
6	6	0	63.246	63.247	-0.0006	1.4691	1.4691	0.00001	1.9
7	5	2	66.151	66.151	0.0002	1.4115	1.4115	0.0000	1.8
8	4	0	67.104	67.104	-0.0002	1.3937	1.3937	0.0000	16.7
8	4	2	68.991	68.991	-0.0003	1.3601	1.3601	0.0000	46.4
9	2	1	69.925	69.926	-0.0008	1.3442	1.3442	0.0000	5.8
6	6	4	70.854	70.855	-0.0008	1.3289	1.3289	0.0000	14.8
8	5	1	71.805	71.779	0.0264	1.3136	1.3140	-0.0004	0.9
9	3	2	73.615	73.612	0.0031	1.2857	1.2857	0.0000	5.5
9	4	1	75.425	75.428	-0.0031	1.2593	1.2592	0.0000	0.9
10	1	1	77.242	77.229	0.0126	1.2341	1.2343	-0.0002	1.7
10	2	0	78.129	78.125	0.0038	1.2223	1.2224	0.0000	4.3
10	3	1	80.798	80.796	0.0022	1.1885	1.1886	0.0000	6.1
10	4	0	83.450	83.446	0.0036	1.1574	1.1574	0.0000	41.0
9	6	1	84.328	84.327	0.0015	1.1476	1.1476	0.0000	3.0
10	4	2	85.212	85.205	0.0067	1.1379	1.1380	-0.0001	18.2
11	2	1	87.842	87.836	0.0063	1.1105	1.1105	-0.0001	5.5
8	8	0	88.711	88.711	-0.0003	1.1018	1.1018	0.0000	19.4
11	3	2	91.339	91.337	0.0022	1.0769	1.0769	0.0000	3.9
10	6	0	92.214	92.212	0.0016	1.0689	1.0689	0.0000	1.8
9	6	5	94.852	94.843	0.0091	1.0460	1.0461	-0.0001	1.5
12	0	0	95.725	95.722	0.0032	1.0388	1.0388	0.0000	8.0
12	2	0	97.488	97.484	0.0043	1.0246	1.0247	0.0000	9.7
10	7	1	98.370	98.367	0.0027	1.0178	1.0178	0.0000	3.8
12	2	2	99.257	99.253	0.0041	1.0111	1.0111	0.0000	17.7
11	6	1	101.930	101.924	0.0061	0.9917	0.9917	0.0000	1.9
9	9	2	105.528	105.528	0.0001	0.9675	0.9675	0.0000	4.7
10	8	2	106.441	106.438	0.0028	0.9617	0.9618	0.0000	0.8

Table 4.7. (*continued*)

h	k	l	$2\theta_{obs}$	$2\theta_{cal.}$	$\Delta(2\theta)$	d_{obs}	d_{cal}	Δd	Int
13	2	1	109.200	109.196	0.0040	0.9450	0.9450	0.0000	2.4
12	4	4	110.126	110.125	0.0007	0.9396	0.9396	0.0000	11.6
12	6	0	112.002	112.001	0.0010	0.9291	0.9291	0.0000	26.8
13	3	2	112.946	112.948	-0.0020	0.9240	0.9240	0.0000	3.2
12	6	2	113.903	113.902	0.0013	0.9190	0.9190	0.0000	8.2
8	8	8	117.786	117.792	-0.0060	0.8997	0.8996	0.0000	6.0
14	1	1	120.791	120.803	-0.0118	0.8860	0.8859	0.0001	1.5
14	2	0	121.812	121.827	-0.0151	0.8815	0.8815	0.0001	0.8
14	3	1	124.967	124.972	-0.0052	0.8686	0.8685	0.0000	4.8
12	8	0	126.037	126.047	-0.0102	0.8644	0.8643	0.0000	4.4
14	4	0	128.235	128.243	-0.0081	0.8562	0.8562	0.0000	21.3
14	3	3	129.353	129.366	-0.0131	0.8522	0.8521	0.0000	0.8
14	4	2	130.501	130.507	-0.0063	0.8482	0.8482	0.0000	17.5
14	5	1	134.064	134.057	0.0075	0.8366	0.8366	0.0000	2.3

Table 4.8. The observed and calculated structure parameters for the europium iron garnet $Eu_3Fe_{4.2}Al_{0.8}O_{12}$. $2\theta_{obs}$–position of the observed Bragg lines in degrees, $2\theta_{cal}$–position of the calculated Bragg lines in degrees, $\Delta(2\theta)$–the difference between $2\theta_{obs}$ and $2\theta_{cal}$ in degrees, d_{obs}–the observed spacing distance in Å, d_{cal}–the calculated spacing distance in Å, $\Delta(d)$ –the difference between d_{obs} and d_{cal} in Å, Int–the relative intensity.

h	k	l	$2\theta_{obs}$	$2\theta_{cal}$	$\Delta(2\theta)$	d_{obs}	d_{cal}	Δd	Int
2	1	1	17.415	17.431	-0.0156	5.0882	5.0837	0.0045	9.0
2	2	0	20.138	20.153	-0.0154	4.4059	4.4026	0.0033	2.3
3	2	1	26.769	26.766	0.0031	3.3276	3.3280	-0.0004	11.8
4	0	0	28.652	28.652	0.0010	3.1131	3.1131	0.0000	23.5
4	2	0	32.122	32.120	0.0018	2.7843	2.7844	-0.0002	100.0
3	3	2	33.742	33.734	0.0083	2.6542	2.6548	-0.0006	0.6
4	2	2	35.287	35.282	0.0052	2.5415	2.5418	-0.0004	39.0
4	3	1	36.777	36.773	0.0041	2.4418	2.4421	-0.0003	2.8
5	2	1	39.619	39.610	0.0090	2.2730	2.2735	-0.0005	15.7
4	4	0	40.977	40.966	0.0107	2.2007	2.2013	-0.0006	3.2
6	1	1	44.843	44.832	0.0109	2.0196	2.0200	-0.0005	17.6
6	2	0	46.074	46.063	0.0112	1.9684	1.9689	-0.0005	0.4
6	3	1	49.621	49.613	0.0082	1.8357	1.8360	-0.0003	2.4
4	4	4	50.763	50.755	0.0084	1.7971	1.7973	-0.0003	18.1
6	4	0	52.993	52.985	0.0084	1.7266	1.7268	-0.0003	37.6
7	2	1	54.082	54.075	0.0068	1.6944	1.6945	-0.0002	7.1
6	4	2	55.158	55.151	0.0071	1.6638	1.6640	-0.0002	38.7
6	5	1	58.304	58.298	0.0057	1.5813	1.5814	-0.0001	4.0
8	0	0	59.329	59.324	0.0055	1.5564	1.5565	-0.0001	15.0
8	1	1	60.338	60.338	0.0001	1.5328	1.5328	-0.0000	0.2
8	2	0	61.351	61.342	0.0088	1.5099	1.5101	-0.0002	0.2
6	5	3	62.342	62.337	0.0051	1.4882	1.4883	-0.0001	1.1
6	6	0	63.326	63.323	0.0033	1.4675	1.4675	-0.0001	0.8
7	5	2	66.232	66.231	0.0007	1.4099	1.4099	-0.0000	0.9
8	4	0	67.190	67.186	0.0039	1.3921	1.3922	-0.0001	9.1
8	4	2	69.081	69.076	0.0048	1.3586	1.3587	-0.0001	22.5
9	2	1	70.015	70.012	0.0027	1.3427	1.3428	-0.0000	2.7
6	6	4	70.947	70.943	0.0042	1.3274	1.3274	-0.0001	6.9
8	5	1	71.869	71.868	0.0009	1.3126	1.3126	-0.0000	0.4
9	3	2	73.709	73.704	0.0046	1.2843	1.2844	-0.0001	2.4
9	4	1	75.529	75.524	0.0053	1.2578	1.2579	-0.0001	0.7
10	1	1	77.329	77.328	0.0008	1.2330	1.2330	-0.0000	0.9
10	2	0	78.228	78.226	0.0025	1.2210	1.2211	-0.0000	2.0
10	3	1	80.906	80.901	0.0050	1.1872	1.1873	-0.0001	3.1
10	4	0	83.563	83.557	0.0064	1.1561	1.1562	-0.0001	18.2
9	6	1	84.442	84.439	0.0035	1.1463	1.1463	-0.0000	1.2
10	4	2	85.324	85.319	0.0050	1.1367	1.1367	-0.0001	7.8
11	2	1	87.962	87.955	0.0072	1.1093	1.1093	-0.0001	2.5
8	8	0	88.837	88.832	0.0049	1.1006	1.1006	-0.0000	8.0
11	3	2	91.466	91.463	0.0026	1.0757	1.0757	-0.0000	1.7
10	6	0	92.343	92.341	0.0021	1.0678	1.0678	-0.0000	0.8
9	6	5	94.982	94.978	0.0045	1.0449	1.0450	-0.0000	0.6
12	0	0	95.860	95.858	0.0016	1.0377	1.0377	-0.0000	3.0
12	2	0	97.628	97.625	0.0033	1.0236	1.0236	-0.0000	4.0
10	7	1	98.510	98.511	-0.0005	1.0167	1.0167	0.0000	1.4
12	2	2	99.396	99.398	-0.0023	1.0100	1.0100	0.0000	7.4

Table 4.8. (*continued*)

h	k	l	$2\theta_{obs}$	$2\theta_{cal}$	$\Delta(2\theta)$	d_{obs}	d_{cal}	Δd	Int
11	6	1	102.073	102.076	-0.0034	0.9907	0.9907	0.0000	0.8
9	9	2	105.693	105.691	0.0024	0.9665	0.9665	0.0000	1.9
10	8	2	106.592	106.604	-0.0116	0.9608	0.9607	0.0001	0.2
13	2	1	109.375	109.370	0.0049	0.9440	0.9440	0.0000	1.0
12	4	4	110.298	110.302	-0.0044	0.9387	0.9386	0.0000	4.3
12	6	0	112.180	112.184	-0.0043	0.9282	0.9281	0.0000	9.6
13	3	2	113.127	113.135	-0.0077	0.9231	0.9230	0.0000	1.2
12	6	2	114.085	114.092	-0.0069	0.9180	0.9180	0.0000	3.3
10	9	3	117.036	117.008	0.0276	0.9033	0.9034	-0.0001	0.2
8	8	8	117.993	117.997	-0.0041	0.8987	0.8987	0.0000	2.9
14	1	1	121.018	121.021	-0.0026	0.8850	0.8849	0.0000	0.5
14	2	0	122.025	122.050	-0.0246	0.8806	0.8805	0.0001	0.3
14	3	1	125.205	125.210	-0.0048	0.8676	0.8676	0.0000	1.6
12	8	0	126.274	126.291	-0.0165	0.8635	0.8634	0.0001	1.4
14	4	0	128.490	128.498	-0.0084	0.8553	0.8552	0.0000	7.6
14	4	2	130.764	130.776	-0.0121	0.8473	0.8473	0.0000	6.6

Table 4.9. The observed and calculated structure parameters for the europium iron garnet $Eu_3Fe_4Al_1O_{12}$. $2\theta_{obs}$–position of the observed Bragg lines in degrees, $2\theta_{cal}$–position of the calculated Bragg lines in degrees, $\Delta(2\theta)$–the difference between $2\theta_{obs}$ and $2\theta_{cal}$ in degrees, d_{obs}–the observed spacing distance in Å, d_{cal}–the calculated spacing distance in Å, $\Delta(d)$ –the difference between d_{obs} and d_{cal} in Å, Int–the relative intensity.

h	k	l	$2\theta_{obs}$	$2\theta_{cal}$	$\Delta(2\theta)$	d_{obs}	d_{cal}	Δd	Int
2	1	1	17.428	17.446	-0.0184	5.0844	5.0791	0.0053	9.5
2	2	0	20.163	20.172	-0.0087	4.4005	4.3986	0.0019	2.2
3	2	1	26.784	26.790	-0.0064	3.3258	3.3250	0.0008	11.3
4	0	0	28.674	28.678	-0.0044	3.1108	3.1103	0.0005	22.0
4	2	0	32.151	32.150	0.0011	2.7818	2.7819	-0.0001	100.0
4	2	2	35.318	35.315	0.0034	2.5393	2.5395	-0.0002	39.7
4	3	1	36.814	36.807	0.0068	2.4395	2.4399	-0.0004	2.4
5	2	1	39.656	39.647	0.0088	2.2709	2.2714	-0.0005	17.8
4	4	0	41.015	41.005	0.0101	2.1988	2.1993	-0.0005	3.6
6	1	1	44.889	44.875	0.0143	2.0176	2.0182	-0.0006	21.5
6	2	0	46.124	46.107	0.0173	1.9664	1.9671	-0.0007	0.6
6	3	1	49.678	49.661	0.0175	1.8337	1.8343	-0.0006	3.3
4	4	4	50.818	50.804	0.0144	1.7952	1.7957	-0.0005	23.2
6	4	0	53.052	53.036	0.0159	1.7248	1.7253	-0.0005	51.6
7	2	1	54.143	54.128	0.0151	1.6926	1.6930	-0.0004	10.0
6	4	2	55.220	55.205	0.0152	1.6621	1.6625	-0.0004	51.9
6	5	1	58.373	58.356	0.0171	1.5796	1.5800	-0.0004	5.5
8	0	0	59.402	59.382	0.0197	1.5547	1.5551	-0.0005	22.0
6	5	3	62.421	62.399	0.0216	1.4865	1.4870	-0.0005	1.5
6	6	0	63.402	63.386	0.0156	1.4659	1.4662	-0.0003	1.4
7	5	2	66.313	66.299	0.0153	1.4084	1.4087	-0.0003	1.4
8	4	0	67.269	67.255	0.0143	1.3907	1.3910	-0.0003	12.5
8	4	2	69.162	69.147	0.0147	1.3572	1.3574	-0.0003	33.6
9	2	1	70.099	70.085	0.0144	1.3413	1.3416	-0.0002	4.0
6	6	4	71.029	71.016	0.0126	1.3260	1.3262	-0.0002	10.3
8	5	1	71.957	71.943	0.0140	1.3112	1.3114	-0.0002	0.9
9	3	2	73.791	73.782	0.0097	1.2831	1.2832	-0.0001	3.7
9	4	1	75.608	75.604	0.0043	1.2567	1.2567	-0.0001	1.1
10	1	1	77.436	77.411	0.0252	1.2315	1.2319	-0.0003	1.3
10	2	0	78.322	78.310	0.0125	1.2198	1.2200	-0.0002	3.4
10	3	1	80.994	80.989	0.0049	1.1862	1.1862	-0.0001	5.3
10	4	0	83.656	83.649	0.0071	1.1551	1.1551	-0.0001	29.4
9	6	1	84.537	84.532	0.0048	1.1452	1.1453	-0.0001	2.1
10	4	2	85.420	85.414	0.0058	1.1357	1.1357	-0.0001	12.0
11	2	1	88.058	88.054	0.0035	1.1083	1.1083	-0.0000	4.6
8	8	0	88.939	88.933	0.0056	1.0996	1.0997	-0.0001	13.2
11	3	2	91.571	91.569	0.0016	1.0747	1.0747	-0.0000	3.3
10	6	0	92.448	92.448	-0.0005	1.0668	1.0668	0.0000	1.4
9	6	5	95.101	95.090	0.0108	1.0439	1.0440	-0.0001	1.1
12	0	0	95.969	95.973	-0.0039	1.0368	1.0368	0.0000	5.1
12	2	0	97.745	97.743	0.0022	1.0226	1.0227	0.0000	6.7
10	7	1	98.628	98.630	-0.0024	1.0158	1.0158	0.0000	2.5
12	2	2	99.521	99.520	0.0009	1.0091	1.0091	0.0000	12.5
11	6	1	102.197	102.204	-0.0072	0.9898	0.9898	0.0001	1.6
9	9	2	105.824	105.827	-0.0030	0.9656	0.9656	0.0000	3.6
10	8	2	106.723	106.742	-0.0193	0.9600	0.9599	0.0001	0.5

Table 4.9. (*continued*)

h	k	l	$2\theta_{obs}$	$2\theta_{cal}$	$\Delta(2\theta)$	d_{obs}	d_{cal}	Δd	Int
13	2	1	109.500	109.516	-0.0160	0.9433	0.9432	0.0001	2.0
12	4	4	110.436	110.451	-0.0149	0.9379	0.9378	0.0001	8.0
12	6	0	112.323	112.338	-0.0152	0.9274	0.9273	0.0001	17.6
13	3	2	113.274	113.291	-0.0173	0.9223	0.9222	0.0001	2.3
12	6	2	114.235	114.251	-0.0164	0.9173	0.9172	0.0001	6.3
8	8	8	118.155	118.169	-0.0142	0.8979	0.8979	0.0001	5.1
14	1	1	121.171	121.204	-0.0325	0.8843	0.8842	0.0001	1.1
14	2	0	122.194	122.236	-0.0424	0.8799	0.8797	0.0002	0.6
14	3	1	125.386	125.409	-0.0235	0.8669	0.8668	0.0001	3.3
12	8	0	126.466	126.495	-0.0288	0.8627	0.8626	0.0001	2.5
14	4	0	128.678	128.713	-0.0349	0.8546	0.8545	0.0001	14.4
14	3	3	129.832	129.848	-0.0160	0.8505	0.8505	0.0001	0.9
14	4	2	130.966	131.002	-0.0361	0.8466	0.8465	0.0001	12.9

Table 4.10. The observed and calculated structure parameters for the sample $Eu_3Fe_{3.5}Al_{1.5}O_{12}$. $2\theta_{obs}$–position of the observed Bragg lines in degrees, $2\theta_{cal}$–position of the calculated Bragg lines in degrees, $\Delta(2\theta)$–the difference between $2\theta_{obs}$ and $2\theta_{cal}$ in degrees, d_{obs}– the observed spacing distance in Å, d_{cal}– the calculated spacing distance in Å, $\Delta(d)$ –the difference between d_{obs} and d_{cal} in Å, Int–the relative intensity.

h	k	l	$2\theta_{obs}$	$2\theta_{cal}$	$\Delta(2\theta)$	d_{obs}	d_{cal}	Δd	Int
2	1	1	17.528	17.514	0.0140	5.0556	5.0596	-0.0040	12.9
2	2	0	20.275	20.250	0.0249	4.3764	4.3817	-0.0053	3.4
3	2	1	26.913	26.895	0.0176	3.3102	3.3123	-0.0021	16.6
4	0	0	28.796	28.791	0.0049	3.0978	3.0984	-0.0005	23.3
4	2	0	32.288	32.276	0.0111	2.7703	2.7713	-0.0009	100.0
3	3	2	33.921	33.898	0.0223	2.6406	2.6423	-0.0017	1.0
4	2	2	35.461	35.454	0.0062	2.5294	2.5298	-0.0004	36.1
4	3	1	36.958	36.953	0.0042	2.4303	2.4306	-0.0003	3.2
5	2	1	39.820	39.806	0.0140	2.2620	2.2627	-0.0008	21.0
4	4	0	41.180	41.169	0.0104	2.1904	2.1909	-0.0005	3.5
6	1	1	45.065	45.056	0.0083	2.0101	2.0105	-0.0004	22.0
6	2	0	46.307	46.294	0.0127	1.9591	1.9596	-0.0005	0.6
5	4	1	47.651	47.507	0.1442	1.9069	1.9124	-0.0055	3.7
6	3	1	49.872	49.864	0.0076	1.8271	1.8273	-0.0003	3.3
4	4	4	51.020	51.013	0.0071	1.7886	1.7888	-0.0002	21.2
6	4	0	53.259	53.256	0.0030	1.7 186	1.7187	-0.0001	40.0
7	2	1	54.359	54.353	0.0059	1.6864	1.6865	-0.0002	9.9
6	4	2	55.442	55.435	0.0067	1.6560	1.6561	-0.0002	42.9
6	5	1	58.608	58.602	0.0060	1.5738	1.5740	-0.0001	5.6
8	0	0	59.625	59.634	-0.0086	1.5494	1.5492	0.0002	24.4
6	5	3	62.651	62.666	-0.0154	1.4 816	1.4813	0.0003	1.3
6	6	0	63.651	63.659	-0.0076	1.4 607	1.4606	0.0002	1.4
7	5	2	66.568	66.587	-0.0186	1.4 036	1.4033	0.0003	1.4
8	4	0	67.540	67.548	-0.0080	1.3858	1.3856	0.0001	9.4
8	4	2	69.445	69.451	-0.0062	1.3523	1.3522	0.0001	27.1
9	2	1	70.388	70.394	-0.0058	1.3365	1.3364	0.0001	3.8
6	6	4	71.322	71.331	-0.0090	1.3213	1.3211	0.0001	6.8
8	5	1	72.275	72.263	0.01200	1.3062	1.3064	-0.0002	0.4
9	3	2	74.124	74.113	0.01120	1.2781	1.2783	-0.0002	3.0
9	4	1	75.987	75.946	0.04120	1.2514	1.2519	-0.0006	0.7
10	1	1	77.756	77.764	-0.0082	1.2272	1.2271	0.0001	0.9
10	2	0	78.666	78.669	-0.0027	1.2153	1.2153	0.0000	2.4
10	3	1	81.357	81.366	-0.0088	1.1818	1.1817	0.0001	4.2
10	4	0	84.039	84.044	-0.0047	1.1508	1.1507	0.0001	18.4
9	6	1	84.929	84.933	-0.0042	1.1410	1.1409	0.0000	1.7
10	4	2	85.820	85.822	-0.0015	1.1314	1.1314	0.0000	7.7
11	2	1	88.482	88.481	0.0010	1.1041	1.1041	0.0000	3.4
8	8	0	89.416	89.367	0.0494	1.0950	1.0954	-0.0005	11.4
11	3	2	92.050	92.023	0.0270	1.0704	1.0706	-0.0002	2.4
10	6	0	92.912	92.909	0.0028	1.0627	1.0627	-0.0000	0.8
9	6	5	95.525	95.573	-0.0478	1.0404	1.0400	0.0004	0.5
12	0	0	96.432	96.463	-0.0311	1.0330	1.0328	0.0003	1.9
12	2	0	98.184	98.249	-0.0645	1.0192	1.0187	0.0005	5.0
10	7	1	99.099	99.144	-0.0452	1.0123	1.0119	0.0003	1.6
12	2	2	100.016	100.042	-0.0261	1.0054	1.0052	0.0002	6.8
11	6	1	102.780	102.752	0.0282	0.9858	0.9860	-0.0002	0.6

Table 4.10. (*continued*)

h	k	l	$2\theta_{obs}$	$2\theta_{cal}$	$\Delta(2\theta)$	d_{obs}	d_{cal}	Δd	Int
9	9	2	106.418	106.412	0.0063	0.9619	0.9619	-0.0000	1.9
13	2	1	110.112	110.142	-0.0299	0.9397	0.9395	0.0002	1.6
12	4	4	111.069	111.088	-0.0188	0.9343	0.9342	0.0001	4.3
12	6	0	113.006	112.998	0.0077	0.9237	0.9238	0.0000	9.4
12	6	2	114.870	114.936	-0.0661	0.9140	0.9137	0.0003	2.7
8	8	8	118.956	118.909	0.0472	0.8942	0.8944	-0.0002	2.4
14	1	1	122.079	121.990	0.0889	0.8804	0.8808	-0.0004	0.5
14	4	0	129.562	129.638	-0.0763	0.8515	0.8512	0.0003	10.7
14	4	2	131.888	131.978	-0.0899	0.8436	0.8433	0.0003	6.9

Table 4.11. The cubic lattice constant a of the $Eu_3Fe_{5-x}Al_xO_{12}$ series.

x	a (Å)
0.0	12.5010(4)
0.1	12.4938(3)
0.15	12.4908(4)
0.2	12.4898(1)
0.3	12.4824(2)
0.5	12.4729(3)
0.6	12.4658(2)
0.8	12.4531(2)
1.0	12.4408(4)
1.5	12.3956(9)

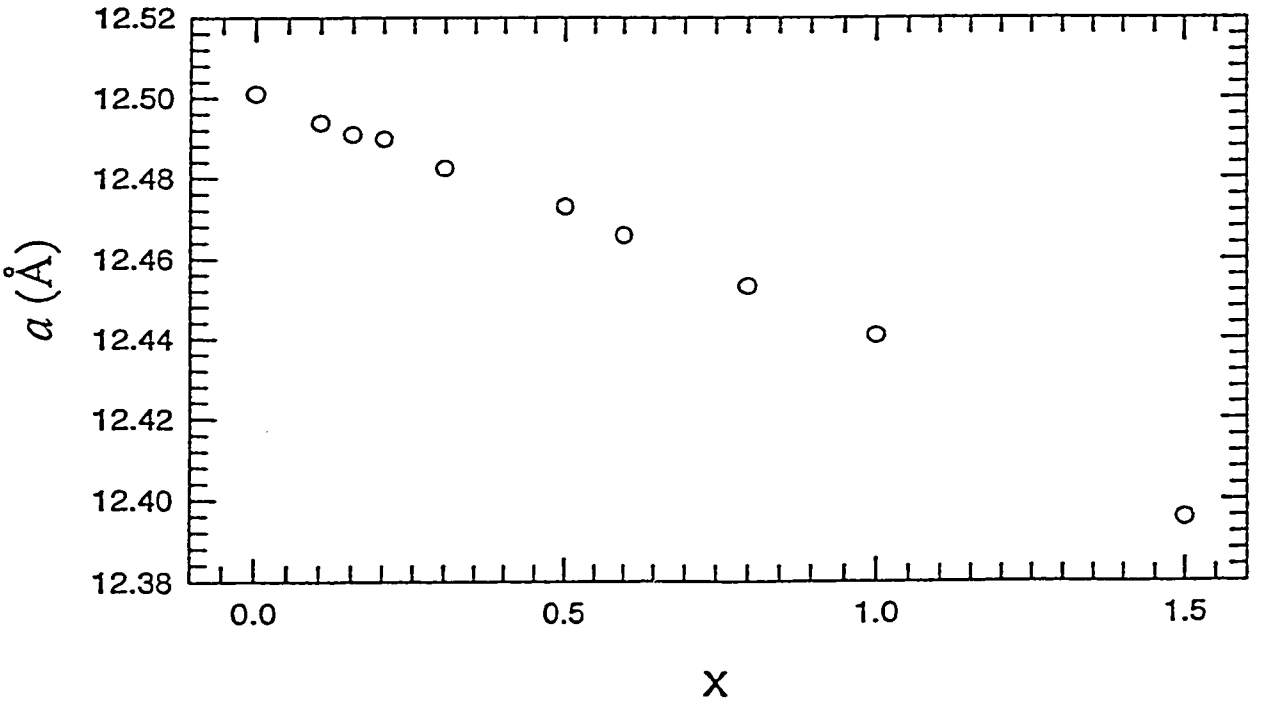

Fig. 4.1 The lattice constant a as a function of the nominal composition x for the $Eu_3Fe_{5-x}Al_xO_{12}$ series.

4.1.2 The Rietveld analysis

Table 4.12 displays the cubic lattice constants (derived from the refinement using all the observed reflections and the structure refined parameters), occupancy factors for each type of atom in each site, calculated compositions and final positions of oxygen ions and R-values. Due to the quality of the collected spectra, only the spectra from polycrystalline samples x = 0.0, 0.1, 0.2, 0.3, 0.5, 0.6, 0.8 and 1.0 could be refined by the Rietveld method. The plots of raw, calculated and difference spectra for the polycrystalline samples are shown in **Figs. 4.2–4.9**. It should be pointed out that the *a* values derived from the Rietveld refinement agree with the values from the peak indexing programs. From the data of occupancy factors, we observe a substitution of Fe ions by Al ions in both the *a* and *d* sites. However, the cation distribution derived from the Rietveld method does not agree with the nominal composition x for each sample due to the close scattering factors of Al and Fe atoms. This fact may indicate that more accurate method should be used to determine the cation distribution for the $Eu_3Fe_{5-x}Al_xO_{12}$ series.

Table 4.12. The refined *a* values, R-values, site occupancies and calculated iron distribution for the $Eu_3Fe_{x-5}Al_xO_{12}$ series. The lattice constants and atomic parameters are in Å. R_B–Rietveld Bragg agreement index, R_P–Rietveld profile agreement index, R_{wp}–weighted Rietveld profile agreement index, R_{wp}(expected)–the expected R_{wp} values.

Nominal composition x	**0.0**	**0.1**	**0.2**	**0.3**	**0.5**	**0.6**	**0.8**	**1.0**
Lattice constant	12.499(8)	12.494(1)	12.487(1)	12.482(6)	12.469(2)	12.464(2)	12.451(1)	12.440(9)
Atomic Parameters (O)								
x	-0.0268(4)	-0.0300(5)	-0.0299(1)	-0.0283(4)	-0.0261(9)	-0.0249(3)	-0.0319(9)	-0.0258(2)
y	0.0576(2)	0.0567(4)	0.0581(3)	0.0584(2)	0.0555(6)	0.0590(5)	0.0544(9)	0.0556(7)
z	0.1515(9)	0.1525(4)	0.11505(1)	0.1507(1)	0.1506(6)	0.1521(4)	0.1512(2)	0.1516(8)
Site occupancy factor								
c: Eu(1/8,0,1/4)	0.25							
a: (0,0,0)								
Fe	0.166(7)	0.1617(6)	0.1545(6)	0.1658(9)	0.1652(6)	0.1661(7)	0.1637(9)	0.1653(1)
Al	0	0.0121(1)	0.0049(1)	0.0007(8)	0.0014(1)	0.0005(1)	0.0028(8)	0.0013(7)
d: (3/8,0,1/4)								
Fe	0.25	0.2473(1)	0.1984(5)	0.1852(5)	0.1878(3)	0.1631(7)	0.2109(7)	0.1883(1)
Al	0	0.0026(9)	0.0515(5)	0.0621(7)	0.0621(7)	0.0868(3)	0.0390(3)	0.0616(2)
Cation distribution								
a: Fe	2.0	1.85(4)	1.94(1)	1.99(1)	1.98(2)	1.99(4)	1.96(5)	1.98(3)
Al	0.0	0.14(6)	0.05(9)	0.009	0.01(8)	0.006	0.03(5)	0.01(7)
d: Fe	3.0	2.96(7)	2.38(1)	2.22(3)	2.25(3)	1.95(8)	2.53(1)	2.25(9)
Al	0.0	0.03(3)	0.61(9)	0.77(7)	0.74(7)	1.04(2)	0.46(9)	0.74(1)
R factors								
R_B	16.34	8.93	10.36	11.22	9.30	10.70	8.19	8.56
R_P	20.25	13.11	14.92	14.39	15.30	14.37	8.94	14.44
R_{wp}	27.87	18.15	21.61	21.08	22.11	19.93	11.70	19.16
R_{wp}(expected)	5.43	3.35	4.45	3.95	5.13	3.70	1.07	3.49

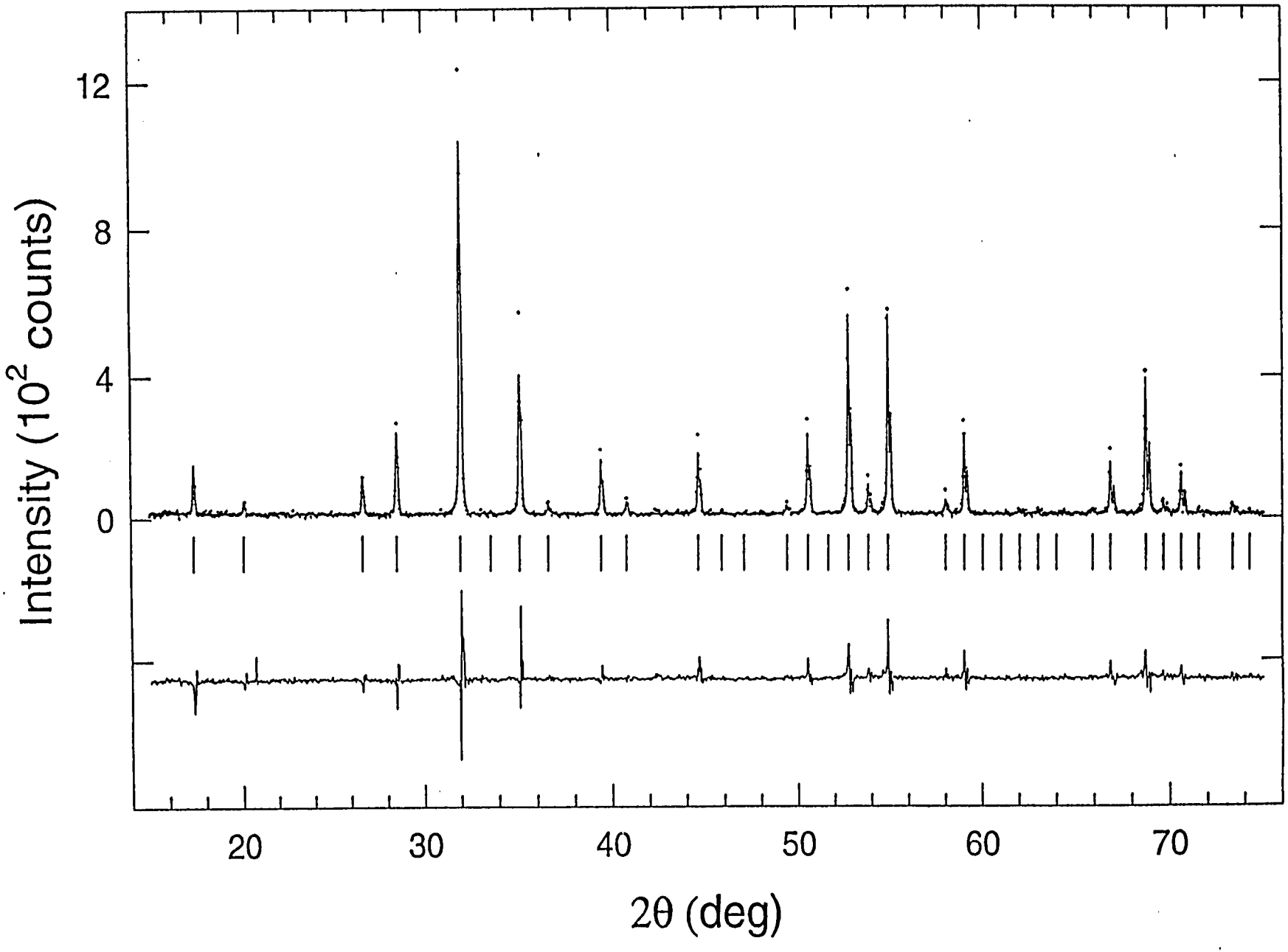

Fig. 4.2. Final Rietveld refinement of the x=0.0 sample. The observed (+), calculated (−) and difference (−) profiles.

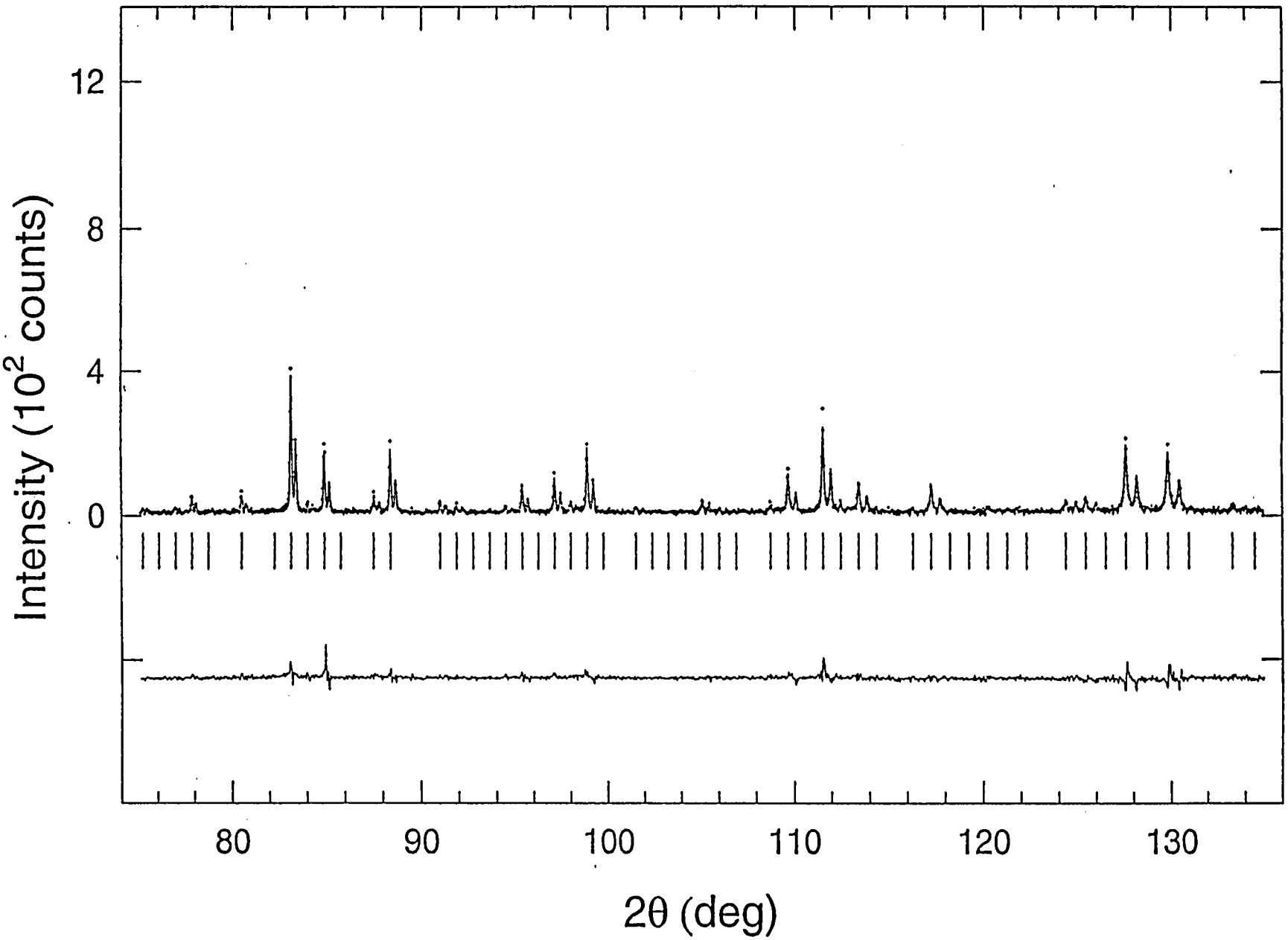

Fig. 4.2. (*continued*)

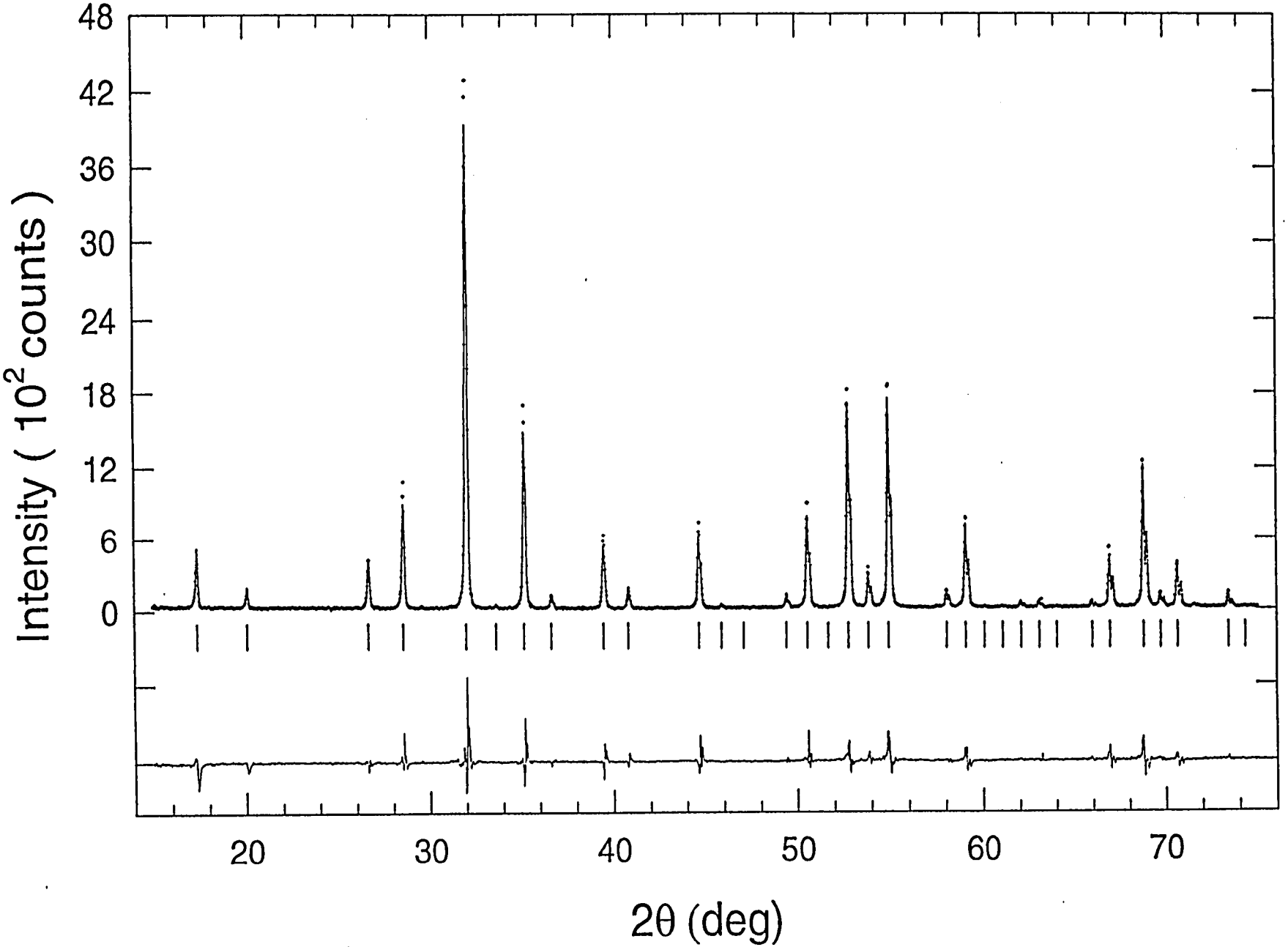

Fig. 4.3. Final Rietveld refinement of the x=0.1 sample. The observed (+), calculated (–) and difference (–) profiles.

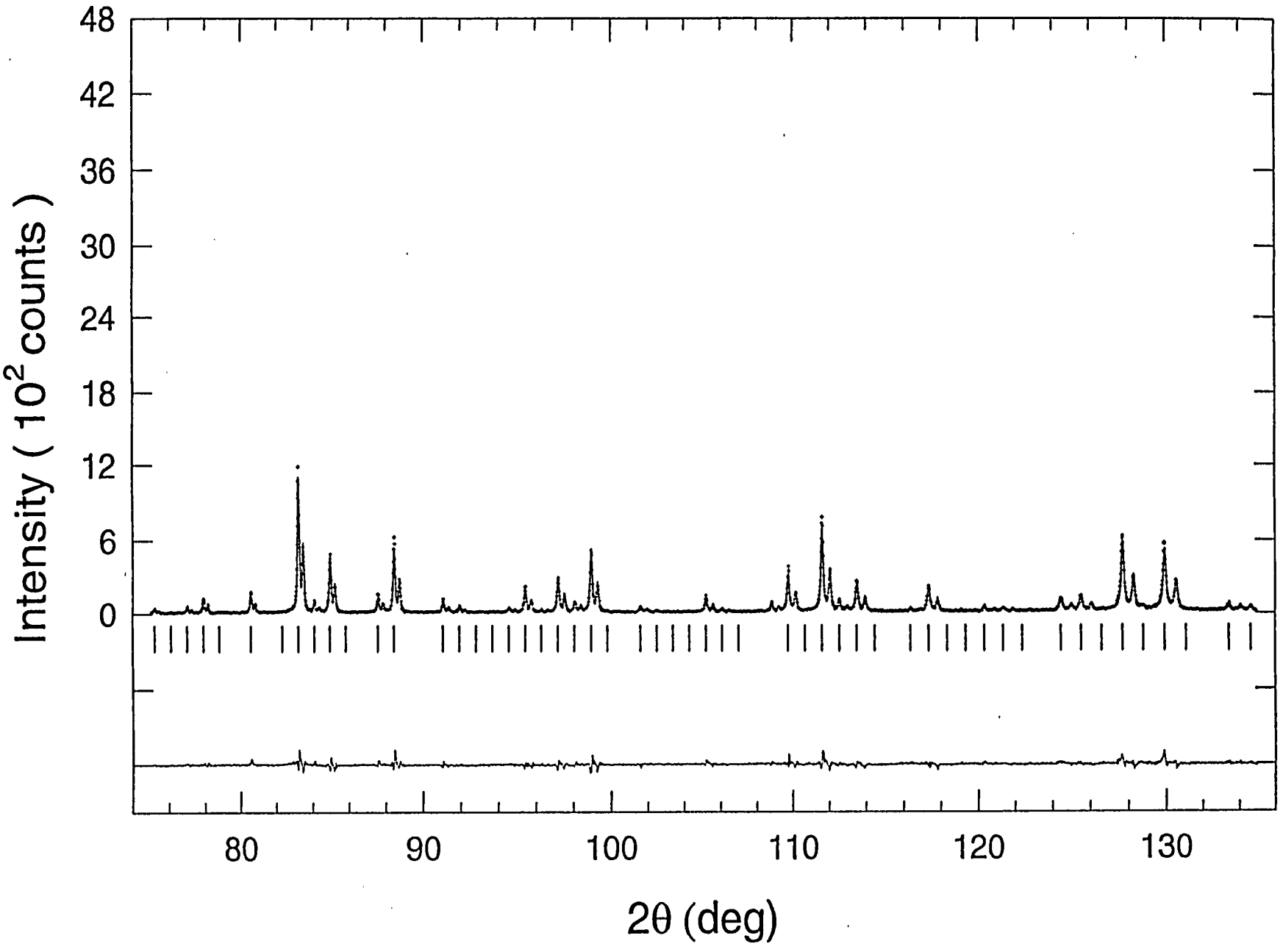

Fig. 4.3. (*continued*)

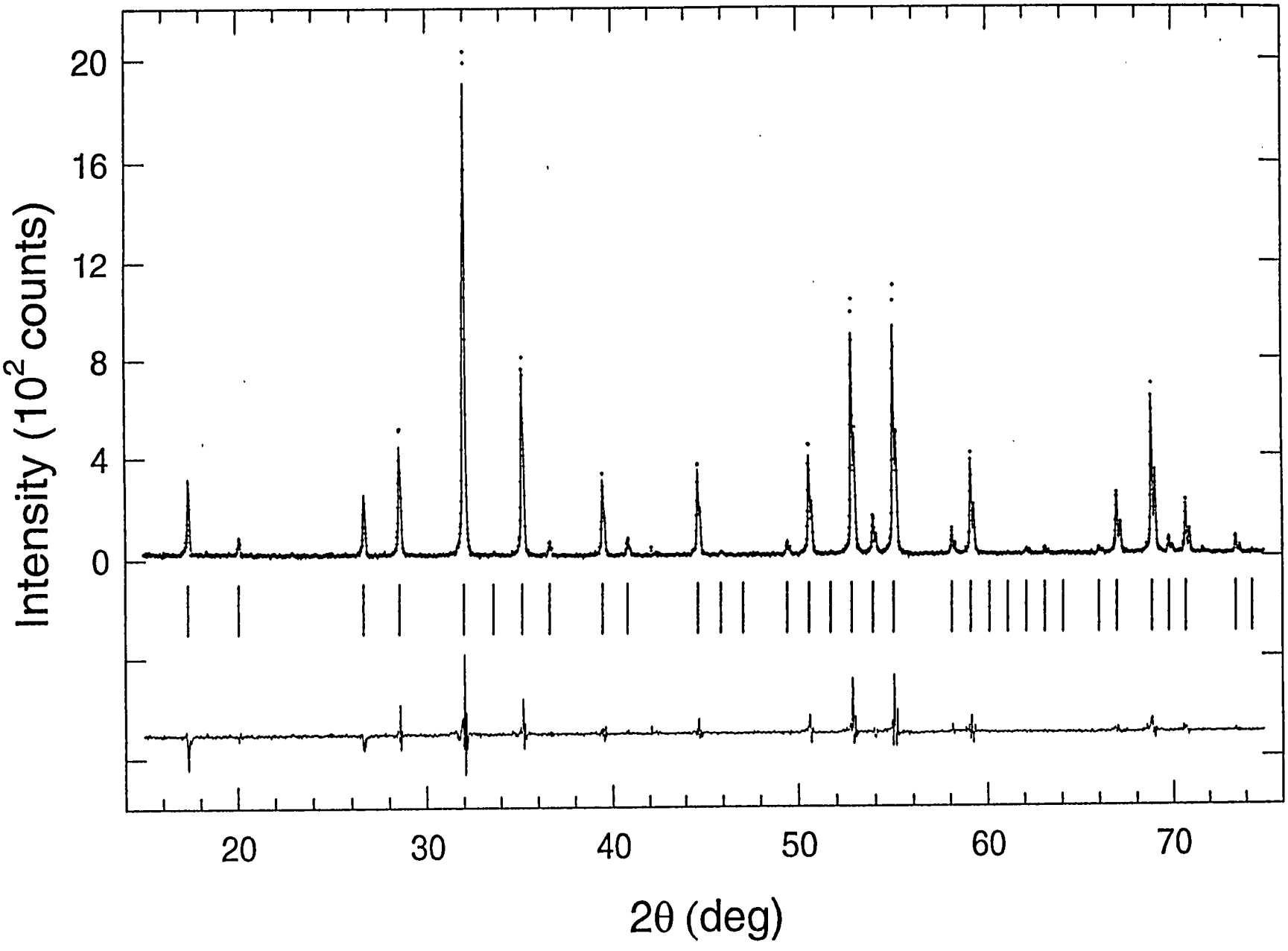

Fig. 4.4. Final Rietveld refinement of the x=0.2 sample. The observed (+), calculated (−) and difference profiles.

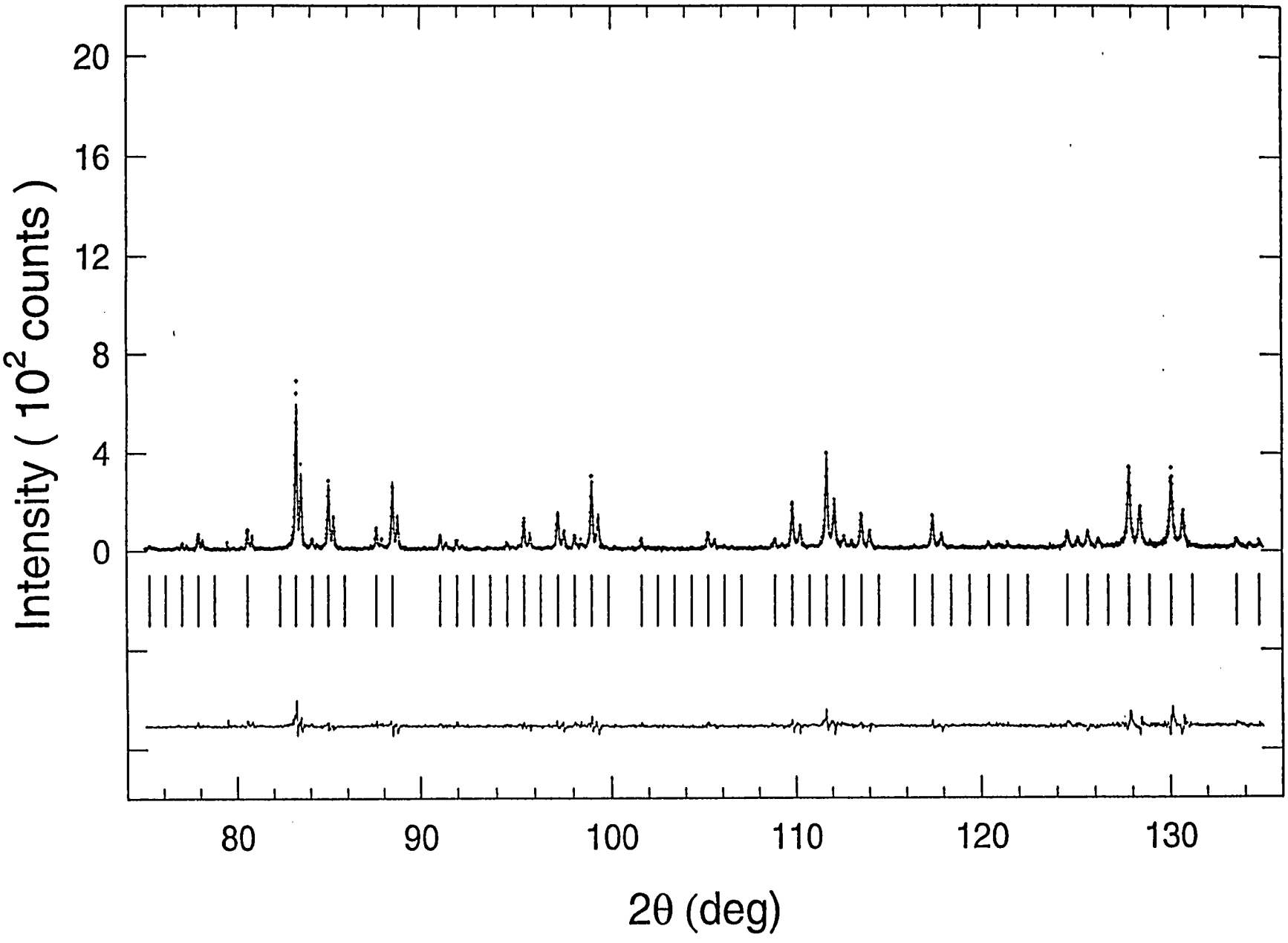

Fig. 4.4. (*continued*)

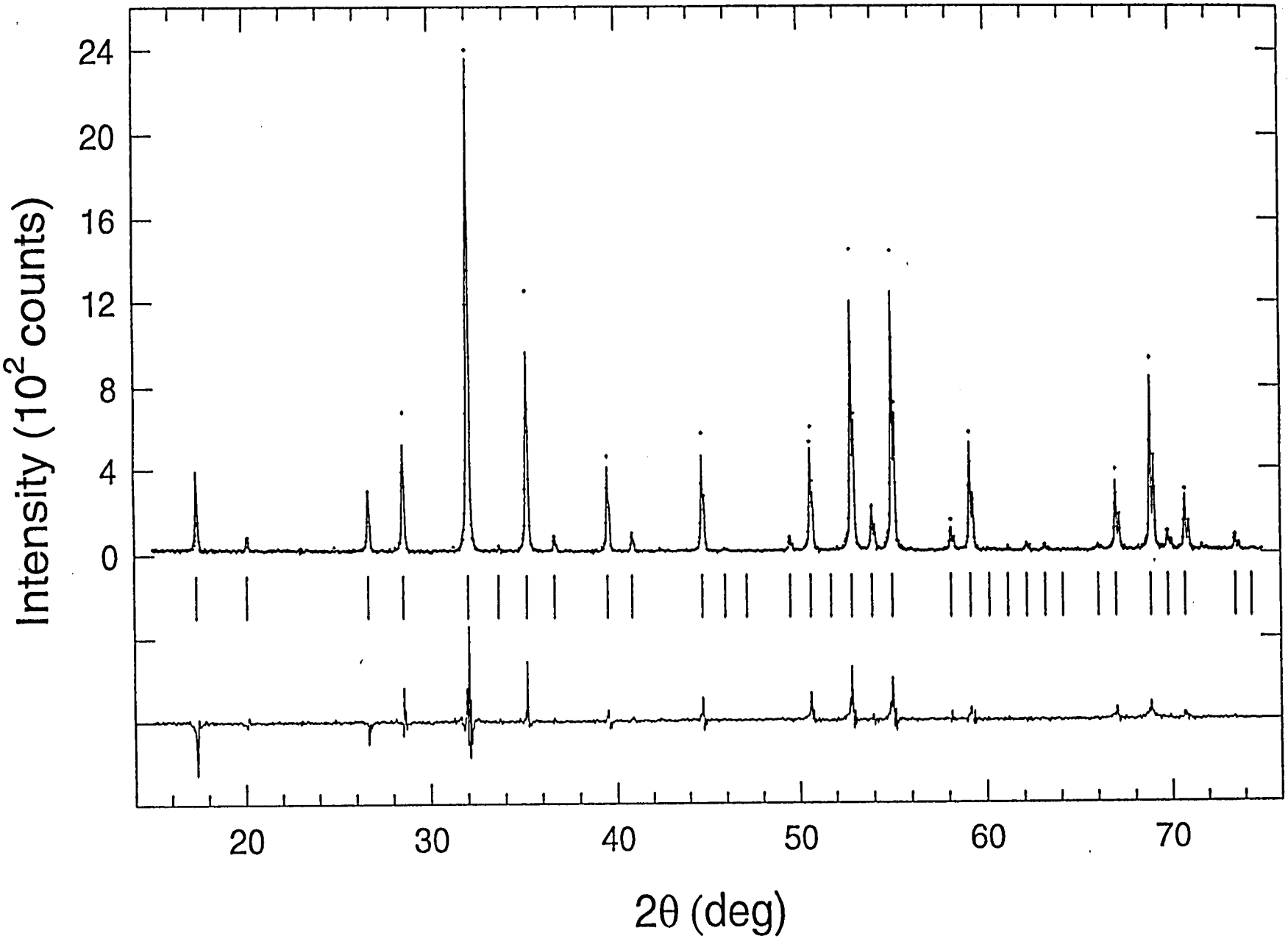

Fig. 4.5. Final Rietveld refinement of the x=0.3 sample. The observed (+), calculated (–) and difference (–) profiles.

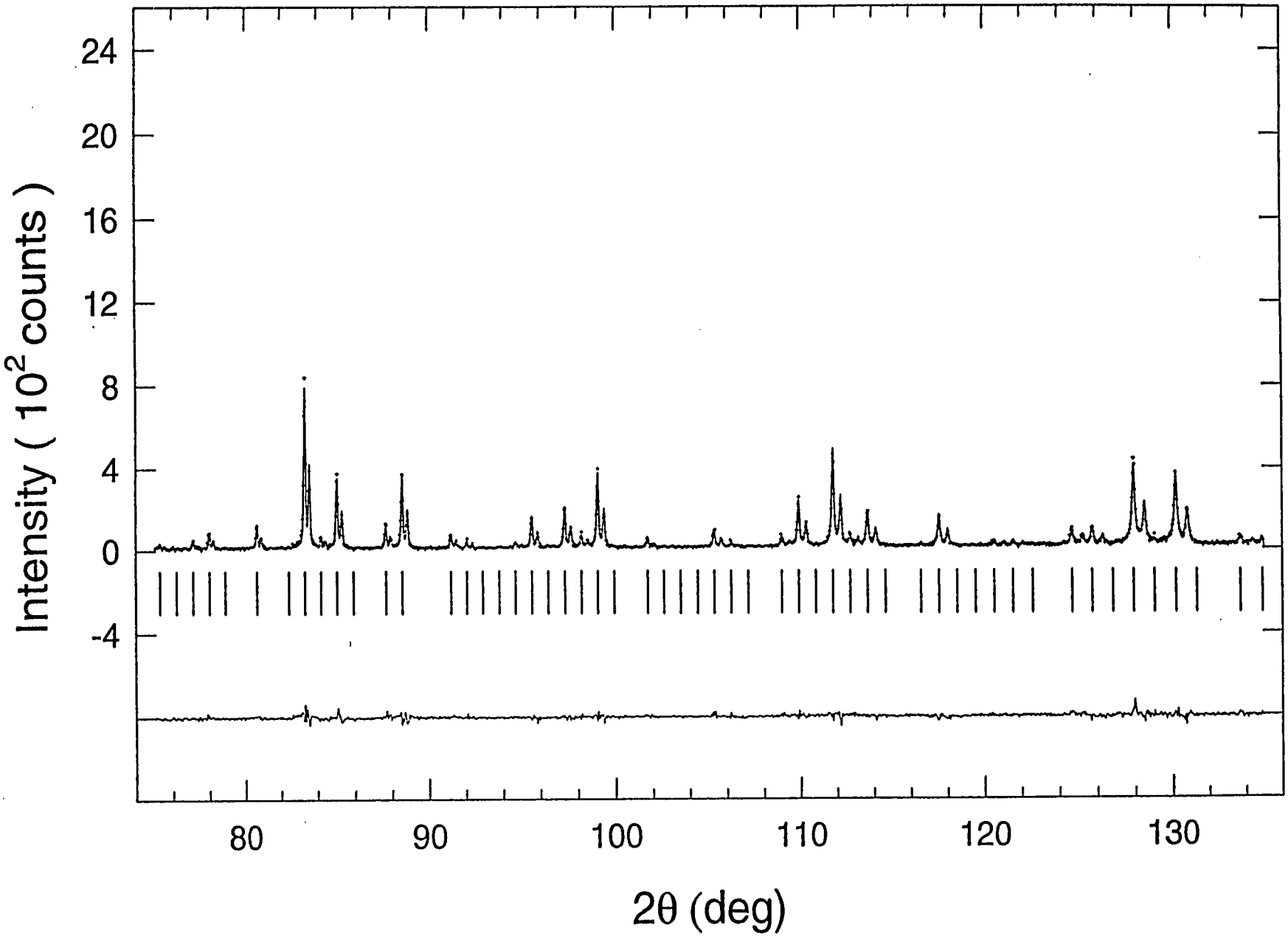

Fig. 4.5. (*continued*)

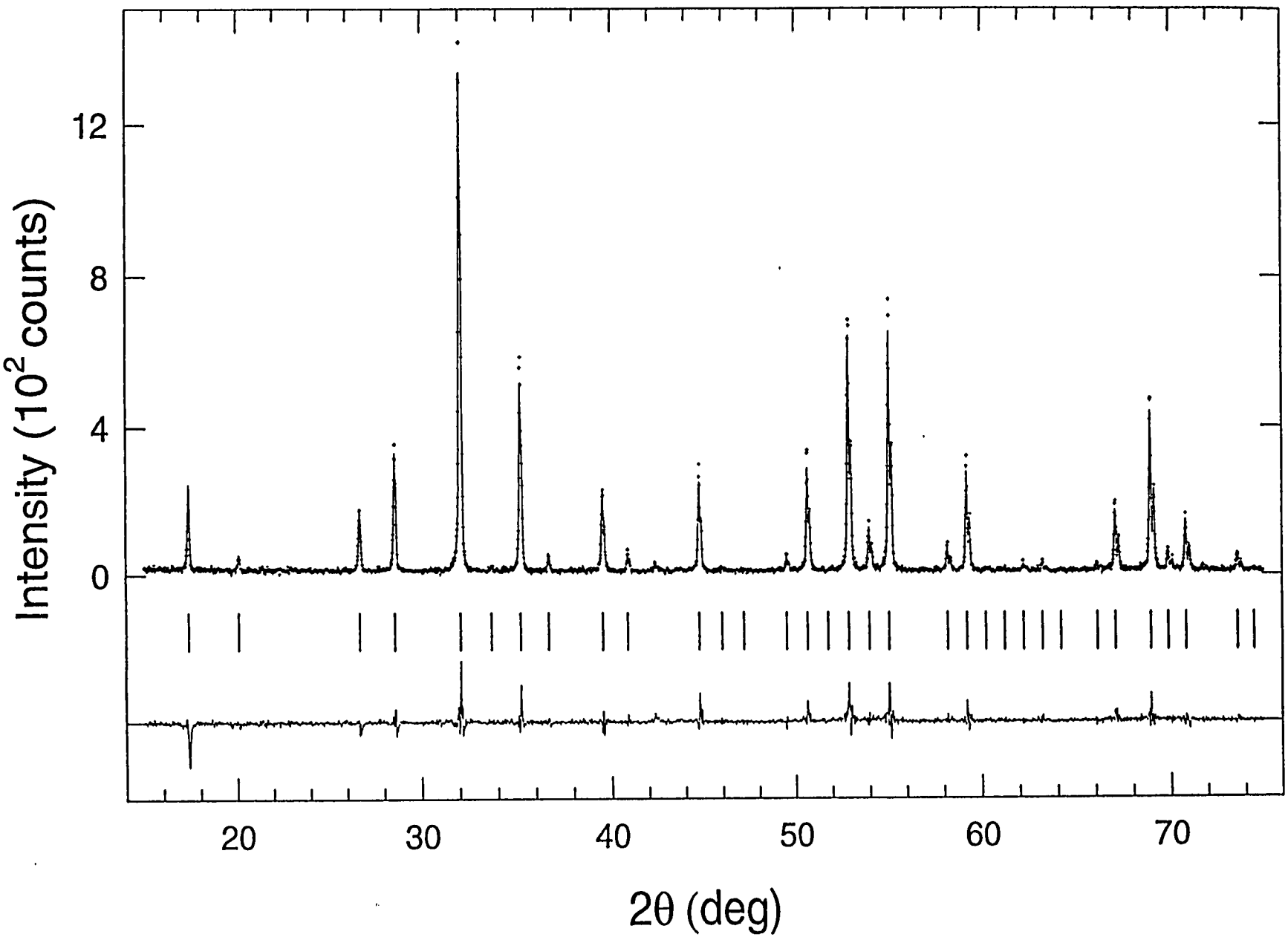

Fig. 4.6. Final Rietveld refinement of the x=0.5 sample. The observed (+), calculated (–) and difference (–) profiles.

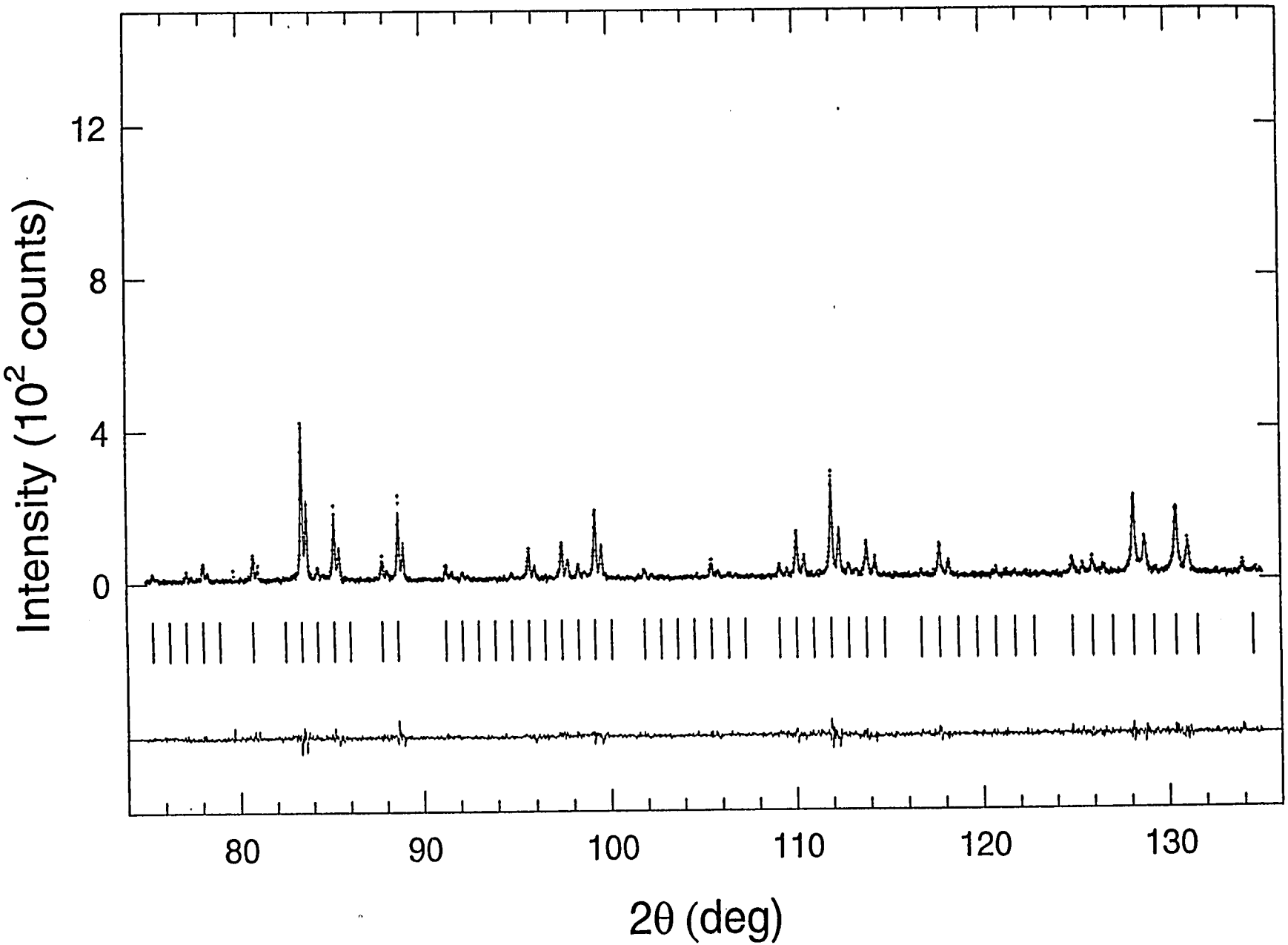

Fig. 4.6. (*continued*)

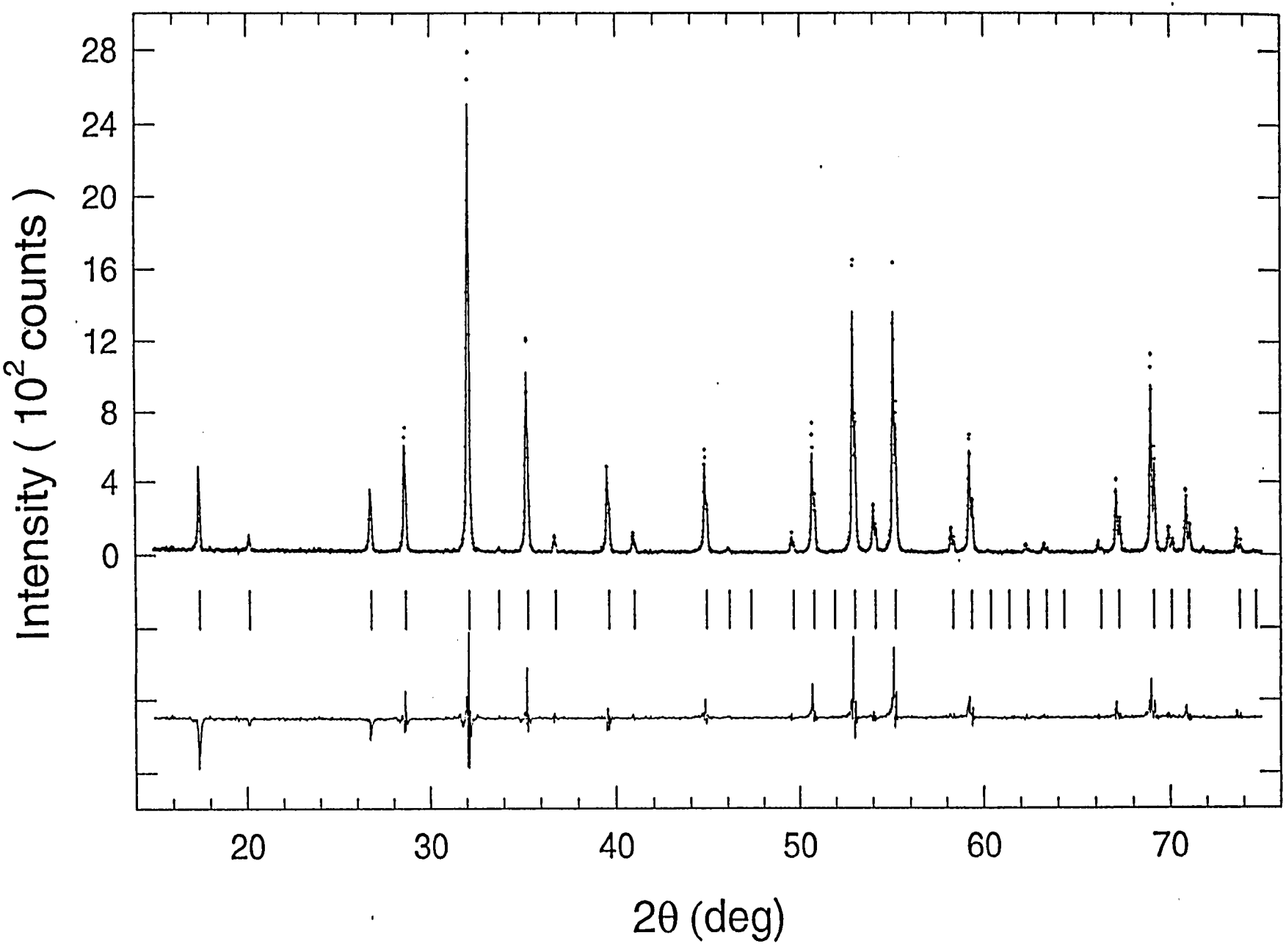

Fig. 4.7. Final Rietveld refinement of the x=0.6 sample. The observed (+), calculated (–) and difference (–) profiles.

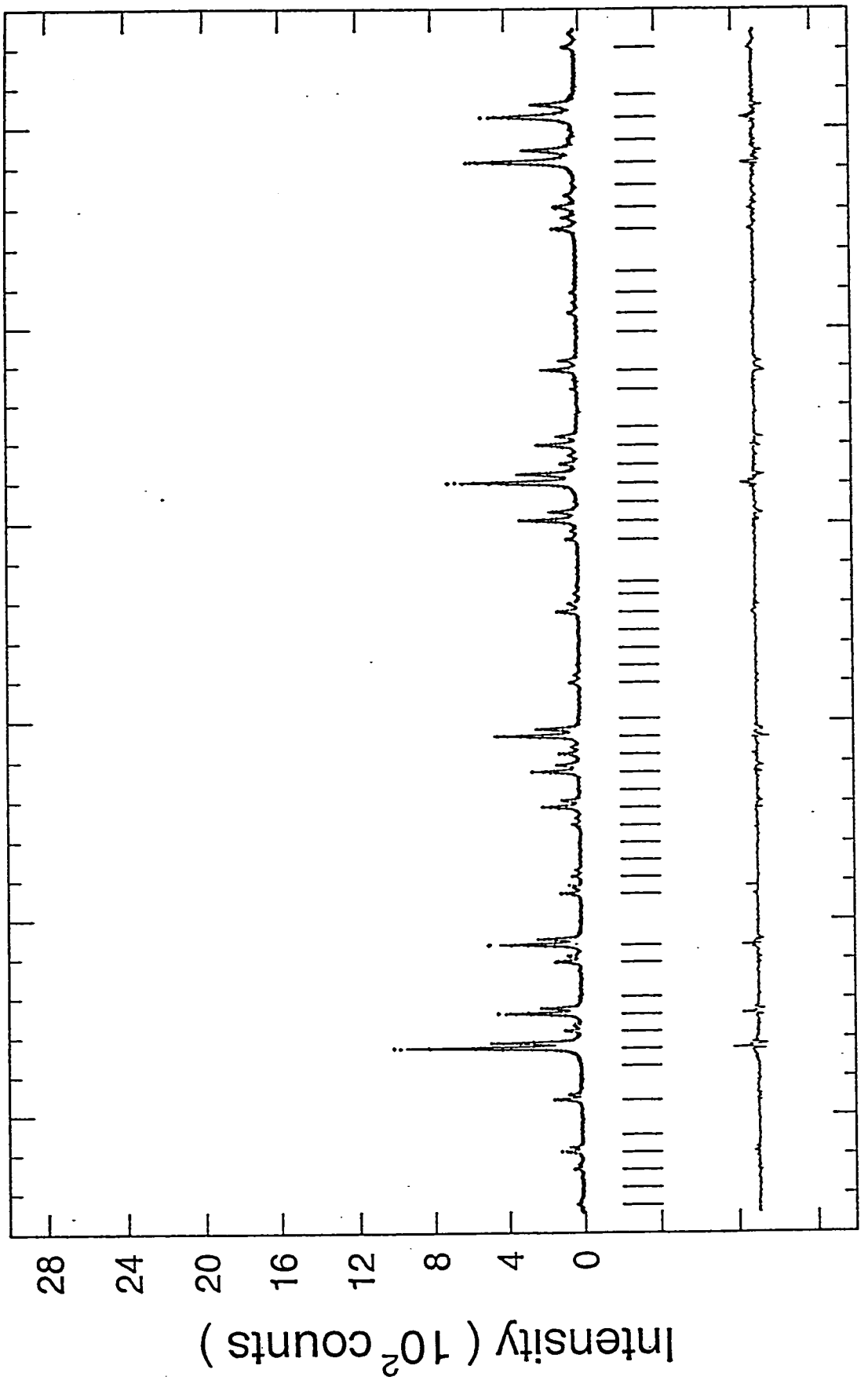

Fig. 4.7. *(continued)*

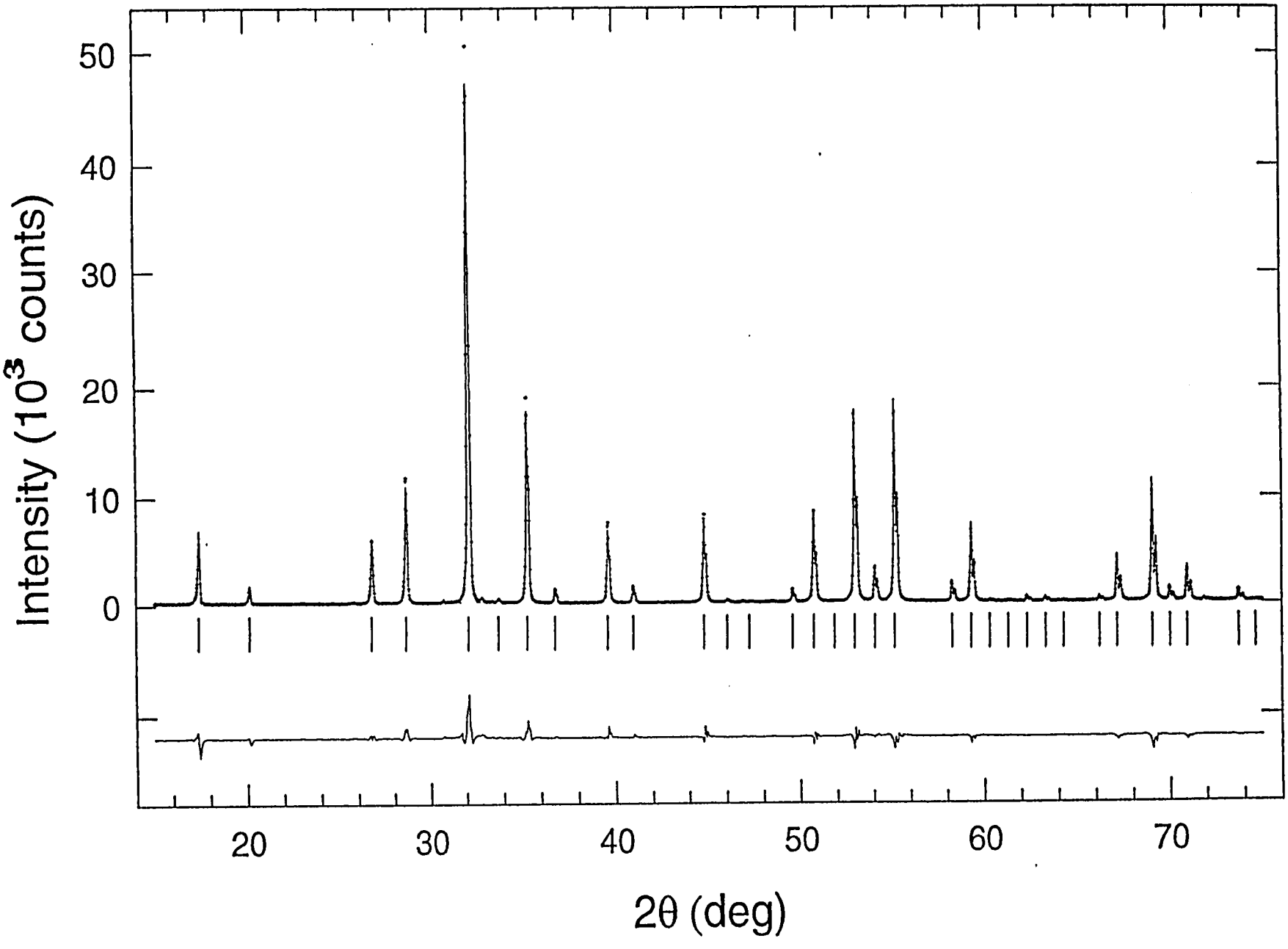

Fig. 4.8. Final Rietveld refinement of the x=0.8 sample. The observed (+), calculated (–) and difference (–) profiles.

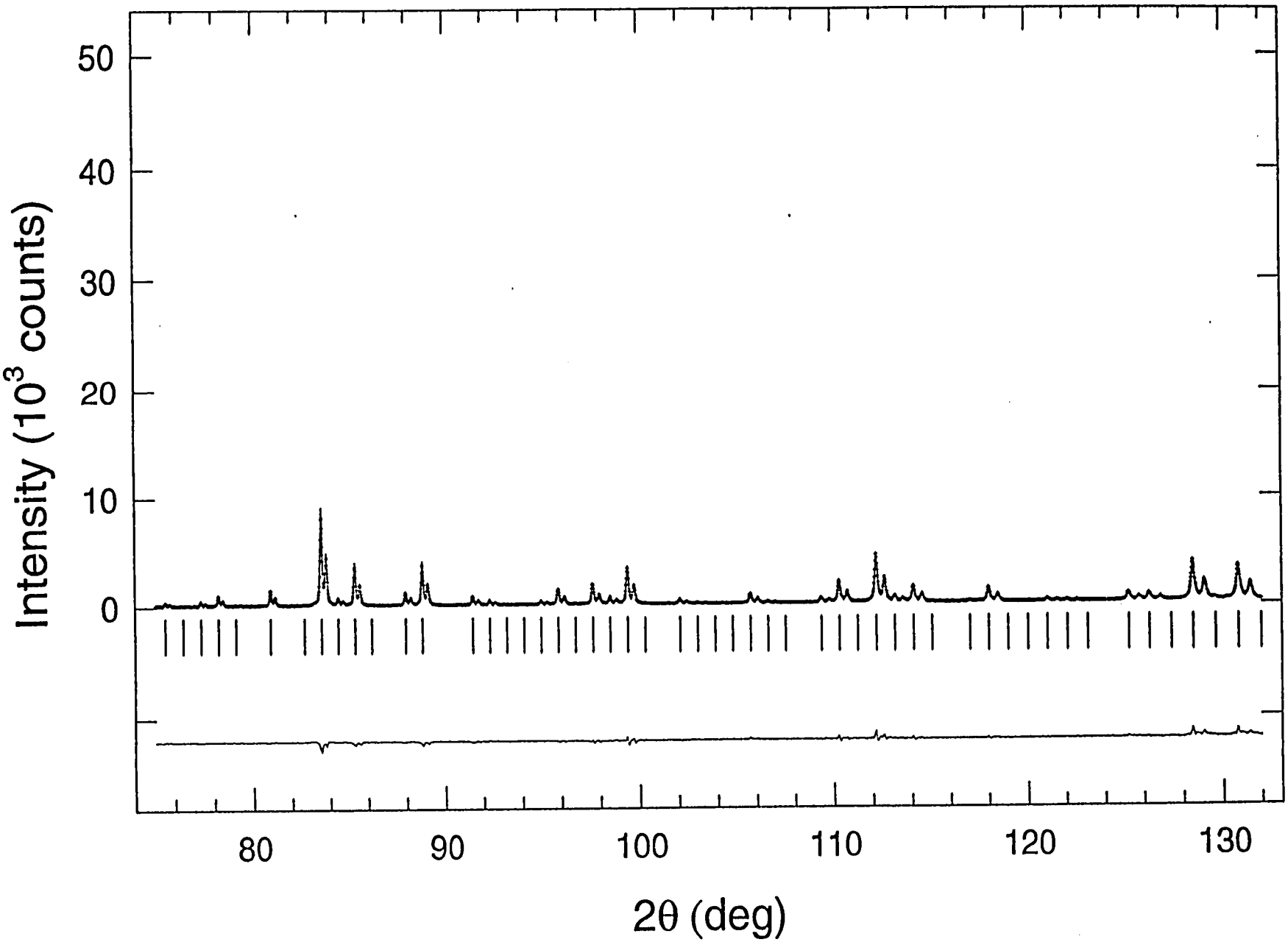

Fig. 4.8. (*continued*)

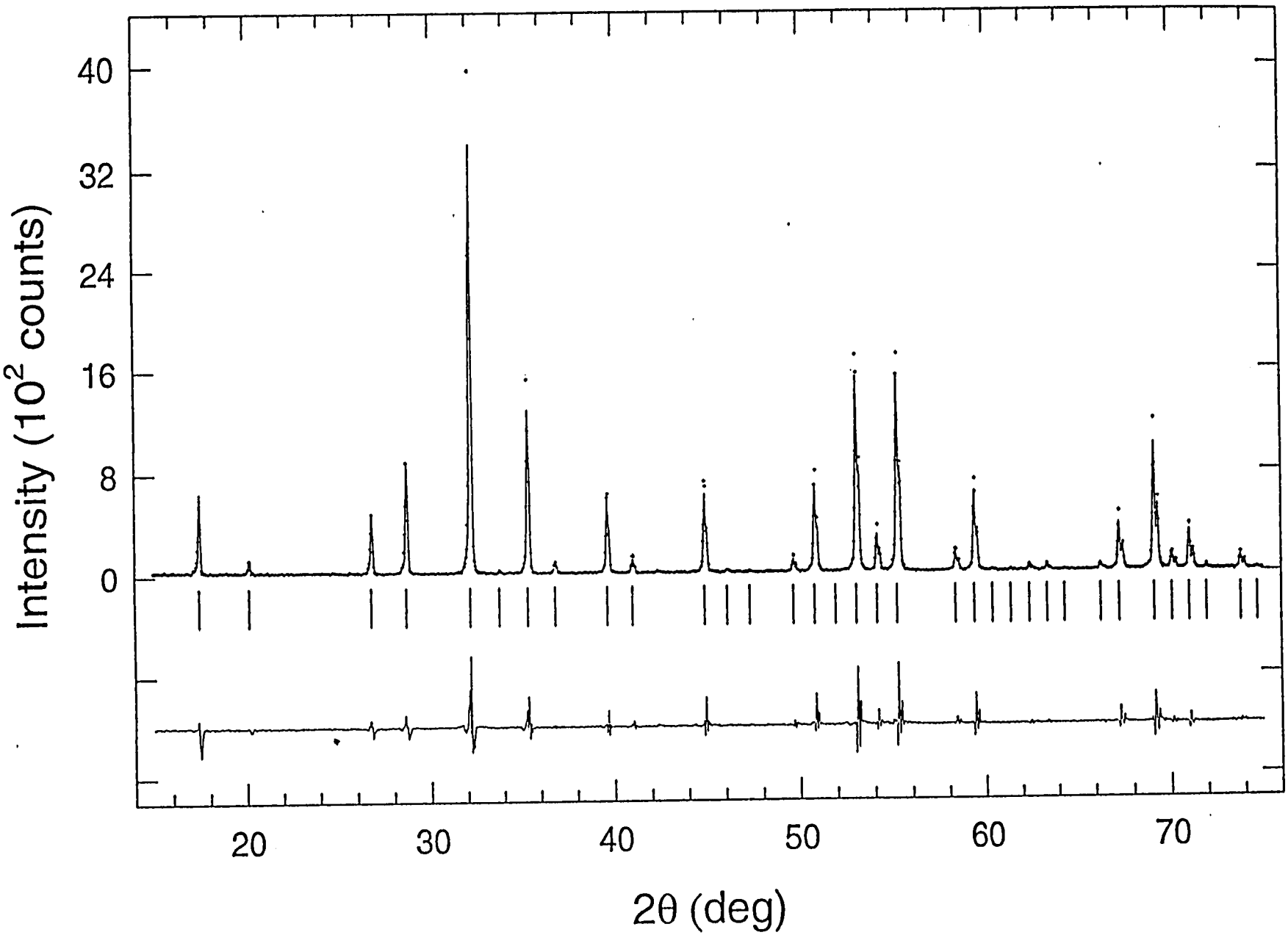

Fig. 4.9. Final Rietveld refinement of the x=1.0 sample. The observed (+), calculated (−) and difference (−) profiles.

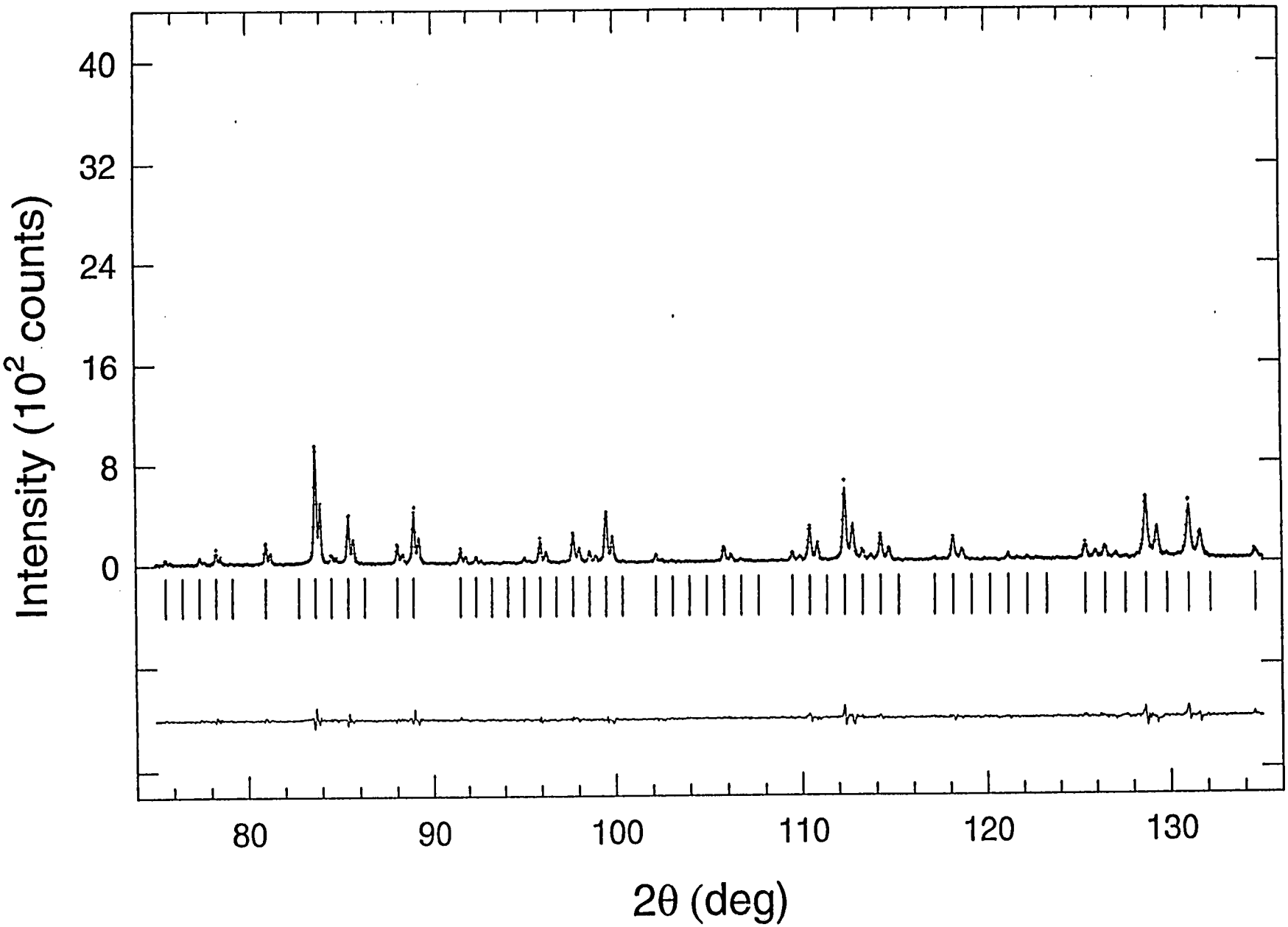

Fig. 4.9. (*continued*)

4.2 ^{57}Fe Mössbauer spectroscopy

In the europium iron garnet series, the iron atoms occupy both the *a* and *d* sites in the crystal structure. Since different sites in the crystal structure have different electronic environments, the iron atoms at different sites will have different quadrupole splittings and isomer shifts if the measurement is made above the Néel temperature of the samples. For examples, the spectra of the studied samples with x = 0.0, 1.0, and 1.5, fitted to two doublets from the Fe atoms in the *a* and *d* sites, are shown in **Figs. 4.10–4.12**. The doublet with larger absorption area is due to Fe^{3+} ions in the *d* site since more Fe atoms occupy the *d* site.

Since two lines overlap in the main absorption line at ~0.4 mm/s in the MS spectra (**Figs. 4.10–4.12**), the spectra are also fitted by trading the places of these two lines. The fitted results show that the area of the doublet from the Fe atoms in the *a* site is larger than that in the *d* site at the temperature above 700 °C. This is at variance with the known fact that there are more Fe atoms in the *d* site than in the *a* site[1,8]. Therefore, the positions of the two doublets are chosen as shown in **Figs. 4.10–4.12**.

The amount of iron atoms in the *a* and *d* sites in the garnet structure is related to the relative area of the corresponding subspectrum. There are many factors that can influence the relative areas[83]. In many cases, those factors are assumed to be equal for the *a* and *d* sites even though they are not in reality. In this thesis, unequal recoil-free fractions were considered for the *a* and *d* sites[84], respectively. The amount of iron atoms in the *a* and *d* sites were derived not only from the raw spectra, assuming that the used Mössbauer absorbers are thin[57-59,85], but also from the thickness-corrected spectra.

Assuming that the Debye model gives a satisfactory description of the vibration modes of the $Eu_3Fe_{5-x}Al_xO_{12}$ series, the temperature dependence of the recoil-free fraction f is given by **Eq. 2.44**. By using this equation, f can be calculated if the Mössbauer temperature θ_D is known. Garnets have a structure which is very complicated. Different sites have different lattice vibrations. Therefore, two Mössbauer temperatures were introduced for the respective a and d sites in this research[86].

When determining the amount of iron atoms in the a and d sites in the $Eu_3Fe_{5-x}Al_xO_{12}$ series by assuming the Debye vibration model, it is necessary to know the respective f or θ_D[87]. It can be seen From **Eq. 2.43** that the area of a doublet in a spectrum is proportional to the product of the number of iron atoms, n, and the corresponding f. In order to determine the Debye temperatures, MS spectra were recorded in the temperature range 298–1023 K for the three samples with x = 0.0, 1.0 and 1.5. The results from the two-doublet fitting model are listed in **Tables 4.13–4.15**. A comparison of the room temperature spectra before and after the temperature scan was performed in order to see if there was any cation redistribution due to the heating process. It should be pointed out that the room temperature spectra of the sample with x = 1.5 before and after the temperature scan showed the rearrangement of iron atoms in the crystal structure. Therefore, only those spectra without cation redistribution were analyzed.

The changes in the absorption area of a doublet $A(T)$ are only proportional to the changes of the f for the relevant site, which can be seen in **Eq. 2.43**. The combination of **Eq. 2.43** and **Eq. 2.44** gives

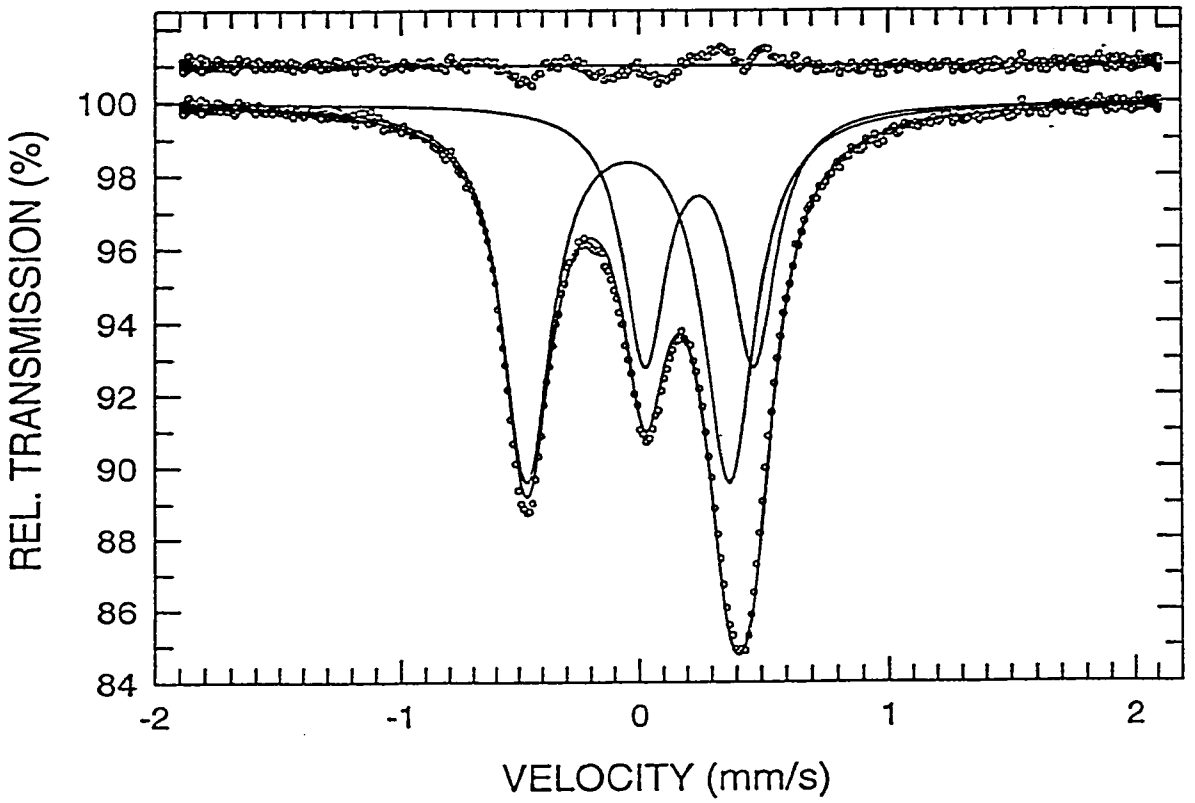

Fig. 4.10. ^{57}Fe MS spectrum of $Eu_3Fe_5O_{12}$ (T = 573 K) fitted with two symmetric doublets corresponding to the *a* and *d* sites, respectively. The velocity scale is relative to iron foil.

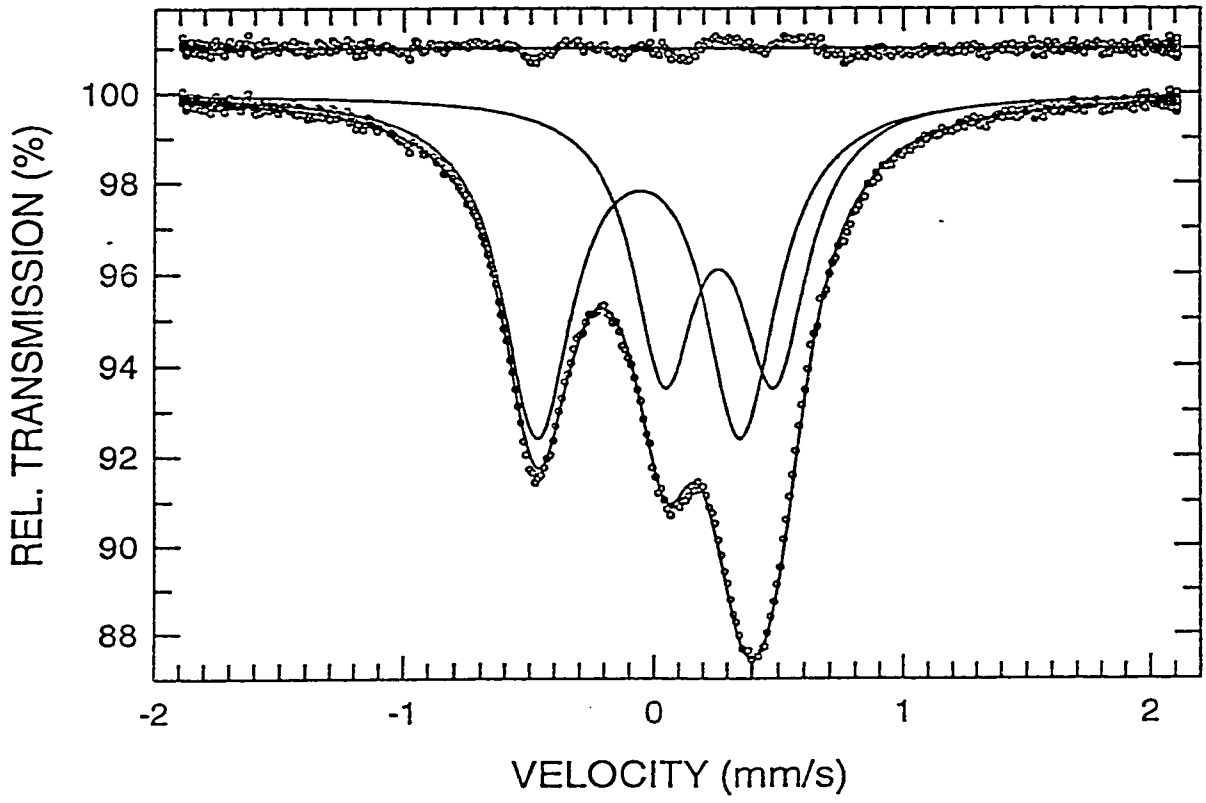

Fig. 4.11. ^{57}Fe MS spectrum of $Eu_3Fe_4Al_1O_{12}$ (T = 573 K) fitted with two symmetric doublets corresponding to the *a* and *d* sites, respectively. The velocity scale is relative to iron foil.

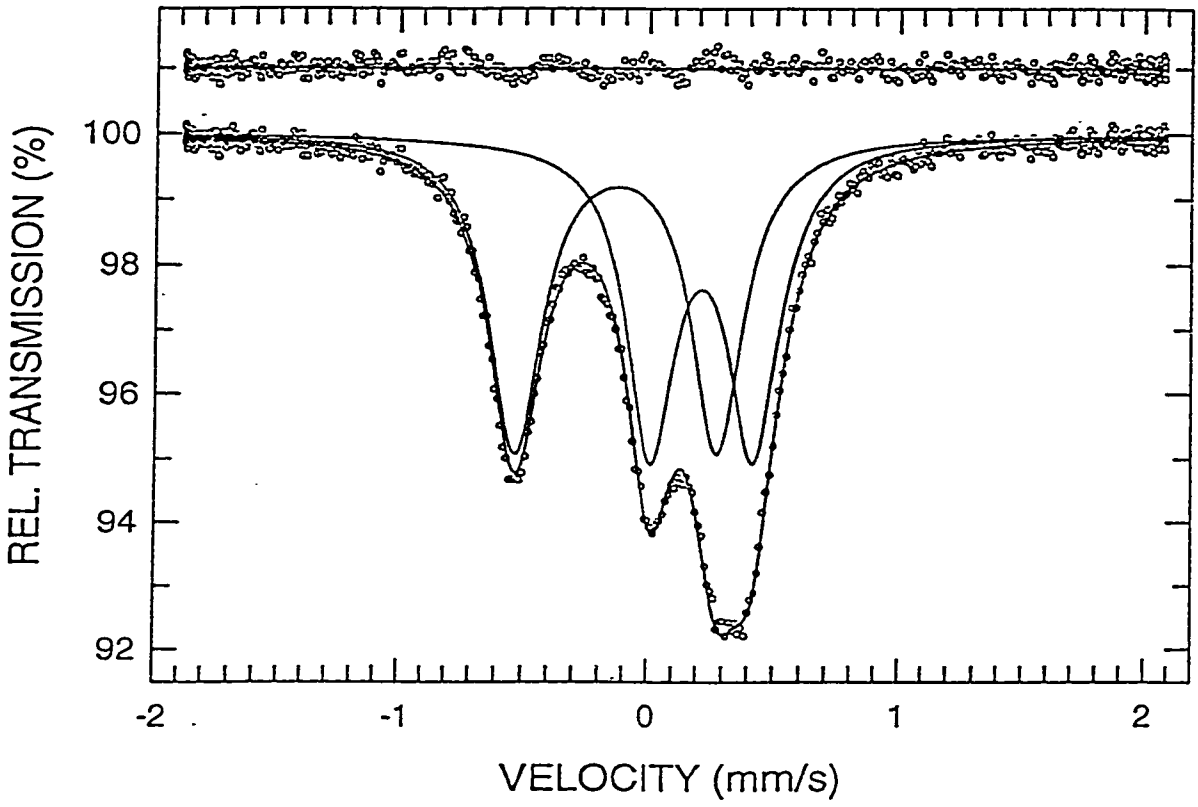

Fig. 4.12. ^{57}Fe MS spectrum of $Eu_3Fe_{3.5}Al_{1.5}O_{12}$ (T = 623 K) fitted with two symmetric doublets corresponding to the *a* and *d* sites, respectively. The velocity scale is relative to iron foil.

$$A(T) = k \cdot n \cdot \exp\left[\frac{-E_\gamma^2}{Mc^2 k\theta_D}\left(\frac{1}{4}+\frac{T^2}{\theta_D^2}\int_0^{\theta_D/T}\frac{xdx}{e^x-1}\right)\right]. \tag{4.1}$$

k and n are constant for each site in a temperature scan if the same absorber is used. Therefore, one finds that

$$\ln\left[\frac{A(T)}{A(RT)}\right] = \ln\left[\frac{f(T)}{f(RT)}\right], \tag{4.2}$$

where $A(T)$ is the doublet area at temperature T, $A(RT)$ is the doublet area at room temperature, $f(T)$ is the recoil-free fraction at temperature T and $f(RT)$ is the recoil-free fraction at room temperature. By combining **Eq. 4.1** and **Eq. 4.2**, it can be seen that the set of data, ln[A(T)/A(RT)] versus temperature T, can be related to θ_D. The θ_D values determined from the relationship ln[$A(T)/A(RT)$] versus T for the samples with x = 0.0, 1.0 and 1.5 are shown in **Figs. 4.13–4.15**. For each sample, the θ_D for the a site is different from θ_D for the d site in the Debye approximation for lattice vibrations.

Based on the θ_D values for each particular site, the corresponding values of f at any temperature can be calculated by using **Eq. 2.44**. The ratio of the doublet areas from the a and d sites for a studied sample can be written as $\frac{A_a}{A_d} = \frac{n_a f_a}{n_d f_d}$, where the subscripts a and d denote the a and d sites, respectively. Therefore, n_a/n_d can be solved. Furthermore, the iron distribution can be calculated since the total amount of iron atoms in one garnet chemical formula for each sample is known from the nominal composition x. The values of θ_D, cation distribution for the respective a and d sites in the three studied

Table 4.13. The MS parameters for $Eu_3Fe_5O_{12}$. CS, QS and A refer to the center shift (relative to iron foil), quadrupole splitting and relative area, respectively.

	a site			d site		
T(K)	CS (mm/s)	QS (mm/s)	A (%·mm/s)	CS (mm/s)	QS (mm/s)	A (%·mm/s)
298	0.306(4)	0.428(1)	0.053(3)	0.015(4)	0.849(8)	0.094(4)
573	0.136(3)	0.447(2)	0.046(1)	-0.157(9)	0.841(1)	0.080(2)
623	0.108(4)	0.447(5)	0.044(7)	-0.188(6)	0.837(2)	0.077(4)
673	0.075(7)	0.449(1)	0.043(3)	-0.222(4)	0.838(4)	0.074(9)
773	0.012(8)	0.451(9)	0.040(2)	-0.284(8)	0.834(1)	0.069(8)
873	-0.046(5)	0.453(1)	0.038(4)	-0.346(9)	0.830(2)	0.064(5)

Table 4.14. The MS parameters for $Eu_3Fe_4Al_1O_{12}$. CS, QS and A refer to the center shift (relative to iron foil), quadrupole splitting and relative area, respectively.

	a site			d site		
T(K)	CS (mm/s)	QS (mm/s)	A (%·mm/s)	CS (mm/s)	QS (mm/s)	A (%·mm/s)
298	0.323(7)	0.442(9)	0.066(6)	0.009(4)	0.836(1)	0.094(5)
473	0.216(5)	0.438(9)	0.060(1)	-0.103(6)	0.826(1)	0.084(2)
573	0.152(1)	0.442(1)	0.057(3)	-0.169(5)	0.822(9)	0.079(1)
673	0.083(1)	0.441(6)	0.054(3)	-0.241(3)	0.816(1)	0.072(9)
773	0.018(8)	0.443(5)	0.049(7)	-0.307(5)	0.817(5)	0.065(9)
873	-0.039(4)	0.443(1)	0.046(7)	-0.370(1)	0.805(4)	0.061(8)
973	-0.097(4)	0.433(9)	0.026(4)	-0.431(1)	0.801(6)	0.032(3)

Table 4.15. The MS parameters for $Eu_3Fe_{3.5}Al_{1.5}O_{12}$. CS, QS and A refer to the center shift (relative to iron foil), quadrupole splitting and relative area, respectively.

	a site			d site		
T(K)	CS (mm/s)	QS (mm/s)	A (%·mm/s)	CS (mm/s)	QS (mm/s)	A (%·mm/s)
298	0.329(2)	0.410(8)	0.041(2)	0.002(1)	0.828(2)	0.046(1)
423	0.248(5)	0.407(4)	0.039(1)	-0.088(6)	0.817(9)	0.042(4)
523	0.179(5)	0.410(5)	0.036(5)	-0.160(1)	0.812(2)	0.040(1)
623	0.111(1)	0.410(1)	0.035(2)	-0.230(1)	0.805(9)	0.037(1)
723	0.045(4)	0.408(3)	0.033(1)	-0.298(5)	0.799(1)	0.034(1)
823	-0.017(6)	0.402(9)	0.032(6)	-0.369(2)	0.785(8)	0.030(1)
923	-0.080(3)	0.400(7)	0.031(7)	-0.436(1)	0.780(7)	0.028(2)
1023	-0.143(1)	0.404(9)	0.027(6)	-0.497(4)	0.769(1)	0.025(1)

samples are given in **Table 4.16**.

It can be seen from the cation distribution given in **Table 4.16** that the Al atoms occupy both the *a* and *d* sites in the studied samples with x > 0. This agrees with the results from the Rietveld analysis in the XRD measurements (**Table 4.12**). Since more Al atoms occupy the *d* site than the *a* site, it can be concluded that Al atoms preferentially enter the *d* sites due to the smaller size of Al atom. This proves that the average Y–O distance is larger than the average Z–O distance in the garnet structure[88]. The cation distribution from the MS measurements are more reliable than the results from the XRD measurements. The main reason for this is that MS is sensitive to the local environment around the iron nucleus at the specific site (the short-range order), whereas XRD parameters are obtained based on the mean structure of the whole crystal (the long-range order).

The effective resonance absorber thickness is defined as $T = nf\sigma_0$, where f is the recoilless fraction, n is the number of resonant nuclei per cm^2 and σ_0 is the maximum resonant cross-section. The values of T for the respective *a* and *d* sites in the three studied samples were calculated based on the corresponding f values[89], as shown in **Table 4.16**. It can be seen that they are all smaller than one at room temperature. Thus the condition $T \ll 1$ is not fulfilled and the assumption of thin absorbers is not valid.

The thickness correction has been done by simulating thin-limit folded spectrum from a statistically ideal fit to the raw folded spectrum using Voigt lines[90–92]. The derived θ_D values based on the thickness correction are presented in **Figs. 4.16–4.18**, and the corresponding cation distributions are also given in **Table 4.16**. It turns out that the cation distributions after the thickness correction are very close to the values without

thickness correction. It can been seen in **Table 4.16** that the θ_D or f values change a lot after the thickness correction. For the thickness-corrected spectra, A(T) for a specific site changes in the same direction as the corresponding f(T). Therefore, the value of n does not change significantly since A(T) and f(T) cancel each other (**Eq. 2.43**).

There is another way to determine the Mössbauer temperatures in the studied samples by assuming the Debye vibration mode. δ is a function of T and θ_D is the only unknown parameter in the expression of $\delta(T)$ (**Eq. 2.47**). Therefore, θ_D can be fitted from δ versus T. In order to use this method, more measurements should be made in the low-temperature region[84].

Table 4.16. The values of θ_D, cation distribution and effective resonance absorber thickness at room temperature T(RT) for the respective a and d sites in the studied samples with nominal composition x = 0.0, 1.0 and 1.5. * denotes the values after thickness correction.

Nominal composition x	a site			d site		
	θ_D (K)	Cation distribution	T(RT)	θ_D (K)	Cation distribution	T(RT)
0.0	485(4)	Fe: 1.779(6) Al: 0.0	0.86(7)	457(3)	Fe: 3.220(3) Al: 0.0	0.47(9)
0.0*	406 (4)*	Fe: 1.753 (9)* Al: 0.0*		474(4)*	Fe: 3.247(8)* Al: 0.0*	
1.0	473(6)	Fe: 1.612(2) Al: 0.387(8)	0.71(8)	429(4)	Fe: 2.387(7) Al: 0.612(3)	0.62(6)
1.0*	397(8)*	Fe: 1.586(4)* Al: 0.413(6)*		503(8)*	Fe: 2.413(6)* Al: 0.586(4)*	
1.5	511(6)	Fe: 1.606(8) Al: 0.393(2)	0.78(8)	440(4)	Fe: 1.893(1) Al: 1.106(9)	0.53(4)
1.5*	458(10)*	Fe: 1.813(6)* Al: 0.186(4)*		450(7)*	Fe: 1.686(4)* Al: 1.313(6)*	

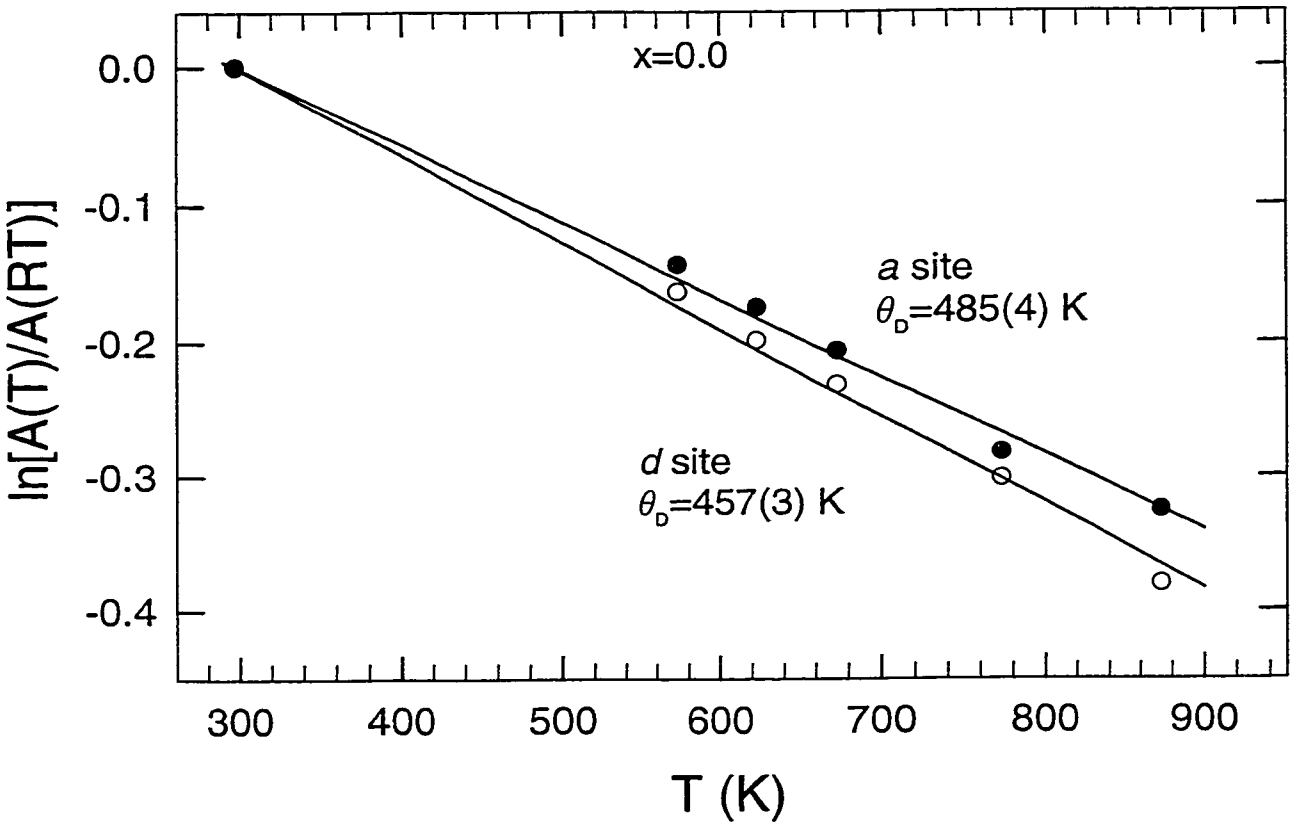

Fig. 4.13. The logarithm of the normalized areas of the two doublets corresponding to the *a* and *d* sites vs. temperature for $Eu_3Fe_5O_{12}$. The areas were obtained from the fits of the raw spectra.

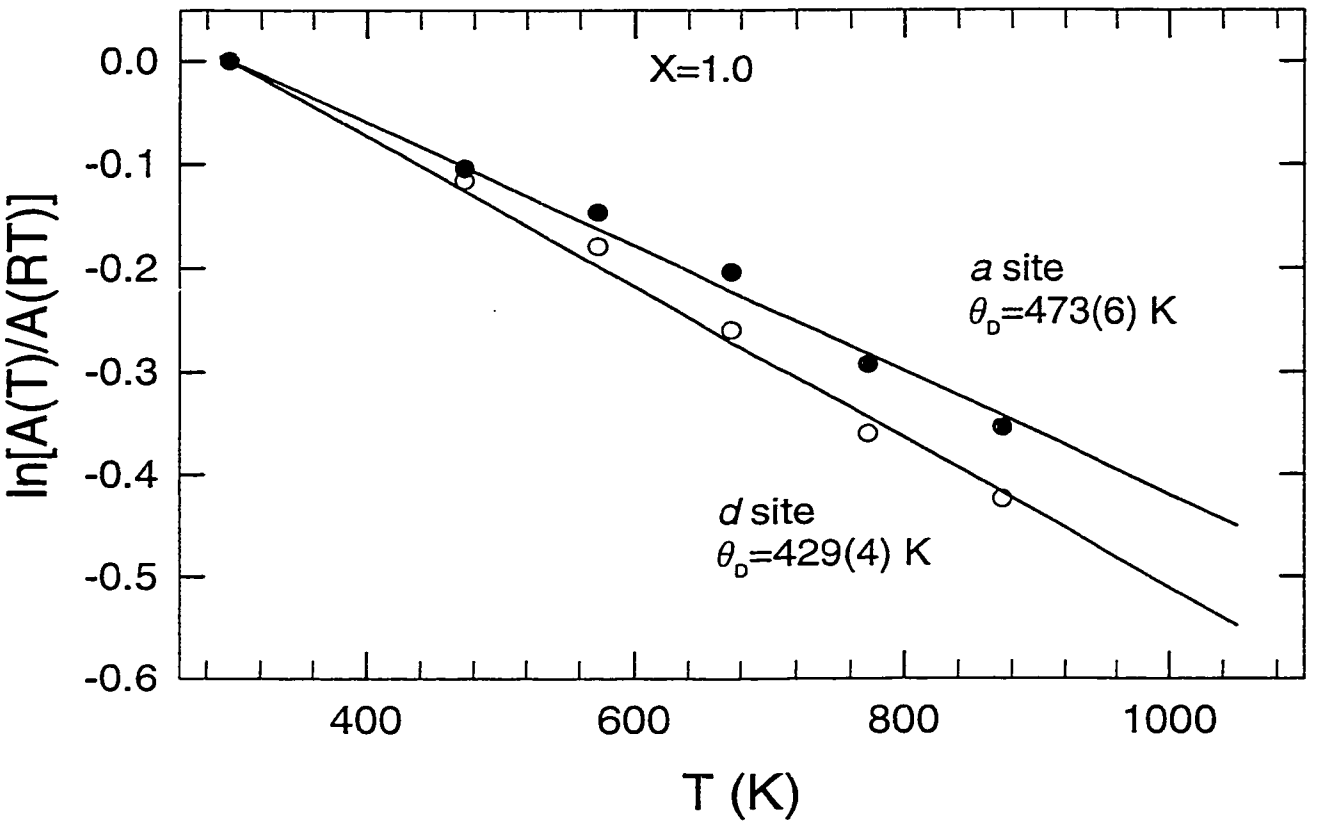

Fig. 4.14. The logarithm of the normalized areas of the two doublets corresponding to the *a* and *d* sites vs. temperature for $Eu_3Fe_4Al_1O_{12}$. The areas were obtained from the fits of the raw spectra.

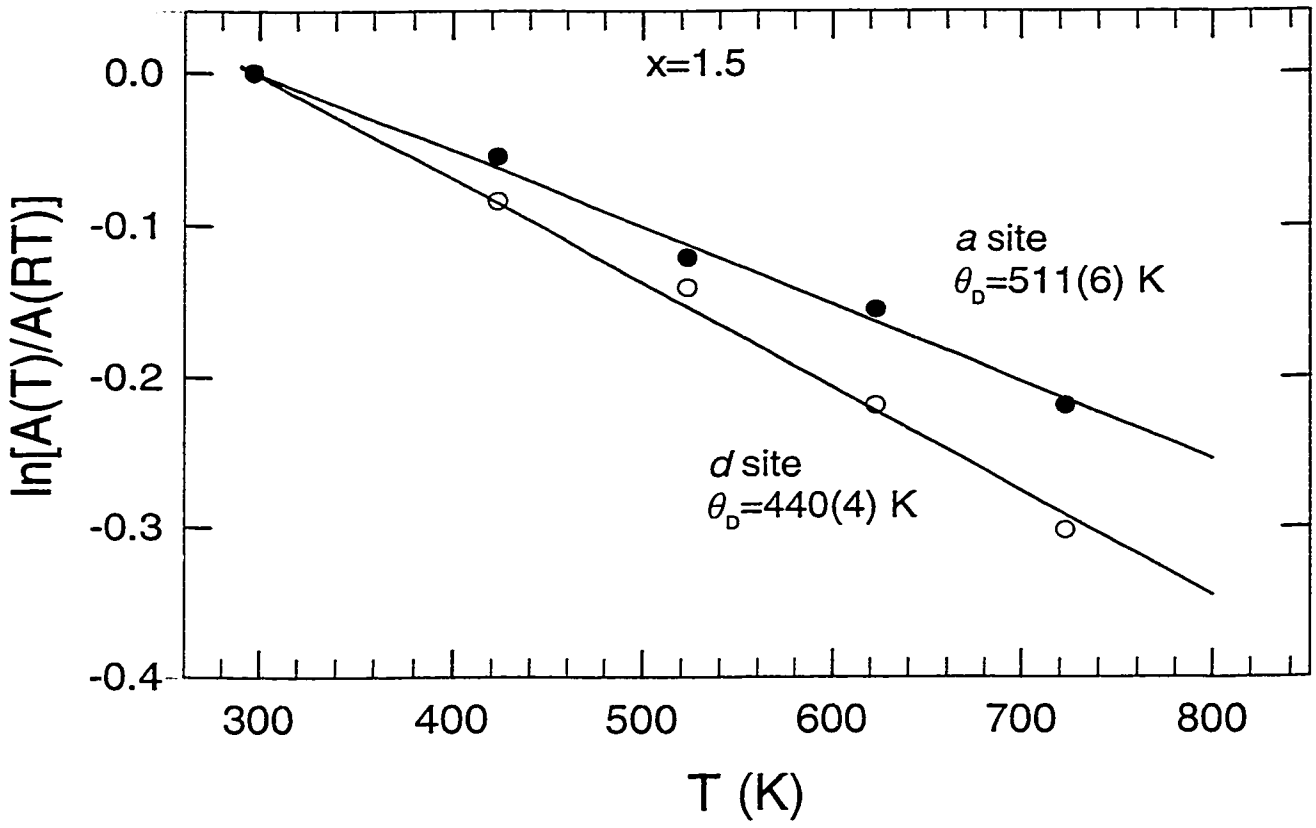

Fig. 4.15. The logarithm of the normalized areas of the two doublets corresponding to the *a* and *d* sites vs. temperature for $Eu_3Fe_{3.5}Al_{1.5}O_{12}$. The areas were obtained from the fits of the raw spectra.

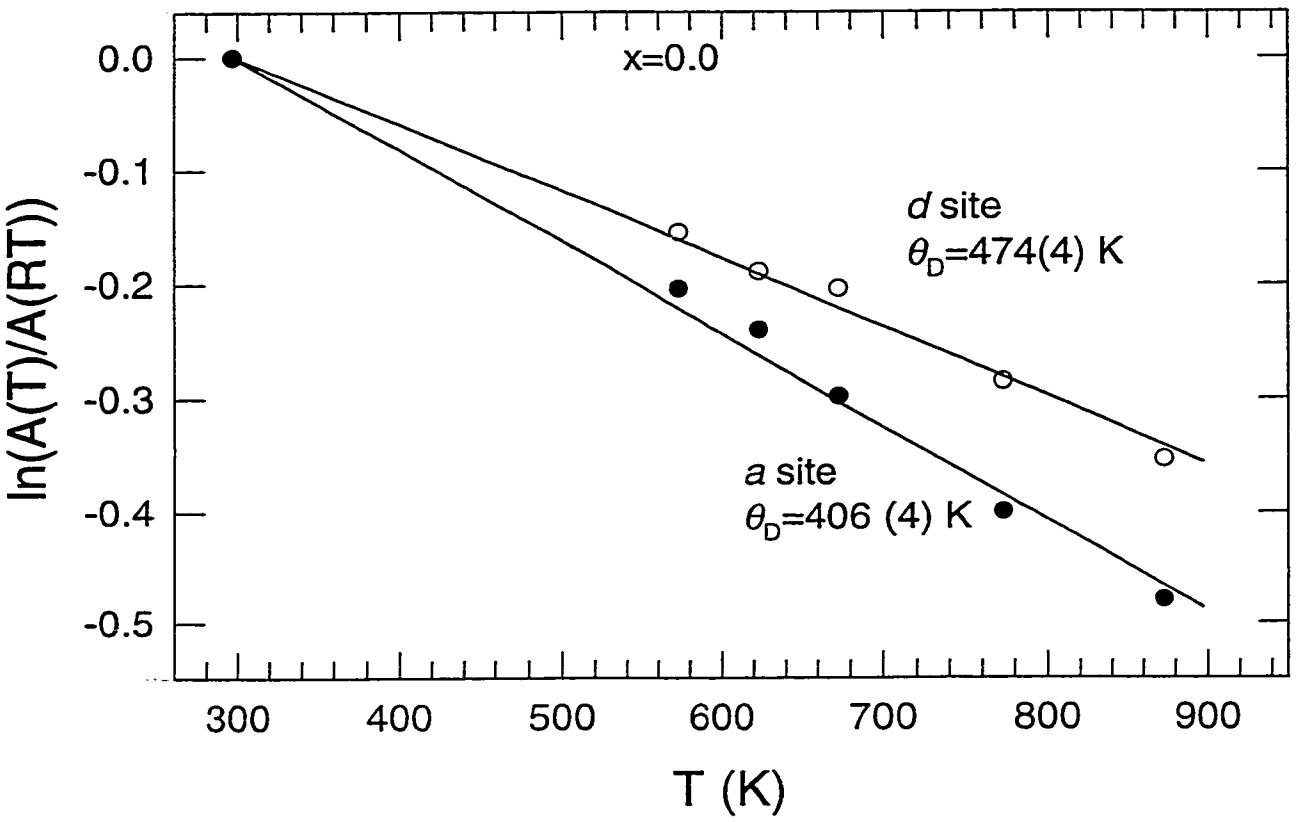

Fig. 4.16. The logarithm of the normalized areas of the two doublets corresponding to the *a* and *d* sites vs. temperature for $Eu_3Fe_5O_{12}$. The areas were obtained from the fits of the thickness-corrected spectra.

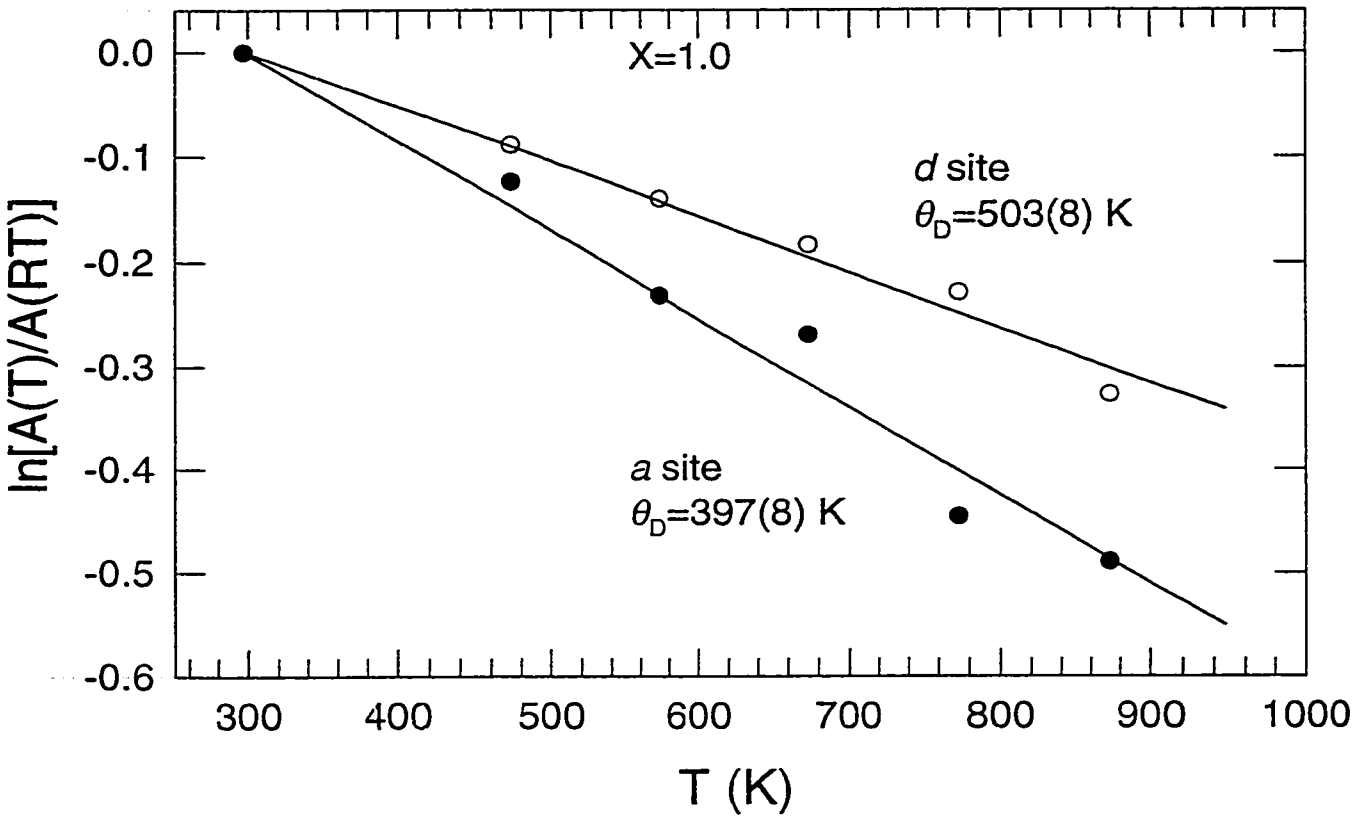

Fig. 4.17. The logarithm of the normalized areas of the two doublets corresponding to the *a* and *d* sites vs. temperature for $Eu_3Fe_4Al_1O_{12}$. The areas were obtained from the fits of the thickness-corrected spectra.

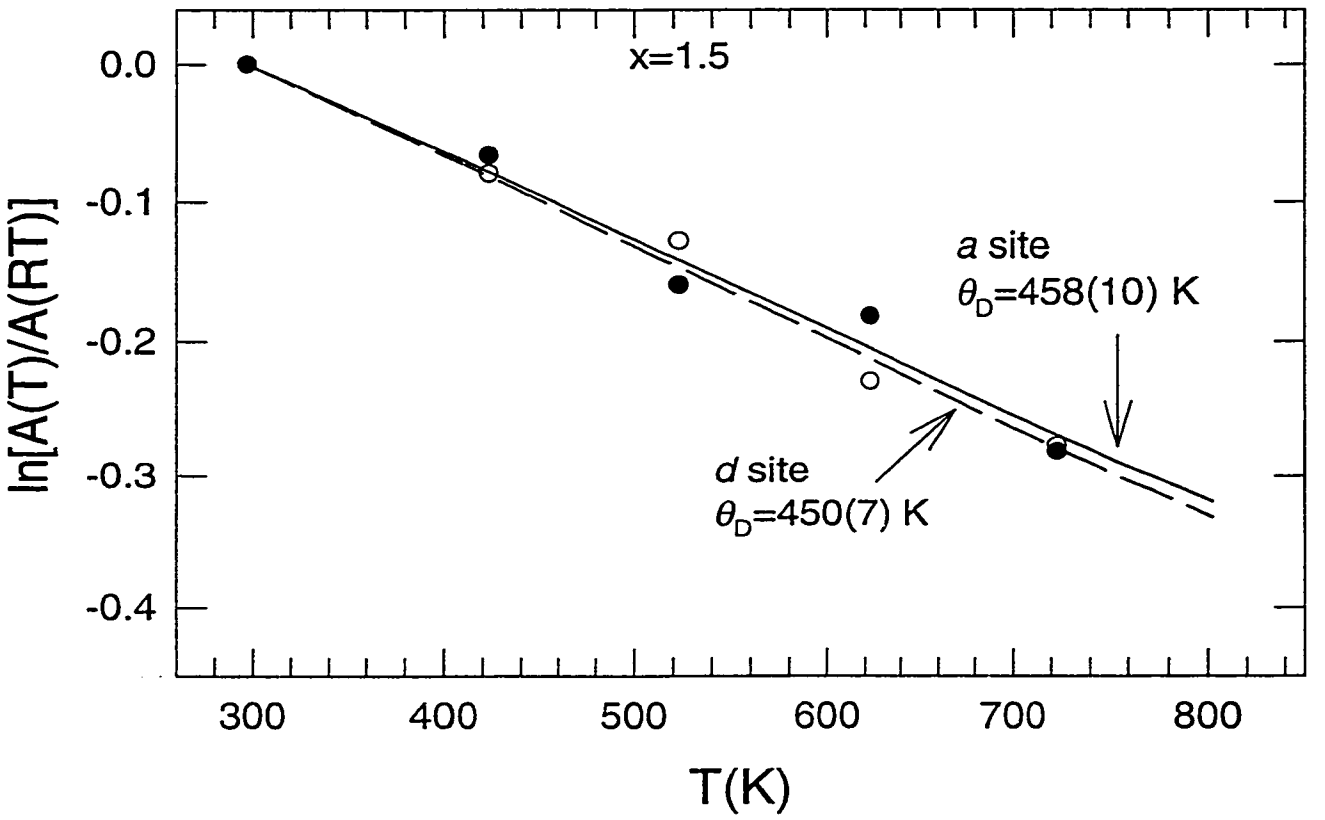

Fig. 4.18. The logarithm of the normalized areas of the two doublets corresponding to the *a* and *d* sites vs. temperature for $Eu_3Fe_{3.5}Al_{1.5}O_{12}$. The areas were obtained from the fits of the thickness-corrected spectra.

Chapter 5

Conclusions

XRD pattern indexing and Rietveld analysis, as one of the two major parts of this thesis, have been performed on the garnet series $Eu_3Fe_{x-5}Al_xO_{12}$. The XRD indexing has been successfully done all Bragg lines, even the very small Bragg lines in the high-angle region, were indexed. The crystal structure of the studied samples is proved to be a body-centered system. The cation distributions in the $Eu_3Fe_{5-x}Al_xO_{12}$ series from the Rietveld analysis have shown that Al atoms occupy both the *a* and *d* sites. MS measurements, as the other major part of the thesis, have also been used to determine the cation distributions in the $Eu_3Fe_{5-x}Al_xO_{12}$ series. The MS data have been analyzed based on the Debye vibration model. The values of θ_D corresponding respectively to the *a* and *d* sites have been derived. The experimental data from the MS method also indicate the existence of Al atoms in both the *a* and *d* sites. Furthermore, the results from the two methods have shown higher Al concentrations in the *d* sites. This is interpreted as evidence of smaller Z–O distance in the garnet structure.

For comparison, the values of θ_D also can be derived from the relationship between δ and T. In this case, the MS measurements on the studied samples should be extended to the low-temperature region.

To confirm the cation distributions in the studied samples, more experimental methods, such as neutron diffraction and infrared and optical absorption, could be useful.

References

[1] S. Geller, Z. Kristallogr. **123**, 1 (1967), and references therein.

[2] B. V. Mill, Neorg. Mater. **5**, 1604 (1969), and references therein.

[3] S. Geller and M. A. Gilleo, J. Phys. Chem. Solids **3**, 30 (1957).

[4] A. Batt and B. Post, Acta Crystallogr. **15**, 1268 (1962).

[5] F. Euler and J. A. Bruce, Acta Crystallogr. **19**, 971 (1965).

[6] G. A. Novak and G. V. Gibbs, Amer. Mineral. **56**, 791 (1971).

[7] F. Bertaud and F. Forrat, Compt. Rend. **242**, 382 (1956).

[8] S. Geller, in *Physics of Magnetic Garnets*, edited by A. Paoletti (North-Holland, Amsterdam, 1977).

[9] J. W. Nielsen and E. F. Dearborn, J. Phys. Chem. Solids **5**, 202 (1958).

[10] F. F. Y. Wang, in *Treatise on Materials Science and Technology*, Vol. **2**, edited by H. Haman (Academic Press, New York, 1973), p. 279.

[11] J. Carda, G. Monros, P. Escribano and J. Alarcon, J. Am. Ceram. Soc. **72**, 160 (1989).

[12] A. F. Wells, *Structural Inorganic Chemistry* (Clarendon, Oxford, 1984), p. 605.

[13] C. P. Khattak and F. F. Y. Wang, in *Handbook on the Physics and Chemistry of Rare Earths*, Vol. **3**, edited by K. A. Gschneidner, Jr. and L. Eyring (North Holland, Amsterdam, 1979), p. 564.

[14] K. Oka and H. Unoki, J. Appl. Phys. **56**, 436 (1984).

[15] G. F. Dionne, J. Appl. Phys. **81**, 5064 (1997).

[16] J. P. Krumme, V. Doormann and P. Willich, J. Appl. Phys. **57**, 3885 (1985).

[17] J. W. Martens, J. Appl. Phys. **59**, 6820 (1986).

[18] J. Ostoreto, M. Guillot and M. Artiniom, IEEE Trans. Magn. **24**, 2560 (1988).

[19] S. Geller, H. J. Williams, R. C. Sherwood and G. P. Espinosa, J. Appl. Phys. **36**, 88 (1965).

[20] S. Geller, R. C. Sherwood, G. P. Espinosa and H. J. Williams, J. Appl. Phys. **36**, 321 (1965).

[21] E. Geustic, J. M. Marcos and L. G. Van Uitert, Appl. Phys. Lett. **4**, 182 (1964).

[22] N. T. McDevitt, J. Opt. Soc. Amer. **59**, 1240 (1969).

[23] D. E. Lacklison and G. B. Scott, IEEE Trans. Magn. **13**, 973 (1977).

[24] B. Hill and K. P. Schmidt, Electron Components Applications **4**, 169 (1982).

[25] J. M. Roberston, J. A. Algra and D. J. Breed, J. Appl. Phys. **52**, 2338 (1981).

[26] J. Krebs, W. G. Maisch, G. A. Prinz and D. W. Forester, IEEE Trans. Magn. **16**, 1179 (1980).

[27] G. B. Scott and D. E. Lacklison, IEEE Trans. Magn. **12**, 276 (1976).

[28] E. M. Gyorgy, J. F. Dillon, Jr. and J. P. Remeika, J. Appl. Phys. **42**, 1454 (1971).

[29] A. J. Henderson, Jr., D. G. Onn, H. Meyer and J. P. Remeika, Phys. Rev. **185**, 1218 (1969).

[30] T. B. Bateman, J. Appl. Phys. **37**, 2194 (1966).

[31] G. S. Parker and W. R. Cox, J. Cryst. Growth **42**, 334 (1977).

[32] Y. Yamaguchi and T. Sakuraba, J. Phys. Chem. Solids **41**, 327 (1980).

[33] J. M. D. Coey, Phys. Rev. B **6**, 3240 (1972).

[34] J. Nicolas, in *Ferromagnetic Materials,* Vol.**2**, edited by E. P. Wohlfarth (North-Holland, Amsterdam, 1980), p. 243.

[35] S. Geller, J. Appl. Phys. **37**, 1408 (1968).

[36] Z. M. Stadnik, J. Phys. Chem. Solids **45**, 311 (1984).

[37] K. Oka and H. Unoki, J. Appl. Phys. **56**, 436 (1984).

[38] I. Ortalli, G. Pedrazzi, E. Schingaro and F. Scordari, Hyperfine Interact. **91**, 727 (1994).

[39] C. Kittel, *Introduction to Solid State Physics* (John Wiley & Sons, New York, 1953), p. 42.

[40] H. P. Myers, *Introductory Solid State Physics* (John Wiley & Sons, New York, 1900).

[41] B. E. Warren, in *X-ray Diffraction*, edited by B. E. Warren and M. Cohen, (Addison-Wesley, London, 1969), p. 41.

[42] H. M. Rietveld, Acta Crystallogr. **A 21**, 228 (1966).

[43] G. Malmros and J. O. Thomas, J. Appl. Crystallogr. **10,** 405 (1977).

[44] R. A. Young, P. E. Mackie and R. B. Von Dreele, J. Appl. Crystallogr. **10**, 262 (1977).

[45] C. P. Khattak and D. E. Cox, J. Appl. Crystallogr. **10**, 253 (1977).

[46] R. A. Young, in *The Rietveld Method,* edited by R. A. Young (Oxford University Press, New York, 1993), p. 11.

[47] H. M. Rietveld, J. Appl. Crystallogr. **2**, 65 (1969).

[48] D. B. Wiles and R. A. Young, J. Appl. Crystallogr. **14**, 149 (1981).

[49] A. March, Z. Kristallogr. **81,** 285 (1932).

[50] G. Will, M. Bellotto, W. Parrish and M. Hart, J. Appl. Crystallogr. **21**, 182 (1988).

[51] H. M. Rietveld, J. Appl. Crystallogr. **22**, 151 (1967).

[52] R. A. Young and D. B. Wiles, J. Appl. Crystallogr. **15**, 430 (1982).

[53] G. Cäglioti, A. Paoletti and F. P. Ricci, Nucl. Instrum. Methods **35**, 8 (1958).

[54] W. James and J. Richardson, in *The Rietveld Method,* edited by R. A. Young (Oxford University Press, New York, 1993), p. 102.

[55] R. A. Young, E. Prince and R. A. Sparks, J. Appl. Crystallogr. **15**, 357 (1982).

[56] R. V. Pound and G. A. Rebka, Phys. Rev. Lett. **3**, 554 (1959).

[57] P. G. Debrunner and H. Frauenfelder, in *Introduction to the Mössbauer Effect,* edited by L. May (Plenum Press, New York, 1971), p. 11.

[58] A. Vertes, L. Korecz and K. Burger, *Mössbauer Spectroscopy* (North-Holland, New York, 1979), p. 35.

[59] P. Gütlich, R. Link and A. Trautwein, *Mössbauer Spectroscopy and Transition Metal Chemistry* (Springer-Verlag, Berlin, 1978).

[60] A. Abragam, *The Principles of Nuclear Magnetism* (Clarendon, London, 1961), p. 161.

[61] I. S. Lyubutin and A. P. Dodokin, Soviet Phys. Crystallogr. **15**, 936 (1971)

[62] G. Amthauer, H. Annersten and S. S. Hafner, Z. Kristallogr. **143**, 14 (1975).

[63] G. A. Sawatzky, F. V. Woude and A. H. Morrish, Phys. Rev. **183**, 383 (1969)

[64] R. V. Pound and G. A. Rebka Jr., Phys. Rev. Lett. **4,** 274 (1960).

[65] Y. Yamaguchi and T. Sakuraba, J. Phys. Chem. Solids **41**, 327 (1979).

[66] PC-Rietveld plus, version 1.01, Philips Analytical X-ray (B. V. Almelo, The Netherlands, 1993).

[67] T. Nakamura, K. Sameshima, K. Okunaga, Y. Sugiura and J. Sato, Powder Diffr. **4**, 9 (1989).

[68] R. Jenkins, in *Modern Powder Diffraction*, vol. **20**, edited by D. L. Bish and J. E. Post (The Mineralogical Society of America, Washington, D. C., 1989).

[69] X'Pert System User Guide, Philips.

[70] R. Jenkins and W. N. Schreiner, Powder Diffr. **4**, 74 (1989).

[71] Standard Reference Material 640b, Silicon Powder 2θ/d-spacing for X-ray Diffraction, Natl. Bur. Stand. (U.S.), edited by S. D. Rasberry (U.S. GPO, Gaithersburg, 1987).

[72] W. N. Schreiner and R. Jenkins, Adv. X-ray Anal. **26**, 141 (1983).

[73] W. Wong-Ng and C. R. Hubbard, Powder Diffr. **2**, 242 (1987).

[74] A. Boultif and D. Louer, J. Appl. Cryst. **24**, 987 (1991).

[75] R. G. Garvey, Least square unit cell refinement with indexing on the personal computer, North Dakota State University (1985).

[76] P. E Werner, Treor 90, University of Stockholm (1990).

[77] J. Carda and G. Monros, J. Sol. State Chem. **108**, 24 (1994).

[78] J. Carda, M. A. Tena, G. Monros, V. Eshvi, M. M. Revintos and J. M. Amigo, Cryst. Res. Technal. **29**, 387 (1994).

[79] S. Margulies and J. R. Ehrman, Nucl. Inst. Methods **12**, 131(1961).

[80] G. J. Long, T. E. Cranshaw and G. Longworth, Mössbauer Effect Ref. Data J. **6**, 42 (1983).

[81] N. N. Greenwood and T. C. Gibb, *Mössbauer Spectroscopy* (Chapman and Hall Ltd., London, 1971), p. 23.

[82] R. A. Brand, *Normos-90 Mössbauer Fitting Program Package User's Guide* (Universität Duisburg, Duisburg, 1995).

[83] D. G. Rancourt, Nucl. Instr. Meth. Phys. Res. B **44**, 199 (1989).

[84] C. A. McCammon, Phys. Chem. Minerals **25**, 292 (1998).

[85] I. Nowik, I. Jacob and R. Moreh, Phys. Rev. B **47**, 723 (1993).

[86] C. W. Burnham, Y. Ohashi, S. S. Hafner and D. Virgo, Am. Mineral. **56**, 850 (1971).

[87] G. A. Sawatzky, F. Van Der Woude and A. H. Morrish, Phys. Rev. **183**, 383 (1969).

[88] S. C. Abrahams and S. Geller, Acta Cryst. **11**, 437 (1958).

[89] B. Kolk, in *Studies of Dynamical Properties of Solids with the Mössbauer Effect*, vol. **5**, edited by G. K. Horton and A. A. Maradudin (North-Holland, Amsterdam 1984), p. 184.

[90] D. G. Rancourt, Nucl. Instr. Meth. Phys. Res. B **44**, 199 (1989).

[91] D. G. Rancourt, J. Y. Ping and R. G. Berman, Phys. Chem. Minerals **21**, 258 (1994).

[92] D. G. Rancourt, A. M. McDonald, A. E. Lalonde and J. Y. Ping, American Mineralogist **78**, 1 (1993).

Statement of originality

This thesis is based on the work carried out as a M. Sc. student under the supervision of Z. M. Stadnik during the period 1996-2000 in the Department of Physics, University of Ottawa. I have involved both the XRD and MS measurements of the studied samples under the guidance of Z. M. Stadnik. All data analysis and calculations were made by me following the ideas and substantial guidance of Z. M. Stadnik.

To the best of my knowledge, no single piece of information presented in this thesis is directly copied from any published paper.